INFLUENCE OF PRESSURE-DAMS IN LIQUID ANNULAR SEALS IN THE LAMINAR FLOW REGIME, MEASURED RESULTS FOR STATIC AND ROTORDYNAMIC CHARACTERISTICS

A Thesis

by

JESUS SALAS III

Submitted to the Office of Graduate and Professional Studies of
Texas A&M University
in partial fulfillment of the requirements for the degree of

MASTER OF SCIENCE

Chair of Committee,	Dara W. Childs
Committee Members,	Luis San Andrés
	Gary Fry
Head of Department,	Andreas A. Polycarpou

May 2016

Major Subject: Mechanical Engineering

ABSTRACT

This thesis presents the test procedures and results of a study to create an alternative to plain annular seals as radial rotor supports in Electrical Submersible Pumps (ESPs). Currently, these pumps are assembled with annular seals which are susceptible to significant circumferential wear, resulting in increased radial clearance and degraded centering capabilities. Centering forces in annular seals arise due to hydrodynamic effects (fluid rotation) and hydrostatic effects (axial pressure drops that use the Lomakin Effect to get centering forces). The author's attempt to circumvent this issue integrates pressure-dams to improve the hydrodynamic centering forces.

Three pairs of seals were manufactured for this study: (1) 1X-clearance smooth seals (baseline pair), (2) 1X-clearance pressure-dam seals, and (3) 2X-clearance pressure-dam seals. The objective was to compare the centering capabilities of the three seals to determine if the pressure-dams were effective. The test rotor diameter was 116.83 mm (4.5998 in.). The 1X-clearance smooth and pressure-dam seals were manufactured to have a minimum 0.127 mm (0.005 in.) radial clearance. The 2X-clearance pressure-dam seals had a radial clearance of 0.254 mm (0.01 in.). Both pairs of pressure-dam seals were machined to include three pressure-dams of equal arc angle and axial length, but different recess depths. The pressure-dams were designed via results from Nicholas.

The pressure-dam seals were tested in two load orientations; load on dam (LOD) and load on land (LOL). Test conditions for all seals includes four rotor speeds (1500, 3000, 4500, and 6000 RPM), four axial pressure drops (2.1, 4.1, 6.2, and 8.3 bar), and four eccentricity ratios (0.0, 0.4, 0.6, and 0.8). The lubricant is ISO VG46 at

115°Fahrenheit, which has a dynamic viscosity of 0.0306 Pa-s.

Static test results include seal loci and seal leakage. The 1X-clearance pressure-dam seal leaks at least twice as much as the 1X-clearance smooth seal in every static position. The 2X-clearance pressure-dam seal leaks nearly 5 times more than the 1X-clearance pressure-dam seal.

Dynamic results include: (1) rotordynamic coefficients (direct stiffness, damping, and virtual mass as well as cross-coupled stiffness and virtual mass) and (2) whirl frequency ratios; the means by which these are arrived at is outlined in the proceeding sections. Results for the pressure-dam seals show a significant number of negative-direct-stiffness coefficients and whirl frequency ratios nearing 1. In general, the pressure-dam seals are out-performed by the smooth seals, which have whirl frequency ratios of approximately 0.5. In addition, their rotordynamic coefficients are sensitive to load orientation, making them poorly suited for vertical operation.

When the radial clearance was doubled, the pressure-dam seals did not have a stable equilibrium position under load; thus, the results are limited to centered (unloaded) conditions. Under these conditions, the pressure-dam seals do not retain their centering forces, and a large portion of the test data reflect negative direct stiffness coefficients ($\geq 50\%$).

XLAnSeal of the XLTRC^2 software suite was used to predict the leakage and rotordynamic coefficients of the smooth seal. Results show good agreement with measurements. No code exists for predicting the static and dynamic characteristics of annular seals with pressure-dams.

All test-flow conditions remained in the laminar regime. The presented results include seal leakage, seal loci under varying load, direct and cross coupled stiffness, damping, and virtual mass coefficients, and whirl frequency ratio.

DEDICATION

For my mother and father who always encouraged me, even when they could tell I had no idea what I was doing.

ACKNOWLEDGMENTS

First and foremost, I would like to thank Dr. Dara Childs for giving me one of the best opportunities I have ever received. I come from small beginnings, and he gave me a shot to do something that will ultimately shape my life and career, and I am deeply grateful for that. Thank you to all the TRC members for their support and allowing me to undertake this project. Thank you to Dr. San Andrès and Dr. Fry for your support and for being on my committee, and thank you to all the Turbolab office staff for handling any and all frantic emails that I ever sent.

I'd also like to thank all my Turbolab friends for their help, guidance, and welcomed distractions. J.Alex, Jose, Matt, Clay, Jimmy, Jennifer, Andrew, Josh, Mauricio, David, and Min. I was fortunate to work at the Turbolab, and maybe even more fortunate to have made such good friends while I was there. Thanks to Mr. Ray Matthews for your advice and for making sure none of us ever wore shorts and sandals in the building. I'd also like to thank coffee, Doritos, and Pandora online radio for their continued, judgement-free support.

NOMENCLATURE

$\boldsymbol{A_{ij}}$	Frequency domain stator acceleration [L/T^2]
C_{ij}	Seal damping coefficients [FT/L]
C_r	Seal Radial clearance [L]
D	Seal Diameter [L]
$\boldsymbol{D_{ij}}$	Frequency domain stator displacement [L]
$\boldsymbol{e_o}$	Eccentricity vector [L]
e_{xo}, e_{yo}	Eccentricity in x and y directions [L]
F_s	Applied static load [F]
f_{sx}, f_{sy}	Seal reaction forces in the x and y directions [F]
$\boldsymbol{F_x}, \boldsymbol{F_y}$	Frequency domain excitation forces in the x and y directions [F]
f_x, f_y	Applied dynamic loads in the x and y directions [F]
$\boldsymbol{H_{ij}}$	Frequency domain dynamic stiffness [F/L]
$\boldsymbol{j}$	Complex operator ($\sqrt{-1}$) [-]
K_{eq}	Equivalent stiffness coefficient [F/L]
K_{ij}	Seal stiffness coefficients [F/L]
L	Seal axial length [L]
L_d	Pressure-dam recess axial length [L]
$\bar{L_d}$	Nondimensional pressure-dam axial length, defined in Eq.(3) [-]
L_s	Pressure-dam recess depth [L]
$\bar{L_s}$	Nondimensional pressure-dam depth, defined in Eq.(3) [-]
M_{ij}	Seal virtual mass coefficients [M]
M_s	Stator mass [M]
$\dot{Q}$	Seal volumetric leakage rate [L^3/T]
Re_z	Axial Reynolds number, see Eq.(C.7) [-]

Re_θ	Circumferential Reynolds number, see Eq.(C.7) [-]
Re	Vector Reynolds number, see Eq.(C.7) [-]
R	Shaft radius [L]
W_o	Lubricant axial velocity [L/T]
$\ddot{x}, \ddot{y}$	Stator accelerations in the x and y directions [L/T^2]

Greek symbols

Δ_x, Δ_y	Relative stator displacement in x and y directions [L]
$\epsilon_{xo}, \epsilon_{yo}$	Static eccentricity ratio in x and y directions [-]
ϵ_o	Static eccentricity ratio [-]
θ_d	Pressure-dam arc length [Angle]
$\bar{\theta_d}$	Nondimensional dam arc length [-]
θ_p	Pad arc length [Angle]
μ	Fluid dynamic viscosity [FT/L^2]
ρ	Lubricant density [M/L^3]
ϕ	Attitude angle [Angle]
Ω	Excitation frequency [1/T]
ω	Rotor speed [1/T]

Abbreviations

DE, NDE	Drive end, non drive end
ESP	Electrical submersible pump
LOL, LOD	Load on land, load on dam
WFR	Whirl frequency ratio, defined in Eq.(C.1)

Subscripts

i,j	interchangeable x and y directions
x, y	x and y directions

TABLE OF CONTENTS

LIST OF FIGURES

LIST OF TABLES

INTRODUCTION

Annular pressure seals reduce the leakage of fluids into regions of differing pressures or compositions. Typically, they are employed in a liquid, gas, or two-phase process and are used in a variety of rotating pumps and compressors [1]. The annular seals discussed here are intended for Electrical Submersible Pumps (ESPs). ESPs are an inexpensive type of down-hole, centrifugal pump, used in the extraction of petroleum.

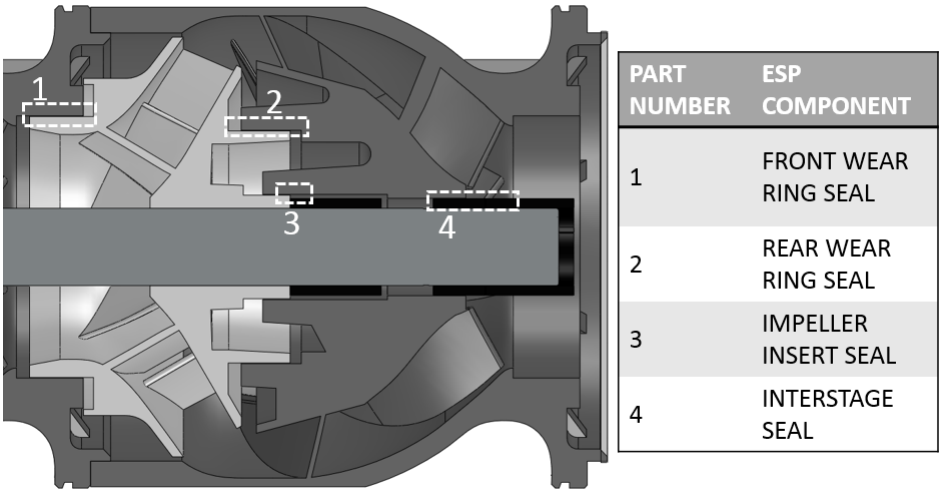

Figure 1: ESP Cutaway with seal components indicated [2]

Figure 1 shows a cutaway view of a single stage of an ESP and indicates the front (1) and rear (2) wear ring seals, the impeller insert seal (3), and the interstage seal (4). This research is aimed at finding a suitable replacement for the interstage seal.

ESP seals have historically employed a plain, cylindrical geometry [3]. Due to the often emulsive and sandy nature of the pump process fluid, the radial clearance of ESP seals have been known to prematurely degrade [4], [5], [6]. The nature of modern ESPs as a commodity has limited studies into enhancing their stability. As a result, the body of literature on ESP seals is limited.

Durham [7] discusses lateral vibration levels of horizontal ESPs to be in excess of 0.254 mm (10 mils) and finds that the the most common failures occured in the motor-bearing and seal assemblies. Salas et al. [8] observed high synchronous and subsynchronous vibration in an ESP due to motor shaft whirling. The authors find that changing the geometry of the motor bearing from cylindrical to an undisclosed "high-stability" design eliminates the issue.

Valantas and Bolleter [9] studied water injection pumps which failed after 700 hours of services due to excessive wear at the balance piston. The authors remedied the issue by filtering the water to reduce the amount of abrasives, increasing the hardness of sacrificial pump components, and including a swirl brake to mitigate fluid rotation. Childs and Norrbin [2] give a comprehensive look at ESP rotordynamics and present simulation results that suggest annular seals with swirl brakes upstream of the flow are a viable solution to mitigate ESP failures.

Annular seals often play the role of hydrodynamic bearings in ESPs, operating with larger clearance-to-radius ratios ($\sim$0.004 versus $\sim$0.001 for bearings) and providing the lateral centering forces that are required for stable pump operation [1]. Most liquid annular seals develop centering forces by two means: (1) hydrodynamic circumferential pressure distribution due to shaft rotation and (2) the Lomakin effect [10] due to axial pressure distributions.

The development of hydrodynamic pressure in bearings is driven by shaft rotation pulling lubricant into the annulus between the rotor and stator walls. As the fluid is dragged into the annulus, its local pressure becomes a function of its circumferential location. The integral of the circumferential pressure field results in a bearing load capacity. A full review of the derivations and applications are given by San Andrès [11] and Childs [12]. For plain journal bearings, cavitation in the diverging portion of the bearing film creates a lift force in the centered position. For a pressurized seal,

cavitation cannot occur, and the seal requires a static offset to produce a centering force.

ΔPs across an annular seal generate a centering force; this phenomena is known as the Lomakin Effect [10]. That is, as stagnant fluid at some supply pressure approaches the seal annulus of an eccentrically positioned seal, fluid is accelerated through the annulus such that the supply pressure is reduced. The losses at the seal inlet result in a local "Bernoulli-like" effect that is modelled by an inlet-loss coefficient. The pressures then drop linearly across the axial length of the seal due to wall friction. The combined effect of the inlet-loss and the axial pressure drop along the seal length force the rotor back into a centered position. An illustration of the Lomakin effect [10] is given in Figure 2.

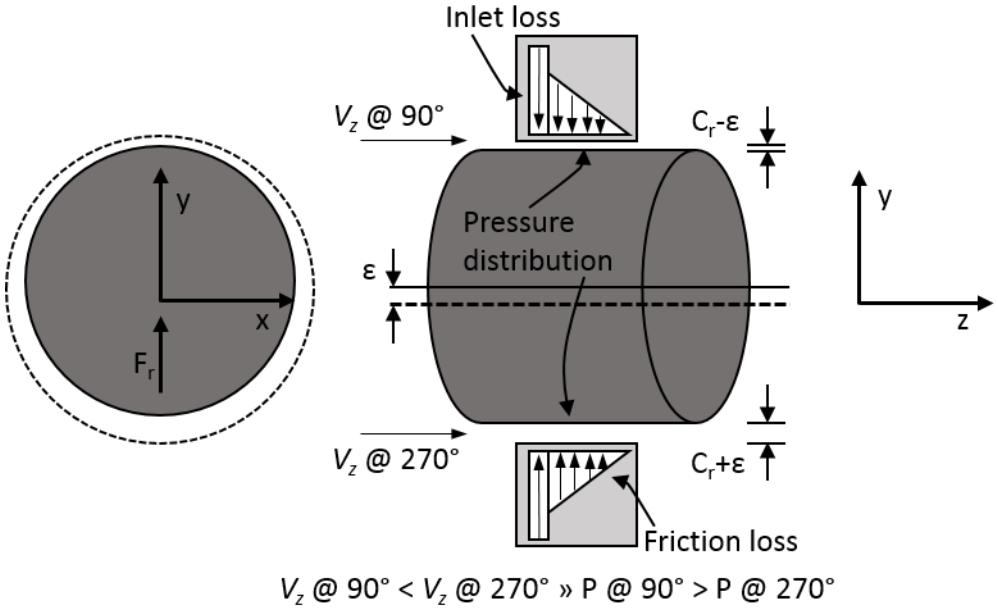

Figure 2: Illustration of the development of centering forces through the Lomakin Effect

The topic of centering forces introduces the idea of rotordynamic coefficients.

Figure 3 represents a traditional KC reaction-force model. The terms represented by springs and dashpots in Figure 3 are known as stiffness (K_{ij}) and damping (C_{ij}), respectively.

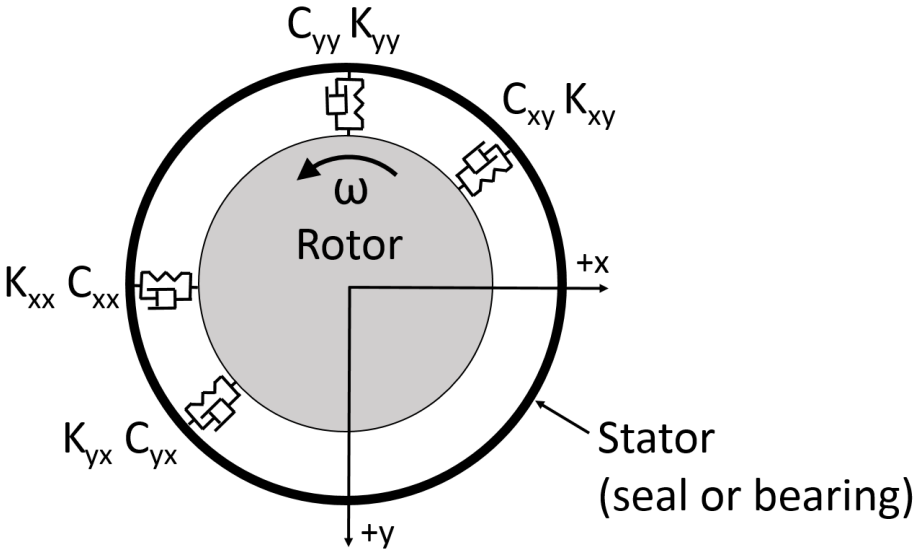

Figure 3: Representation of rotordynamic coefficients developed in a bearing or seal annulus

Traditional lubrication theory based on the Reynolds equation neglects the effect of fluid inertia [11]. Childs [12] derives a KCM reaction-force bulk-flow model which accounts for the inertial or virtual mass terms, represented as M_{ij} in Eq.(1). This model is appropriate for the current series of tests, as the resulting virtual mass terms are found to be significant.

$$-\begin{Bmatrix} f_{sx} \\ f_{sy} \end{Bmatrix} = \begin{bmatrix} K_{xx} & K_{xy} \\ K_{yx} & K_{yy} \end{bmatrix} \begin{Bmatrix} \Delta x \\ \Delta y \end{Bmatrix} + \begin{bmatrix} C_{xx} & C_{xy} \\ C_{yx} & C_{yy} \end{bmatrix} \begin{Bmatrix} \Delta \dot{x} \\ \Delta \dot{y} \end{Bmatrix} + \begin{bmatrix} M_{xx} & M_{xy} \\ M_{yx} & M_{yy} \end{bmatrix} \begin{Bmatrix} \Delta \ddot{x} \\ \Delta \ddot{y} \end{Bmatrix} \quad (1)$$

The terms in-line with the x and y axes are known as direct terms ($i = j$) and

the terms in the off-axis directions are known as cross-coupled terms ($i \neq j$). The author states that this model is valid for small motion about a centered position.

Kanki and Kawakami [13] measured rotordynamic coefficients of short and long (L/D = 0.2, 1.0) plain annular seals out to eccentricities of 0.9. Test conditions included speeds from 500 to 4000 RPM and ΔPs of 0.5 to 10 bar. The seals were water-lubricated. The authors show that, for long seals, stiffness and damping change as much as an order of magnitude as the seals go from centered to eccentric positions. They tested both laminar and turbulent flow seals.

Nelson and Nguyen [14] used a bulk-flow model to predict the rotordynamic coefficients of short, plain annular seals out to eccentricity ratios of 0.7. They compare their analytical model to the test results and finite element predictions of Falco et al. [15]. The authors find that their model is more accurate than the model of Falco et al. [15]. Note that these analyses are done for water-lubricated seals with an L/D of 0.25 at a rotor speed of 4000 RPM and ΔP of 10 bar.

Marquette et al. [16] give test results for annular seals operating at eccentricity ratios out to 0.5. The authors extend the model of Childs [12] to find eccentricity-dependent rotordynamic coefficients. The authors test at speeds from 10200 to 24600 RPM and pressure drops from 40 to 69 bar.

Childs et al. [17] tested short, eccentric smooth and grooved annular seals at speeds up 10000 RPM and pressure-drops up to 70 bar. Their flow is all laminar. San Andrès et al. [18] developed a finite element model for direct comparison to the results from Childs et al. [17]. The authors achieve good agreement for seal rotordynamic coefficients at low eccentricity ratios.

The Texas A&M Turbomachinery Laboratory has produced a large amount of literature on the static and dynamic characteristics of oil buffer seals, both through testing and through simulation [17, 18, 19, 20, 21]. Oil buffer seals were formerly

used in centrifugal compressors but have been subsequently replaced by dry-gas seals. Their C_r/R ratios are on the order of 0.001 and they absorb high ΔPs, on the order of 70 bars. Their flow is always laminar. The seals in this test program exhibit C_r/R ratios of 0.002 and 0.004 for the 1X and 2X-clearance seals, respectively. Childs and Norrbin [2] state that for a typical ESP, the ΔP across a single stage is roughly 2.5 bar (35 psi). In this test program, the ΔPs range from 2.1 to 8.3 bar (30 to 120 psi). When pumping high-viscosity emulsions, the seal flow in ESPs is nominally laminar.

The effect of annular seals on the stability of a turbomachine is partially characterized by the seal whirl frequency ratio (WFR). The WFR of a bearing or seal, in rotordynamics, is typically taken as the ratio of the rotor's first flexural natural frequency (ω_n) to its onset speed of instability (OSI), or:

$$WFR = \frac{\omega_n}{OSI} \Longrightarrow OSI = \frac{\omega_n}{WFR}; \tag{2}$$

The seals tested in this research are orthotropic ($K_{xx} \neq K_{yy}$), the effects of which must be considered in the formulation of the WFR. Lund [22] and San Andrès [23] each give an equation for WFR that can be solved for using rotordynamic coefficients. The difference between the two formulations appears when cross-coupled virtual mass coefficients are significant in magnitude and of opposite signs. San Andrès' model accounts for the cross-coupled virtual mass terms; Lund's does not. In this study, cross-coupled virtual mass terms are found to be significant. As a result, San Andrès' model is used, given in Appendix C.

A WFR at or close to zero is desirable, indicating that the rotor in question can be run in a stable condition well beyond its natural frequency without approaching instability. Plain journal bearings (and seals handling high-viscosity fluids) have a WFR of about 0.5, meaning that a flexible rotor can be run up to twice its first

flexural natural frequency on these bearings before stability is of concern.

A pressure-dam bearing (or step journal bearing), illustrated in Figure 4, is a plain journal bearing which has steps and usually a relief track cut into its circumference. The principle of operation is circumferential fluid flow, driven by the rotor surface speed, enters the step at the leading edge and exits at the trailing edge, creating a high pressure region at the step and forcing the rotor to operate eccentrically. Pressure-dam bearings often exhibit lower WFRs than plain journal bearings. Nicholas [24] creates the following set of non-dimensionalized design parameters for optimizing pressure-dam geometry:

$$\bar{L_d} = \frac{L_d}{L}; \qquad \bar{\theta_d} = \frac{\theta_d}{\theta_p}; \qquad \bar{L_s} = \frac{L_s}{C_r}, \tag{3}$$

where L is the total axial length of the seal insert, θ_p is the pad arc angle, and C_r is the seal radial clearance. He states that stability problems and whirling are typically related to light loads and high speeds, which can be circumvented by these "self-loading" bearings. Nicholas' design recommendations for single pressure-dam bearings are $\bar{L_d}$ of 0.75, $\bar{\theta_d}$ of 0.72, and $\bar{L_s}$ between 3.0 and 6.0. He lists decreases in WFR when following these guidelines. Allaire and Nicholas [25] analyze the pressure-dam bearings to include the effects of turbulent flow at the leading edge of the dam.

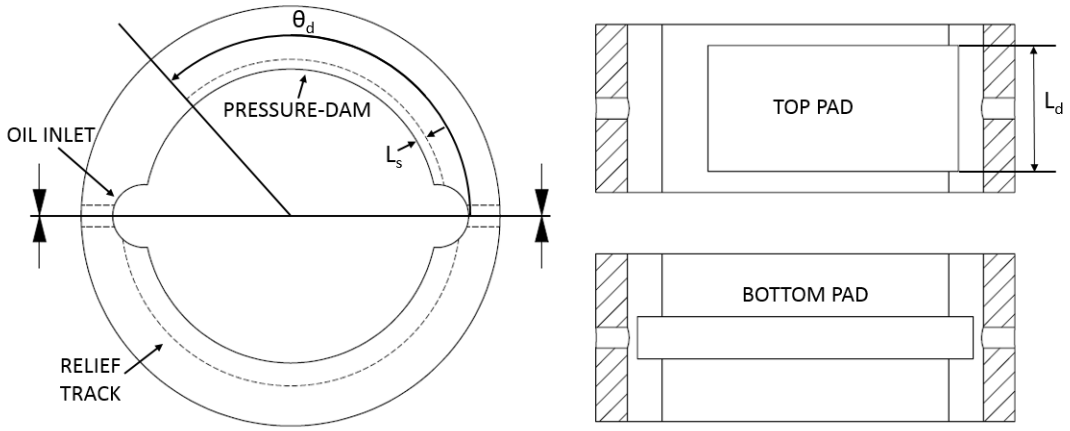

Figure 4: Two-pad pressure-dam bearing with a single dam and a relief track

Mehta and Rattan [26] analyze three-pad pressure-dam bearings with preload using a finite element solution to the Reynolds equation. Their bearings include two pressure-dams in the top pads (unloaded) and a relief track in the lower pad (load direction). They predict that, at high loads, the WFR of the bearing is zero, and at low loads it is nearly 0.1. The authors designed their bearing based on Nicholas [24], except for $\bar{L}_s$, which is set to 1.5. Mehta and Rattan [27] also study the effect of load orientation on a similar three-lobe pressure-dam bearing with preload. They find that the WFR of these bearings depends on load direction.

TEST RIG DESCRIPTION

Testing the annular seals was carried out on an existing rig for testing hydrodynamic journal bearings. The rig was designed by Kaul [28] and built in 1999 at the Texas A&M Turbomachinery Laboratory in College Station, Texas.

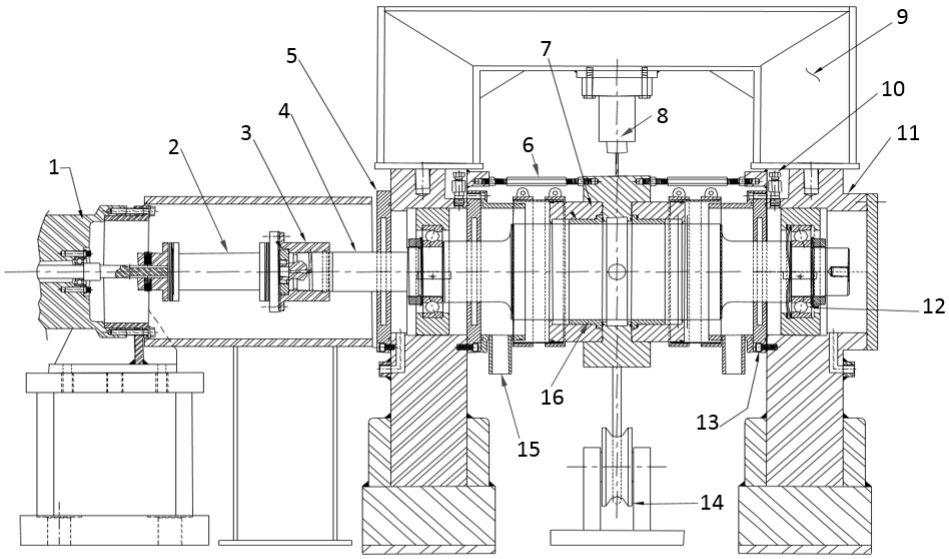

1. Air turbine	5. Vacuum seal	9. Shaker mount	13. Air buffer seal
2. Coupling	6. Pitch stabilizer	10. Mist oil inlet	14. Pulley
3. Rotor hub	7. Seal endcap	11. Test rig pedestal	15. Oil outlet
4. Test rotor	8. Hydraulic shaker	12. Ball bearing	16. Seal insert

Figure 5: Side view of annular seal test rig at the Texas A&M Turbomachinery Laboratory, designed by Kaul [28]

The rig was developed to conduct tests on laminar-flow annular seals to study their static and dynamic characteristics and their effects on the stability of turbomachines as well as their leakage characteristics. Shown in Figure 5, the rig utilizes the idea of a "floating stator", which was pioneered by Glienicke [29].

Kaul's design, shown in Figures 5 and 6, uses hydraulic shakers attached to a pair of stingers to support and dynamically load the stator and a pneumatic cylinder in series with an extension spring to apply static loads. The test frame consists of

the following major components: (1) the main test section (stator, rotor, pedestals, shaker mounts, air turbine), (2) the oil supply system, (3) the hydraulic shakers and static load assembly, and (4) instrumentation and data acquisition. The base of the test frame supports the test frame as well as the air turbine and turbine mount. Figure 6 shows the static load assembly.

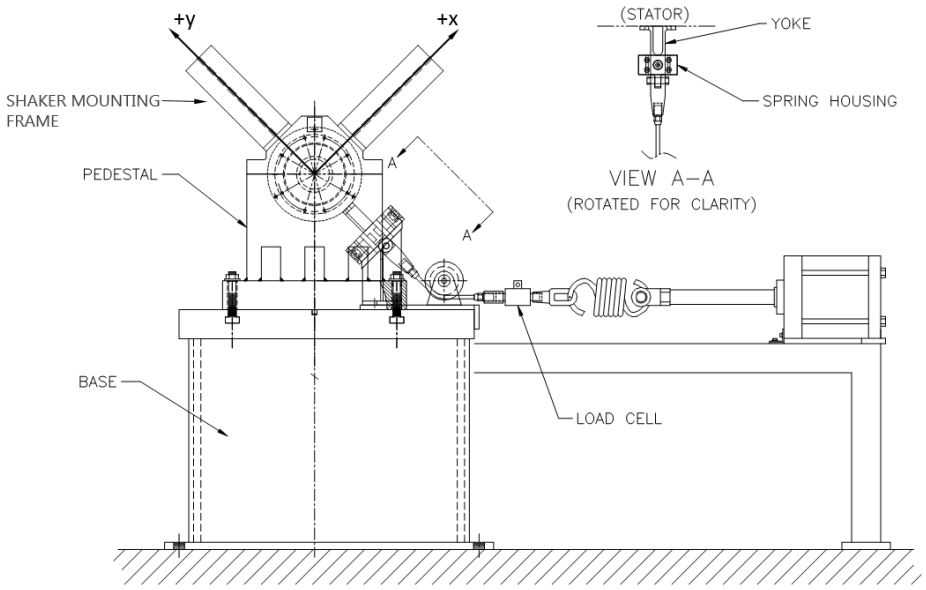

Figure 6: End view of annular seal test rig to show static load assembly [28]

Main Test Section

A 33 kW (45 hp) air turbine with a maximum speed of 17 krpm (283 Hz) acts as the system prime mover. The turbine output shaft is coupled to the test rotor through a hydraulically-mounted disc-pack coupling hub. The rotor has a test section diameter of 117 mm (4.5988 inches). Angular-contact ball bearings and bearing cartridges are mounted on each end of the rotor. Two rotor pedestals support the test rotor and house the ball bearings. The bottom halves of the pedestals are rigidly mounted to the test-frame bed plate. The top halves of the pedestals are integrated

into the hydraulic shaker mounts. When fastened together, the pedestals and shaker mounts also create an isolated cavity where each of the ball bearings can be lubricated via oil mist. This isolated form of lubrication also requires the use of air buffer seals to separate the oil mist from the test lubricant.

An assembled stator is composed of a pair of 660 Bronze seal inserts, a pair of seal endcaps, and the aluminum stator housing. Figure 7 shows the assembly process for the stator.

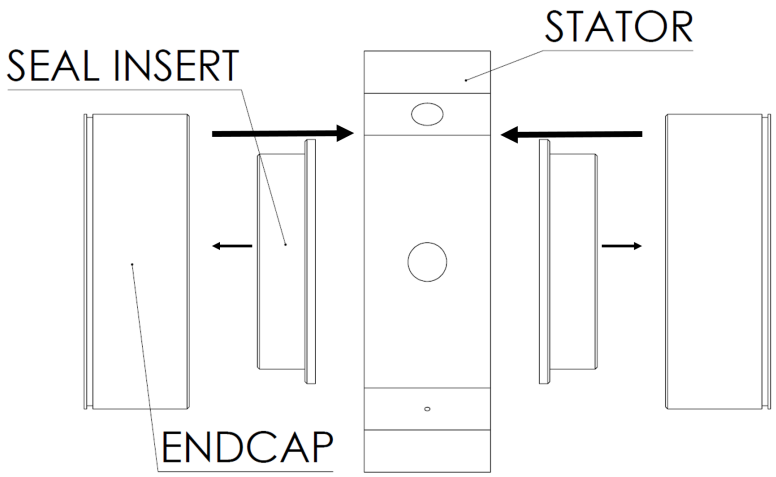

Figure 7: Decomposed view of stator, endcap, and seal insert

The seal inserts are pressed into an endcap. These seals have been manufactured to have a "line-to-line" fit; that is, as the seal is pressed into the endcap, there should be no elastic or plastic deformation of the components, such that the inner diameter of the seals is preserved. Once the seals are pressed into the endcaps, one endcap is installed on each side of the stator housing in a counter-bore. The entire installation process is performed on an alignment mandrel with a 0.04 mm (0.0016 in) diametral clearance between it and the test seals. This tight clearance minimizes misalignment during the assembly process. Once all components of the stator are in place, they are bolted together on the mandrel and placed on the test rotor.

Figure 8 shows the assembled stator and the centrally-located oil-inlet port. Once in place on the test frame, the stator can be aligned to remove any angular misalignment with the use of pitch stabilizers and two pairs of eddy current probes, one set on the drive end (DE) and one set on the non-drive end (NDE).

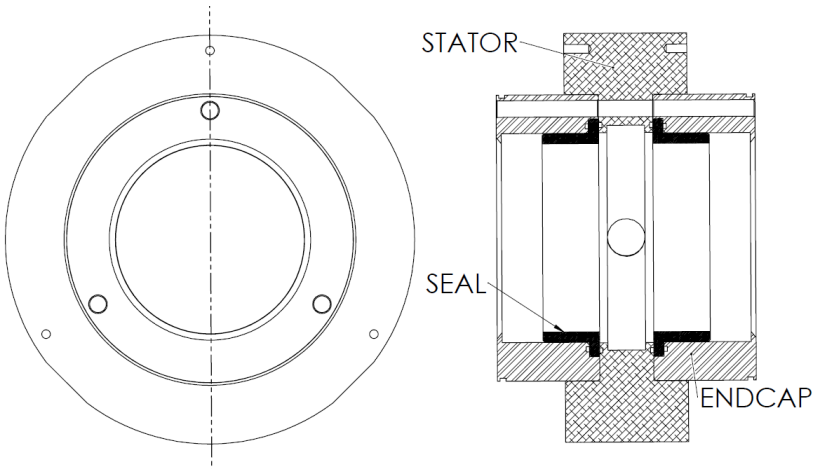

Figure 8: Cross sectional view of test stator, showing seal, endcap, and stator arrangement

Note that tests are done with nominally radial injection of lubricant upstream of the seals. Also note that the inlet circumferential velocity of the lubricant is not measured.

Static and Dynamic Loads

The hydraulic shakers serve not only to perturb the stator housing but also to support it in a "floating" configuration. The shakers are attached to the stator through connections known as stingers, which were designed as per guidelines set by Mitchell and Elliot [30]. The shakers are each driven by a Zonic Corporation hydraulic-powered exciter head and dual-loop master controller. The exciter head contains a hydraulic solenoid valve, which is driven by a 206 bar (3000 psi) power supply. The exciters can apply variable frequency dynamic loads to the stator. As

shown in Figure 6, the hydraulic shakers are oriented in two orthogonal directions to provide a bi-directional excitation.

Figure 6 also illustrates the coordinate system utilized for testing, viewed from the non-drive end (NDE). The exciter which acts in the y direction can supply tensile loads of up to 4500 N (1000 lbf) and compressive loads of up to 9000 N (2000 lbf). The exciter which acts in the x direction can supply compressive and tensile loads of up to 4500 N (1000 lbf). Furthermore, the unit allows for active control of dynamic gains, allowing for a constant amplitude excitation even as the reference frequency is increased.

The static load assembly, as shown in Figure 6, uses a pneumatic cylinder in series with an extension spring and a load cell. A cable extends from the spring and attaches to the stator. As a static load is applied in the $-y$ direction, the stationary rotor appears to move in the $+y$ direction. This motion direction is due to the placement of the eddy-current probes on the stator and the fact that this coordinate system is stator-fixed.

Instrumentation

Figure 9 illustrates and lists the instrumentation used in the acquisition of data during the conducted experiments.

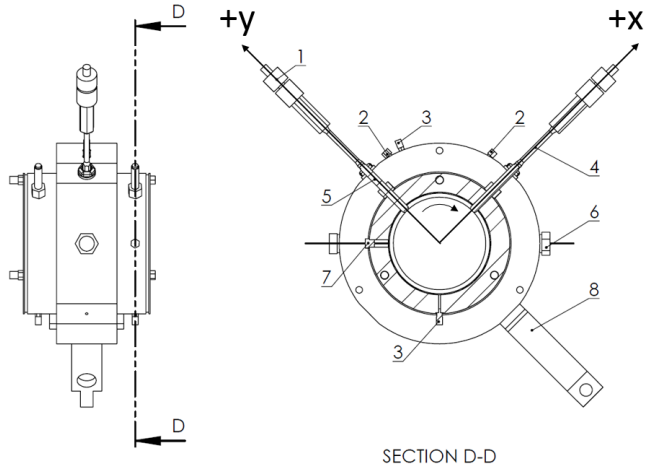

Part	Description	Quantity
1	Load cell	2
2	Accelerometer	2
3	Pressure transducer	3
4	Stinger	2
5	Eddy current probe	4
6	Oil inlet port	2
7	Thermocouple probe	3
8	Static load attachment	1

Figure 9: NDE view of assembled stator and accompanying instrumentation

In series with the shakers and stingers are a pair of load cells (1) for measuring dynamic loads during excitations. The acceleration and relative displacement of the stator is measured using a pair of PCB accelerometers (2) and a set of 3300 Series Bentley Nevada eddy-current probes (5), respectively.

The pressure differential from the upstream and downstream sides of the seal inserts are measured with pressure transducers at the oil inlet and outlets (3). The transducers were Kulite XTM-190 series with maximum pressure ratings of 17 bar (250 psi). The inlet pressure transducer is on the top half of the stator, and the outlet pressure transducers are on the bottom half of the DE and NDE endcaps. Temperature measurements were also taken at the upstream and downstream locations of the seal insert with type J thermocouples (7).

All temperature, pressure, acceleration, and displacement measurements were sampled at 10 kHz using two National Instruments data acquisition cards. The cards were read into a single data acquisition chassis, and the raw voltage signals relayed into a personal computer where the resulting values were analyzed.

Oil System and Lubricant

The test oil supply system was composed of two GEARTEK pumps, a 950 liter (250 gallon) main tank, and a 380 liter (100 gallon) sump tank, both containing ISO VG 46 turbine oil. The target test temperature for these tests was roughly 46°Celsius (115°Fahrenheit), at which the dynamic viscosity and density of ISO VG 46 oil are 0.0306 Pa-s and 861 kg/m exp 3.

The lubricant supply system is controlled by a series of pneumatic valves which are wired into a PID temperature controller. The PID controller enables, with some patience, temperature control within ± 2°Fahrenheit. Reaching steady state temperature goals was achieved by running the rig for 1 to 2 hours prior to recording any data.

Target pressure differentials across the test seals were achieved by varying the lubricant flow rate. Seal leakage is taken as one half of the total oil flow rate into the stator.

Testing Procedure

Prior to running any dynamic tests, a "cold clearance" measurement is taken. This involves using the x direction and y direction shakers in a "displacement" mode that slowly precesses the stator about the rotor. This precession allows the eddy current probes to take measurements of the stator-to-rotor displacement out to its furthest (contacting) position. This displacement measurement results in a circular clearance with a diameter that is roughly the diametral clearance of the seals at room

temperature. Once a cold clearance is taken, a baseline test can then be completed.

A baseline test involves measurement of the test rig dynamic stiffness coefficients when assembled, but before any lubricant has been run through the system. This is also known as a "dry-shake", due to the absence of lubricant. The baseline dynamic stiffness is subtracted from the measured dynamic stiffness to provide a measurement for the seals alone.

Static Measurements

At this point, the stator is centered about the rotor, the oil pumps are activated and begin to fill the annulus with lubricant, and the rotor is run up to the target speed. The rig is run at the target speed and pressure drop until steady state operation is reached, at which point a "hot clearance" is taken to measure the seal radial clearance at the target temperature.

A "hot clearance" involves safely stopping the test rotor and flow of lubricant to the stator and taking a seal-clearance measurement. The rig is then quickly restarted such that steady state operation is re-achieved shortly. Once the rig returns to steady state, a static data condition is measured. This entails measuring lubricant flow rate ($\dot{Q}$), lubricant inlet and outlet temperature, lubricant pressure drop (ΔP), and rotor-stator relative location. Rotor speed (ω) and static load (F_s) are also measured. The reader should note that, while the seals are tested in pairs, the data are reduced to reflect a single seal. That is, the static results and the dynamic results of the proceeding section represent one seal, not a pair of seals.

Figure 10 reminds the reader that, from the NDE, the static loader moves the stator in the $-y$ direction with clock-wise shaft rotation. To relate the position of the stator to the rotor, we define the quantities eccentricity ratio (ϵ) and attitude angle (ϕ), to be defined later.

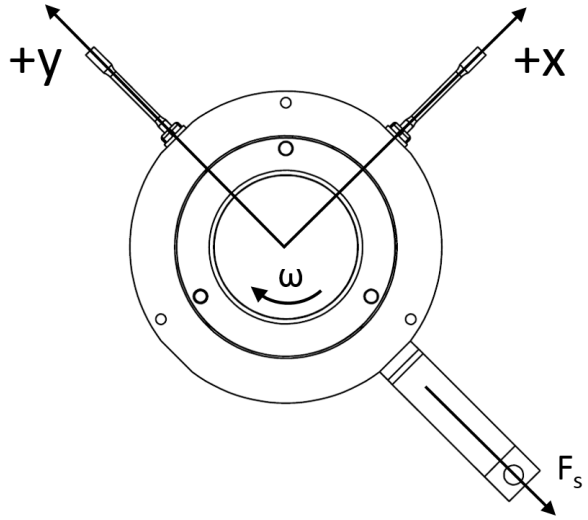

Figure 10: NDE view of stator and established coordinate system

As shown in Figure 11, the eccentricity vector is defined in terms of it's components e_x and e_y in the x and y directions, respectively. ϕ is measured as the angle between the $\boldsymbol{e}$ vector and the load direction, measured in the direction of rotation. The distinction between displacement and eccentricity ratio is explained in Eqs.(4)-(6).

$$\Delta e_{xo} = e_{xo} - \overline{e}_{xo}; \quad \Delta e_{yo} = e_{yo} - \overline{e}_{yo}; \tag{4}$$

$$\epsilon_{xo} = \frac{\Delta e_{xo}}{C_r}; \quad \epsilon_{yo} = \frac{\Delta e_{yo}}{C_r}; \tag{5}$$

$$\epsilon_o = \sqrt{\epsilon_{xo}^2 + \epsilon_{yo}^2}; \quad \phi = tan^{-1}\frac{\epsilon_{xo}}{\epsilon_{yo}}; \tag{6}$$

Here, $\bar{e}_{xo}$ and $\bar{e}_{yo}$ define the geometric center of the seal clearance and Δe_{xo} and Δe_{yo} are the change in position from the center. Note that ϵ_o defines the relative seal-to-rotor position where $\epsilon_o = 0.0$ is centered, and $\epsilon_o = 1$ indicates a 'rubbing' or contacting position.

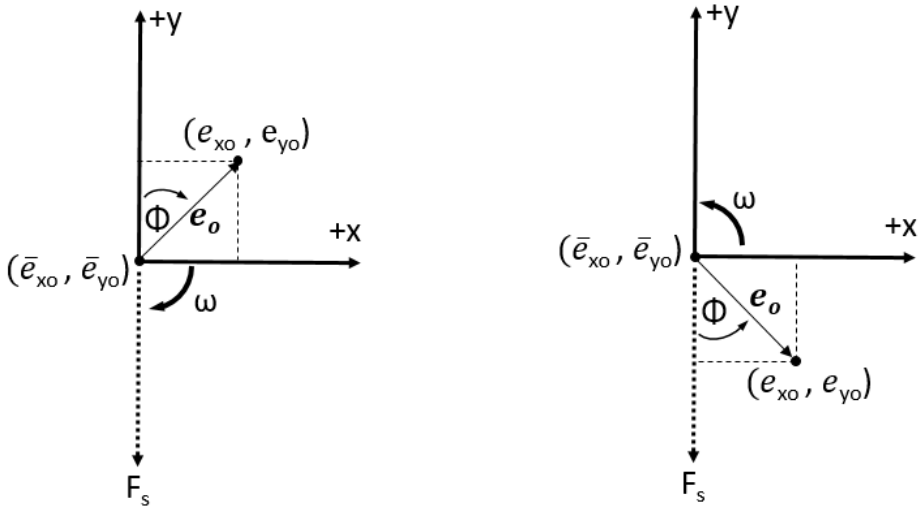

(a) Rig eccentricity definition **(b) Presented eccentricity defintion**

Figure 11: Explanation of static eccentricity measurements

Dynamic Measurements

The equation of motion of the stator is:

$$\begin{Bmatrix} M_s\ddot{x} \\ M_s\ddot{y} \end{Bmatrix} = \begin{Bmatrix} f_x \\ f_y \end{Bmatrix} + \begin{Bmatrix} f_{sx} \\ f_{sy} \end{Bmatrix}, \tag{7}$$

where M_s is the stator mass, $\ddot{x}$ and $\ddot{y}$ are the stator acceleration components in the x and y directions, f_x and f_y correspond to the dynamic forces applied by the stingers

in the x and y directions, and f_{sx} and f_{sy} are the seal reaction forces in the x and y directions. The summation of seal reaction forces is equated to a linearized set of stiffness, damping, and virtual mass coefficients. Solving for and plugging in the seal reaction forces of Eq.(7) into Eq.(1), we arrive at

$$\begin{Bmatrix} f_x - M_s\ddot{x} \\ f_y - M_s\ddot{y} \end{Bmatrix} = \begin{bmatrix} K_{xx} & K_{xy} \\ K_{yx} & K_{yy} \end{bmatrix} \begin{Bmatrix} \Delta x \\ \Delta y \end{Bmatrix} + \begin{bmatrix} C_{xx} & C_{xy} \\ C_{yx} & C_{yy} \end{bmatrix} \begin{Bmatrix} \dot{\Delta} x \\ \dot{\Delta} y \end{Bmatrix} + \begin{bmatrix} M_{xx} & M_{xy} \\ M_{yx} & M_{yy} \end{bmatrix} \begin{Bmatrix} \ddot{\Delta} x \\ \ddot{\Delta} y \end{Bmatrix} \quad (8)$$

This system of linearized equations are only valid for "infinitesimally" small amplitudes of motion. As a rule of thumb, the excitations amplitudes are monitored in real-time during tests and are not to exceed 1/10 of the seal radial clearance. For the present tests, a seal with a 0.127 mm (0.005 in) the amplitudes did not exceed, 0.0127 mm (0.0005 in). Note the presence of virtual mass terms in Eq.(8).

The method by which dynamic stiffnesses and rotordynamic coefficients are approximated has been adapted from Rouvas et al.[31] and Childs and Hale [32]. The dynamic shakers use a pseudo-random waveform that excites the stator at frequencies from 9.765 Hz to roughly 150 Hz, in increments of 9.765 Hz. By using a non-integer increment, the user avoids interference due to electrical noise.

Output voltages from the accelerometers, eddy-current probes, and dynamic load cells are measured to find acceleration $(\ddot{x}, \ddot{y})$, displacement (Δ_x, Δ_y), and force (f_x, f_y) in the x and y directions, respectively. During tests, these parameters are measured in the time domain and converted into the frequency domain. The result is a set of frequency domain excitation forces $(\boldsymbol{F_x}, \boldsymbol{F_y})$, relative stator displacements $(\boldsymbol{D_x}, \boldsymbol{D_y})$,

and accelerations ($\boldsymbol{A_x}, \boldsymbol{A_y}$).

$$\begin{Bmatrix} \boldsymbol{F_x} - M_s\boldsymbol{A_x} \\ \boldsymbol{F_y} - M_s\boldsymbol{A_y} \end{Bmatrix} = - \begin{bmatrix} \boldsymbol{H_{xx}} & \boldsymbol{H_{xy}} \\ \boldsymbol{H_{yx}} & \boldsymbol{H_{yy}} \end{bmatrix} \begin{Bmatrix} \boldsymbol{D_x} \\ \boldsymbol{D_y} \end{Bmatrix} \tag{9}$$

Equation (9) introduces the notion of an impedance or dynamic stiffness coefficient, denoted by $\boldsymbol{H_{ij}}$, where i and j denote the x and y directions, respectively. The physical meaning of dynamic stiffness is a ratio of applied force to a resulting displacement. The dynamic stiffness coefficients can be readily solved for with the frequency domain forces, accelerations, and relative displacements. Alternate shakes in two orthogonal directions are completed to arrive at four independent, linearized equations and four unknowns as shown in Eq.(10).

$$\begin{bmatrix} \boldsymbol{F_{xx}} - M_s\boldsymbol{A_{xx}} & \boldsymbol{F_{xy}} - M_s\boldsymbol{A_{xy}} \\ \boldsymbol{F_{yx}} - M_s\boldsymbol{A_{yx}} & \boldsymbol{F_{yy}} - M_s\boldsymbol{A_{yy}} \end{bmatrix} = - \begin{bmatrix} \boldsymbol{H_{xx}} & \boldsymbol{H_{xy}} \\ \boldsymbol{H_{yx}} & \boldsymbol{H_{yy}} \end{bmatrix} \begin{bmatrix} \boldsymbol{D_{xx}} & \boldsymbol{D_{xy}} \\ \boldsymbol{D_{yx}} & \boldsymbol{D_{yy}} \end{bmatrix} \tag{10}$$

The means by which dynamic stiffness $\boldsymbol{H_{ij}}$ is decomposed into the desired rotordynamic coefficients is related by Eq.(11).

$$\boldsymbol{H_{ij}} = (K_{ij} - M_{ij}\Omega^2) + \boldsymbol{j}(\Omega C_{ij}), \tag{11}$$

where K_{ij}, C_{ij}, M_{ij}, and Ω are rotordynamic stiffness, damping, virtual mass, and excitation frequency, respectively. Note that i is the direction of the excitation force and j is the direction of rotor-to-stator relative motion. Also, note that there is an imaginary part of the dynamic stiffness ($\boldsymbol{j} = \sqrt{-1}$) and a real part. The stiffness and virtual mass are solved for using a linear curve fit in Ω^2 of the real component of the dynamic stiffness, where the stiffness is the y-intercept and the virtual mass is the slope. The damping is estimated as the slope from a linear fit of the complex

component of the dynamic stiffness in Ω.

Uncertainty Analysis

To decrease the variation of the resulting dynamic stiffness, 32 shakes are performed at discrete frequencies a total of 10 times each. The 10 tests at each frequency are averaged and a set of dynamic stiffness values at frequencies from 20 to 320 Hz is the output. The uncertainty of the dynamic stiffness is taken as twice the standard deviation of the 10 averaged dynamic stiffness points taken at each discrete frequency.

A least squares regression analysis is used to determine the goodness of fit of the dynamic stiffness curve fits. The method shown here is given in greater detail by Figliola and Beasley [33]. Least-squares provides an *mth*-order fit of the data of the form

$$y_c = a_0 + a_1 X + a_2 X^2 + ... + a_m X^m \tag{12}$$

To perform a simple linear regression of both the real and complex parts of the dynamic stiffness, Ω^2 is replaced with Λ. This results in a dynamic stiffness that resembles

$$\boldsymbol{H_{ij}} = (K_{ij} - M_{ij}\Lambda) + \boldsymbol{j}(\Omega C_{ij}) \tag{13}$$

This representation of the dynamic stiffness is a first order for both the real and complex parts; the same linear regression model can be used with the form

$$Y_f = a_1 X_i + a_0, \tag{14}$$

where Y_f is the best fit line of the dynamic stiffness, X_i is the square of the excitation

frequency, and the coefficients a_0 (Y-intercept) and a_1 (slope) can be solved for through:

$$a_0 = \frac{\sum_{i=1}^{N} X_i \sum_{i=1}^{N} X_i Y_i - \sum_{i=1}^{N} X_i^2 \sum_{i=1}^{N} Y_i}{(\sum_{i=1}^{N} X_i)^2 - N \sum_{i=1}^{N} X_i^2} \tag{15}$$

$$a_1 = \frac{\sum_{i=1}^{N} X_i \sum_{i=1}^{N} X_i - N \sum_{i=1}^{N} X_i Y_i}{(\sum_{i=1}^{N} X_i)^2 - N \sum_{i=1}^{N} X_i^2} \tag{16}$$

X_i and Y_i in equations (15) and (16) are the squares of the excitation frequency and the measured dynamic stiffness, respectively. This results in a fit of the data that minimizes the sum of the squares of the deviations of the fit from the actual test points. To assess the "goodness" of the fit, the standard error, s_{YX} and the square of the correlation coefficient, or r^2, are also found through:

$$s_{yx} = \sqrt{\frac{\sum_{i=1}^{N} (Y_i - Y_{ci})^2}{N-2}} \tag{17}$$

$$r^2 = \frac{s_{XY}^2}{s_{XX} s_{XY}} \tag{18}$$

where s_{XX} is defined by Figliola as

$$s_{XX} = N \sum_{i=1}^{N} X_i^2 - (\sum_{i=1}^{N} X_i)^2 \tag{19}$$

Appendix B lists values for dynamic stiffness as well as their standard deviations and their r^2 values. Dynamic stiffness, rotordynamic stiffness, damping, and mass are all presented as with their 95% confidence bounds.

SEAL GEOMETRY AND TESTING CONDITIONS

The pressure-dam seals feature three evenly spaced and sized pressure dams. The dams were designed as per geometric relations made by Nicholas [24]. The dam geometries are specified by three non-dimensional parameters; the recess axial length ($\bar{L_d}$), arc length ($\bar{\theta_d}$), and the step depth ($\bar{L_s}$). The nominal radial clearance of the seals was 0.127 mm (0.005 in), which was determined through measurements made on an ESP interstage seal.

Figure 12 illustrates the different pressure-dam seal geometry parameters. Note that, unlike the pressure-dam bearing of Figure 4, the inner diameter of the pressure-dam seal is void of axial feed-grooves. The smooth seal has a similar geometry, except that they do not exhibit any pressure-dams; they exhibit a constant inner diameter. For all intents and purposes, the term "clearance" will refer to the radial clearance of the seal lands, and 1X will refer to the nominal-clearance seals, versus 2X or double-clearance seals.

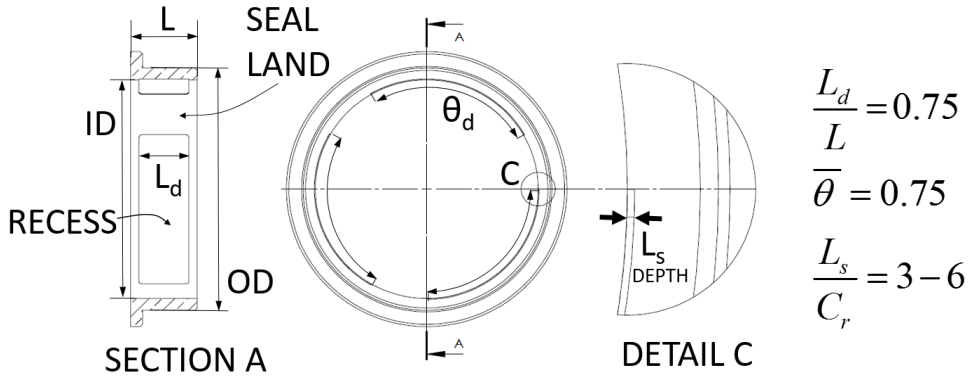

Figure 12: Pressure-dam seal insert with labeled geometry

Table 1 lists the dimensional seal geometries of this test program. The 1X pressure-dam seal has a recess depth $\bar{L_d}$ of 0.75 (26.3 mm), $\bar{L_s}$ of 4.0 (0.52 mm), and $\bar{\theta_d}$ of 0.75 (90°). The 2X pressure-dam seal has a clearance of 0.254 mm (0.01 in)

and, accordingly, a $\bar{L_s}$ value of 1.5 (0.38 mm), but has identical $\bar{L_d}$ and $\bar{\theta_d}$ to that of the 1X seals. The smooth seal is intended to be a baseline and has a constant 0.127 mm (0.005 in) clearance.

Table 1: Tabulated nominal seal geometries

Seal Geometry	C_r[mm(in)]	C_r/R[-]	L/D[-]	L_d[mm(in)]	L_s[mm(in)]
Pressure-dam seal, 1X[a]	0.109 (0.0043)	0.0021	0.3	26.3 (1.035)	0.51 (0.020)
Pressure-dam seal, 2X	0.226 (0.089)	0.0043	0.298	26.3 (1.035)	0.38 (0.015)
Smooth seal, 1X	0.109 (0.0043)	0.0021	0.3	-	-

[a] $\theta_d = 90°$for both pressure-dam seals

Two load orientations were used to test both the 1X and 2X clearance pressure-dam seals; load on land (LOL) and load on dam (LOD). These load orientations are located 60 degress apart and are illustrated by Figure 13.

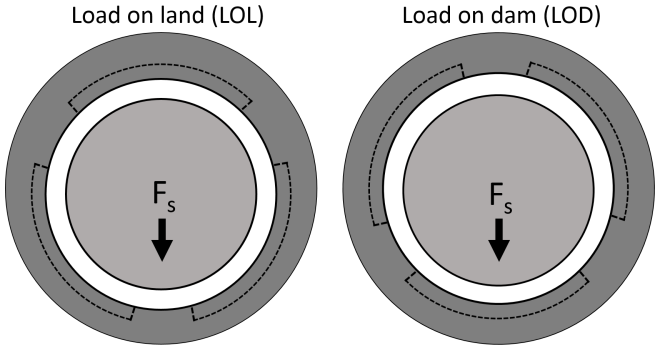

Figure 13: Illustration of LOL and LOD load configurations for the pressure dam seals

Statement of Work

The author is unaware of any literature for pressure-dam bearings with multiple dams and without a relief track. The same goes for annular seals with pressure-dams. This thesis will quantify the static and dynamic characteristics of pressure-dam seals in two load orientations and at two radial clearances. Results will assess the sensitivity of the pressure-dam seals to load direction, as well as determine if they offer enhanced stability over smooth annular seals.

Additionally, literature on smooth annular seals with low rotor speeds and ΔPs is limited. This work will provide smooth seal measurements versus predictions for leakage and rotordynamic coefficients. The predictions have been generated in XLAnSeal of the XLTRC^2 software suite.

The test conditions for each pair of seals include four speeds (1500, 3000, 4500, and 6000 rpm), four axial pressure drops (2.1, 4.1, 6.2, and 8.3 bar), and four eccentricity ratios (0.0, 0.4, 0.6, and 0.8). This amounts to 64 points per seal. The fluid is injected radially upstream of the seals with no circumferential pre-rotation.

STATIC RESULTS

The static results of the seal tests include volumetric seal leakage rate ($\dot{Q}$) and locus plots. The seal leakage is taken as the required oil flow-rate required to reach a target axial pressure drop, divided by two. The locus plots illustrate the motion of the seal center in the x and y directions. Recall that the applied static load is in the $-y$ direction. A static point is taken just before a dynamic point to record steady state measurements of seal leakage and static position, as well as oil inlet and outlet pressures and temperatures.

The measured radial clearance of the 1X clearance smooth and pressure-dam seals is 0.109 mm. This 14% reduction from the target value of 0.127 mm was due to a discrepancy in the test rotor diameter. This change is reflected for all 1X and 2X-clearance seals and in the calculations of eccentricity ratio as well as in the dynamic predictions of the following section. The tabulated measured cold and hot clearances of the pressure-dam and smooth seals are shown in Table 2; these are average radial clearance, measured during baseline testing and just before dynamic measurements. The reader should note that the clearance that is used to calculate eccentricity ratio is the cold clearance, although the hot and cold clearances of the smooth and pressure-dam seals vary only slightly ($\geq 0.5\%$).

During tests, the goal was to reach eccentricity ratios of 0.0, 0.4, 0.6, and 0.8. However, the pressure-dam seal exhibited sporadic seal motions under load. To avoid a "rubbing" incident, the seals were loaded out to "safe" eccentricity ratios. As a result, the eccentricity ratios in the following results vary.

Table 2: Average cold and hot radial seal clearance

Seal	Cold Clearance [mm (mils)]	Hot Clearance [mm (mils)]	% Difference [-]
1X Smooth	0.1094 (4.31)	0.1097 (4.32)	0.3
1X Pressure-dam	0.1092 (4.30)	0.1089 (4.29)	0.23
2X Pressure-dam	0.227 (8.94)	0.227 (8.97)	0.33

The flow in the seal annuli for both smooth and pressure-dam seals is decidedly laminar. The equations for calculating axial, circumferential, and vector Reynolds numbers are given in Appendix C.

Table 3: Largest Reynolds numbers for smooth and pressure-dam seals. Highest values for the 1X seals occur at 6000 RPM and 8.3 bar. The highest values for the 2X seals occur at 6000 RPM and 7.4 bar.

Seal	Circumferential	Axial	Vector
1X Smooth	143	12	144
1X Pressure-dam	710	141	719
2X Pressure-dam	690	245	673

The clearance used in the calculation of Reynolds numbers for the pressure-dam seal is the clearance in the recess, which is 5 times greater than on the land. All Reynolds numbers are well below 1000, indicating laminar flow for all test cases.

1X-Clearance Seals

Figure 14 shows $\dot{Q}$ for the smooth and LOD pressure-dam seal versus ϵ_o. As expected, the pressure-dam seal exhibits nearly identical leakage in the LOD and

LOL orientations; hence, only the $\dot{Q}$ of the pressure-dam seal in the LOD orientation is shown. Static results for all seals are tabulated in Appendix A.

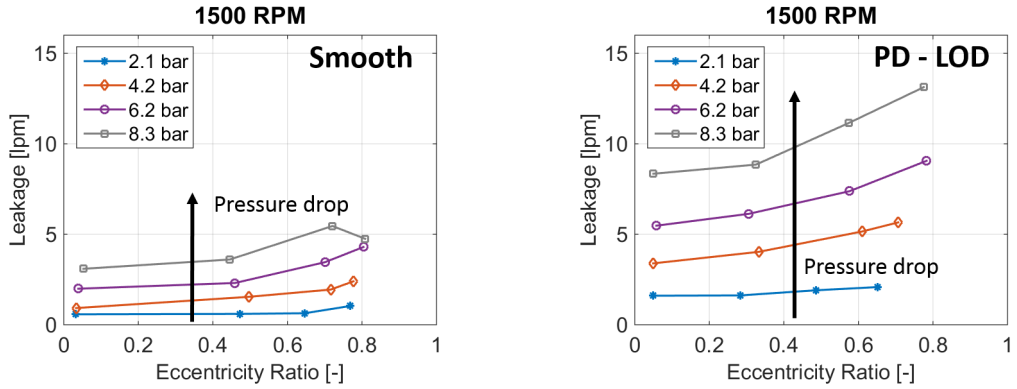

Figure 14: $\dot{Q}$ at 1500 RPM for (a) smooth and (b) LOD pressure-dam seals

The largest $\dot{Q}$ value of the pressure-dam seal (roughly 13 lpm) is nearly 2.5 times higher than the highest observed leakage of the smooth seal. In general, the pressure-dam seal leaks at least twice as much as the smooth seal at equal speeds and axial pressure drops. $\dot{Q}$ for all seals tested increases slightly with ϵ_o and is found to be a stronger function of ΔP than ω. These results agree with that of Childs et al. [21] for smooth seals.

Figure 15 shows the loci for the LOD pressure-dam seal at 2.1 bar and 1500 RPM. The applied static load is in the $-y$ direction (recall Figure 11). As ω increases, Figure 15a shows the seal attitude angle increasing beyond 90°, opposite to the direction of the applied load. When ω is held constant, the increased ΔP generally results in a lower attitude angle with increased eccentricity ratio.

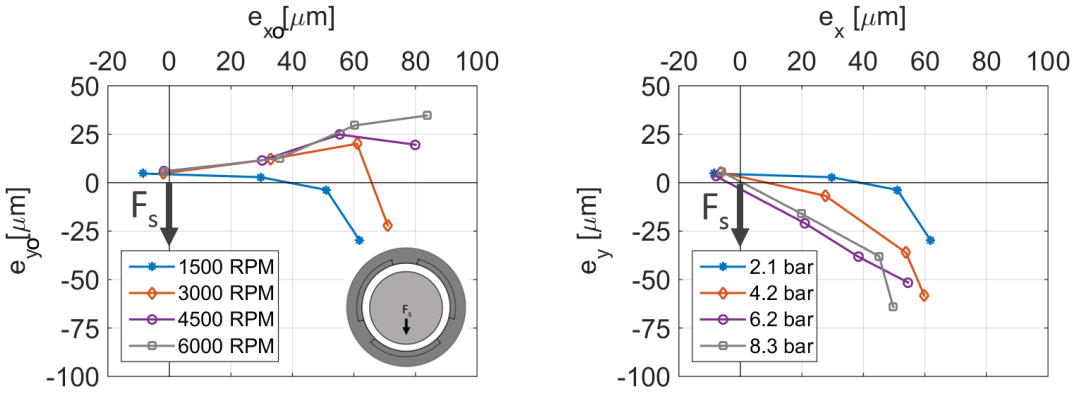

(a) (b)

Figure 15: Loci for LOD pressure-dam seal at (a) $\Delta P = 2.1$ bar with varying ω and (b) $\omega = 1500$ RPM with varying ΔP

Figure 16 shows the attitude angle, ϕ, versus ϵ_o for the LOD pressure-dam seals. Again, the seals exhibit attitude angles that systematically exceed 90°, and even get as high as 110°. In general, the motion of the pressure-dam seal in the LOD orientation is affected by both changes in ω and in ΔP.

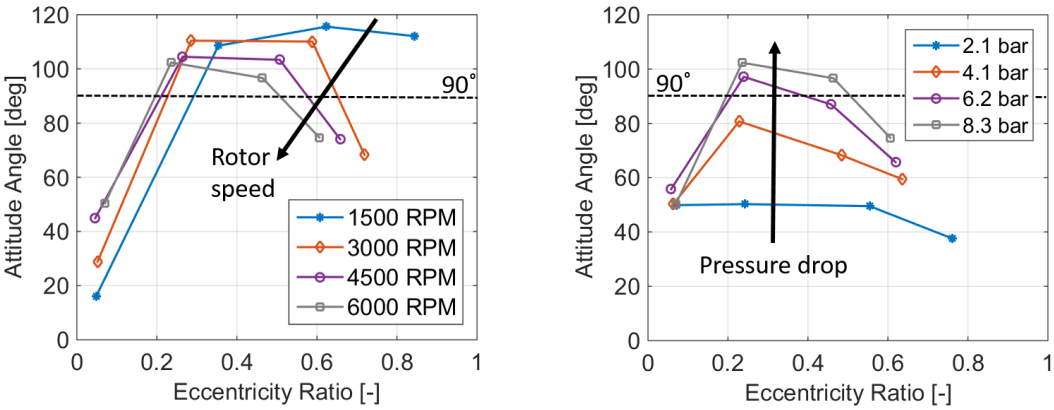

(a) (b)

Figure 16: Attitude angle (ϕ) for LOD pressure-dam seal at (a) $\Delta P = 8.3$ bar with varying ω and (b) $\omega = 6000$ RPM with varying ΔP

Figure 17 shows the loci of the LOL pressure-dam seal at 8.3 bar and 6000 RPM.

Note the indicated load direction. For a given load, the seal motion is nearly constant, regardless of increased ω or ΔP. The seal attitude angles are consistently between 65 and 75 degrees.

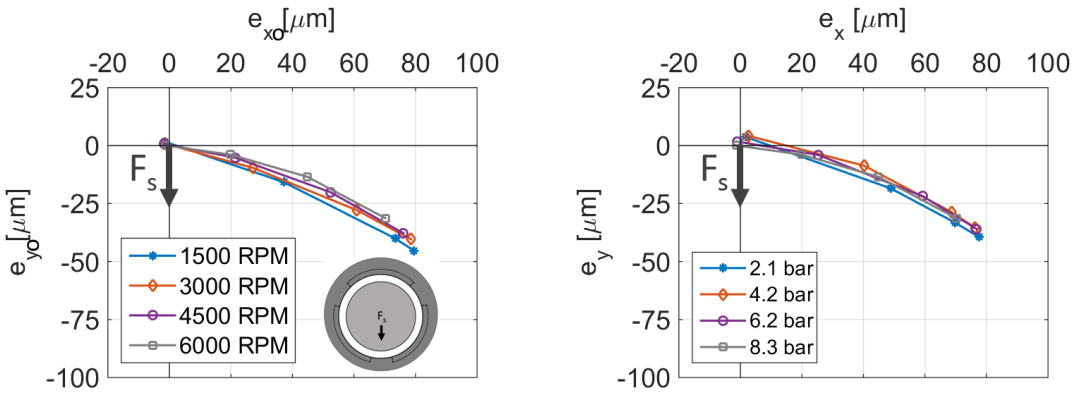

(a) **(b)**

Figure 17: Loci for LOL pressure-dam seal at (a) ΔP = 8.3 bar with varying ω and (b) ω = 6000 RPM with varying ΔP

Figure 18 shows the loci of the smooth seal at 2.1 bar and 1500 RPM.

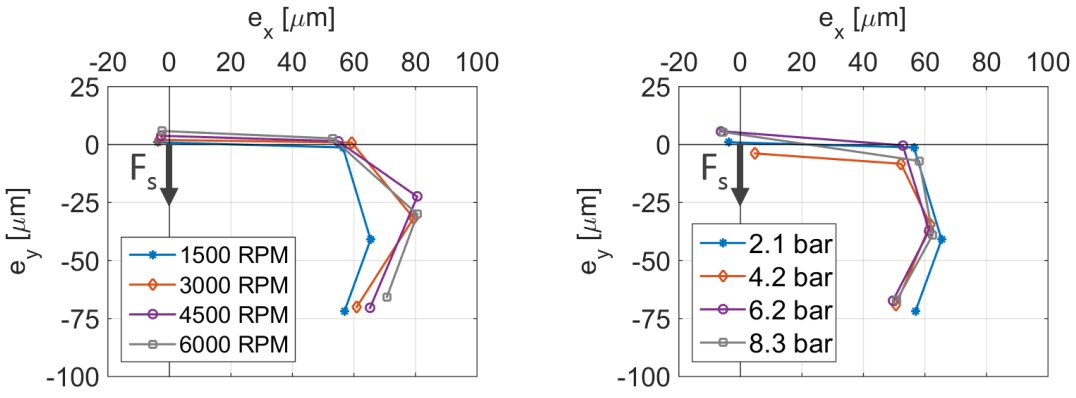

(a) **(b)**

Figure 18: Loci for smooth seal at (a) ΔP = 2.1 bar with varying ω and (b) ω = 1500 RPM with varying ΔP

The seal motion varies only slightly across ω and ΔPs. These results are consistent with smooth seal results from Childs et al. [21]. For all seals, major seal motion in a direction perpendicular to the applied static load signifies the expected presence of cross-coupled forces.

The following figure illustrates the disparity in static load capacity for the smooth and pressure-dam seals.

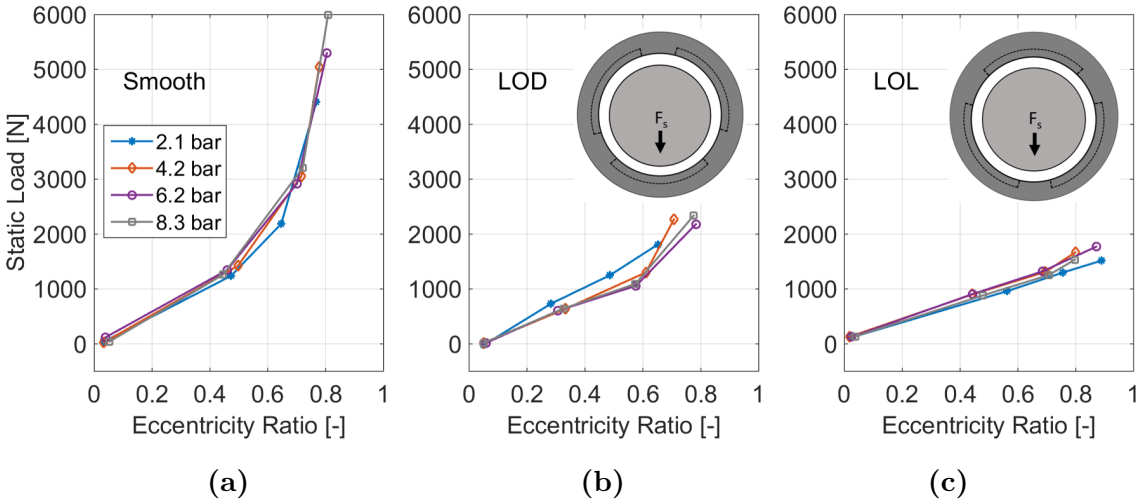

Figure 19: Applied static load versus ϵ_o for the smooth, LOD, and LOL pressure-dam seals at 1500 RPM

The applied static load required two reach $\epsilon_o = 0.8$ for the smooth seal is more than twice the load required for the pressure-dam seal in either load orientation. This trend is observed across all rotor speeds. The reader should note that the smooth seal curve shows an asymptotic behavior as the rotor is approaching the seal wall. The pressure-dam seals do not exhibit the same trend because their geometry is able to break up the circumferential fluid flow, effectively decreasing the hydrodynamic bearing effect.

2X-Clearance Seal

As previously mentioned, a pair of pressure-dam seals were manufactured to have a 2X-clearance. These seals could not react a significant static load in either the LOL or LOD orientation; therefore, data was only taken at zero-load. As a result, the data are plotted against ΔP (as opposed to ϵ_o), and these results only include 16 points per pair (as opposed the 64 points of the 1X seals).

Figure 20 shows $\dot{Q}$ of the 2X LOL pressure-dam seal and the 1X smooth and LOL pressure-dam seals. For brevity, only $\dot{Q}$ at 1500 and 6000 RPM are presented. $\dot{Q}$ is again seen only to be a function of ΔP and not ω. Note that the max attainable ΔP that the lubrication system could supply was 7.2 bar (105 psi) for the 2X-clearance seal.

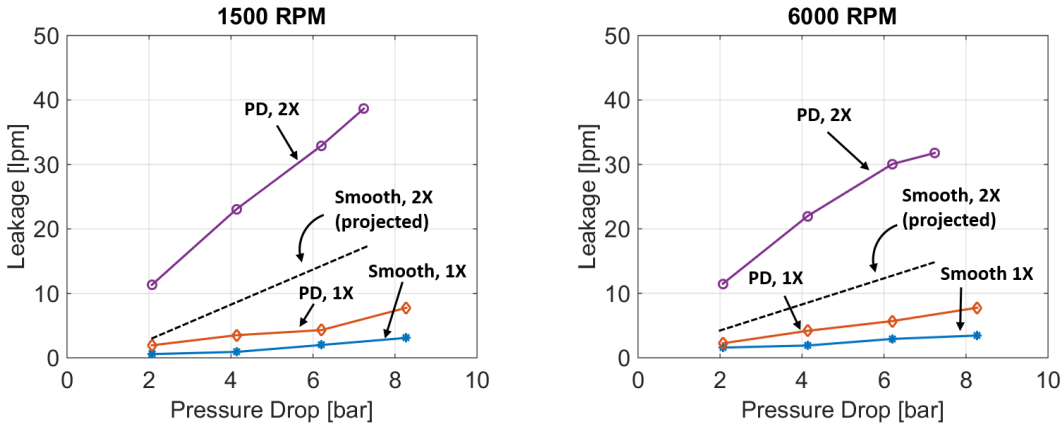

(a) (b)

Figure 20: Seal leakage at (a) 1500 and (b) 6000 RPM for 1X smooth, 2X smooth (projected), 1X LOL pressure-dam and 2X LOL pressure-dam seals

On average, $\dot{Q}$ of the 2X pressure-dam seal in the centered position is 460% larger than that of the 1X pressure-dam seal.

During testing, the 2X pressure-dam seal exhibited non-zero ϵ_o values, even with-

out an applied static load. Figure 21 shows the static position of the rotor in the seal clearance at all test speeds.

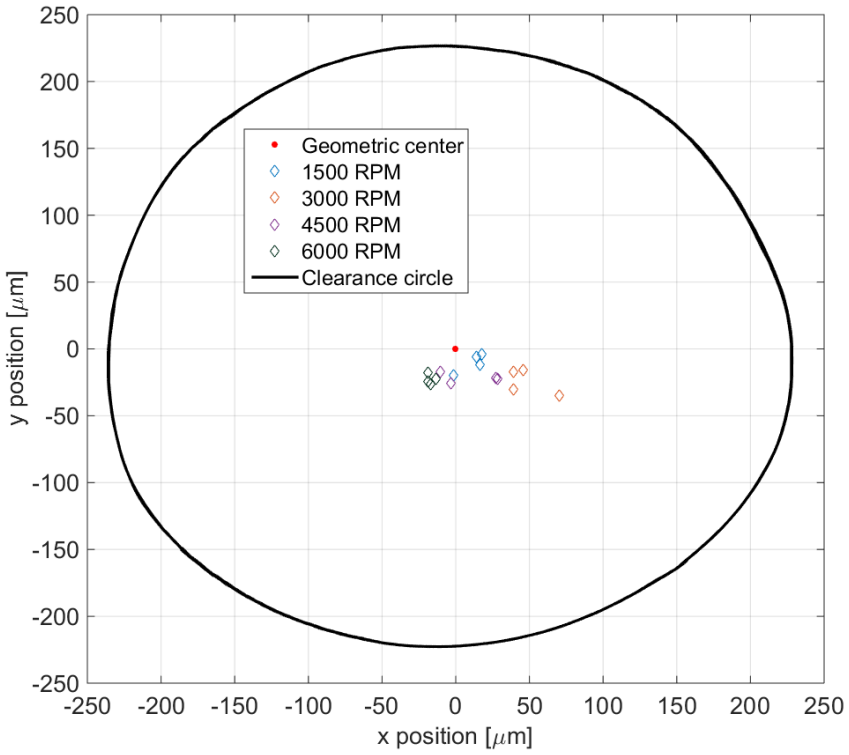

Figure 21: 2X pressure-dam seal clearance, geometric center, and static positions at all speeds

The method by which a seal is centered involves using feedback from the eddy-current probe system and using the hydraulic head unit to position the stator. Even when centered, the 2X pressure-dam seal tended to drift to an off-center position. While not a consistent trend, the seal exhibited large static eccentricity ratios and negative attitude angles while unloaded, as shown in Figure 21.

DYNAMIC RESULTS

This section outlines the dynamic results for selected seal tests. 1X pressure-dam seal rotordynamic coefficients are presented first, with comparisons of LOD to LOL orientation. These results are followed by a comparison of rotordynamic coefficients for 1X and 2X pressure-dam seals. Dynamic results for the 1X pressure-dam seal are also compared to that of the smooth seal. Lastly, predictions for smooth seal $\dot{Q}$ and rotordynamic coefficients are presented versus the measured values.

Before any lubricant is introduced to the test rig, the baseline dynamic stiffness of the "dry" rig is measured. This facilitates a data reduction that results in only the dynamic stiffness of the fluid film. Figure 22 shows the real part of $\boldsymbol{H_{ij}}$ for smooth seal at 6000 RPM, 2.1 bar ΔP, and $\epsilon_o = 0.7$. Note the smallness of the baseline measurement, which is also shown.

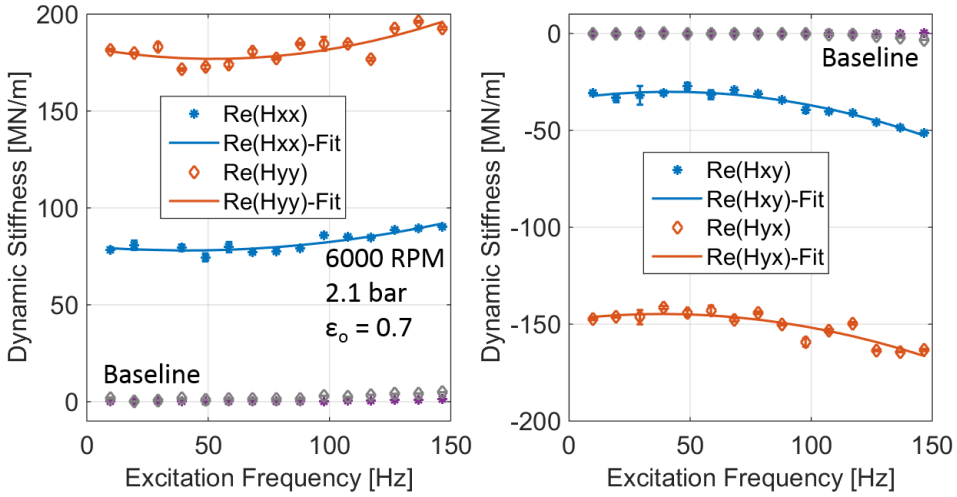

Figure 22: Real part of $\boldsymbol{H_{ij}}$ for a smooth seal baseline point and a test point at 6000 RPM, 2.1 bar, and $\epsilon_o = 0.70$

Dynamic stiffness is measured up to a nominal frequency of 150 Hz, corresponding to ω = 9000 RPM. Recall that stiffness and virtual mass are derived from the y-

intercept and slope of the real part of the dynamic stiffness, respectively. Figure 23 shows the real part of the dynamic stiffness for the LOD pressure-dam seal at 6000 RPM, 2.1 bar, and an eccentricity ratio of 0.74. Note that the y-intercepts of Figure 23 are markedly dissimilar to that of Figure 22. This is discussed further in the proceeding section.

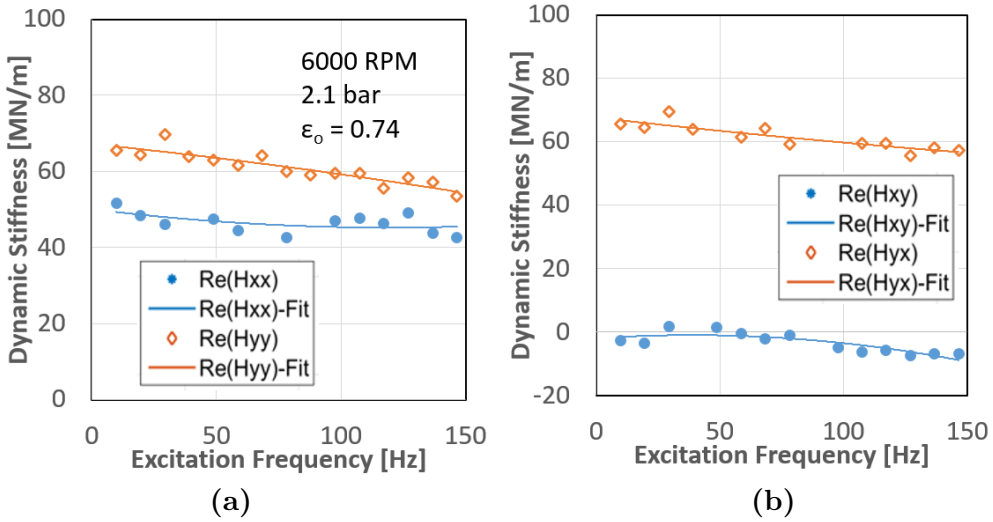

Figure 23: Real part of H_{ij} for a pressure-dam seal in the LOD orientation at 6000 RPM, 2.1 bar, and $\epsilon_o = 0.78$

Figure 24 shows the imaginary part of the dynamic stiffness for the same test point as Figure 22, as well as the imaginary part of the baseline. Recall that the damping coefficients come from the slope of the imaginary part of the dynamic stiffness.

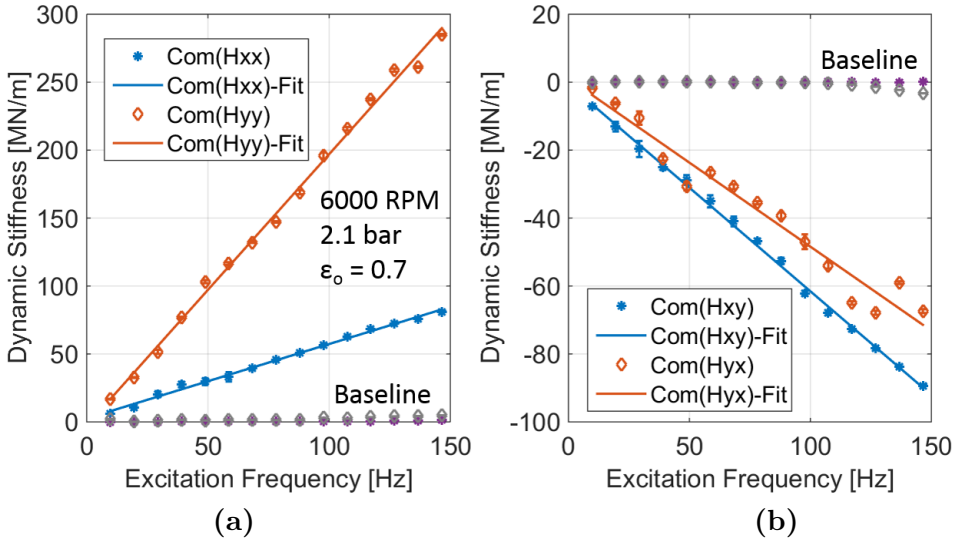

Figure 24: Imaginary part of H_{ij} for a smooth seal baseline point and a test point at 6000 RPM, 2.1 bar, and 0.7 eccentricity ratio

Results for rotordynamic stiffness, damping, and virtual mass are presented with their 95% confidence interval, which is arrived at through a linear least squares regression, detailed in Eqs.(14)-(19). A large confidence interval indicates a poor correlation between the measured dynamic stiffness and the curve fit. This can be the case for seals with low stiffness, as their confidence intervals can be as large as the measured values. Large confidence intervals, however, do not indicate poor repeatability, they suggest poorly curve-fitted data.

Rotordynamic Coefficients: 1X-Clearance Pressure-dam Seal

Rotordynamic coefficients for the 1X pressure-dam seal are presented versus ϵ_o at a fixed ΔP and varied ω or at a fixed ω and varied ΔP. In most cases, the rotordynamic coefficients of the pressure-dam seal vary with both ΔP and ω, but typically the correlation is stronger with ω. All rotordynamic coefficients are tabulated in Appendix B.

Figure 25 shows K_{xx} (unloaded direction) versus ϵ_o of the pressure-dam seal in

the LOD orientation. At $\Delta P = 2.1$ bar, K_{xx} is only slightly affected by the increase in ω. At $\Delta P = 8.3$ bar, the effect is more pronounced and the stiffness coefficients go from negative values at 1500 and 3000 RPM to all positive values at 4500 and 6000 RPM.

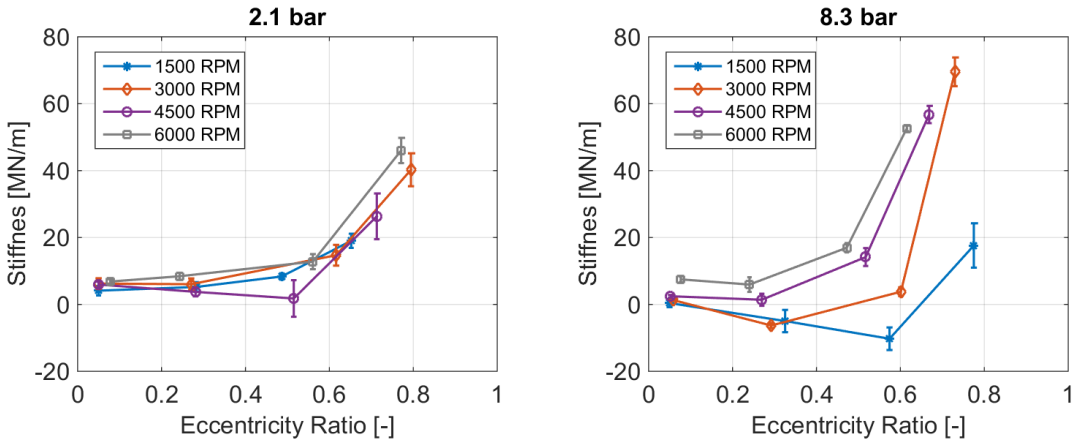

(a) **(b)**

Figure 25: K_{xx} (unloaded direction) vs. ϵ_o of the LOD pressure-dam seal at (a) 2.1 bar and (b) 8.3 bar

Figure 26 shows that the effect of ω on K_{yy} (loaded direction) is more pronounced at ΔP = 2.1 bar than at 8.3 bar. While the trend is not consistent, the peak direct stiffness at 2.1 bar is 64 MN/m, versus 19.5 MN/m at 8.3 bar.

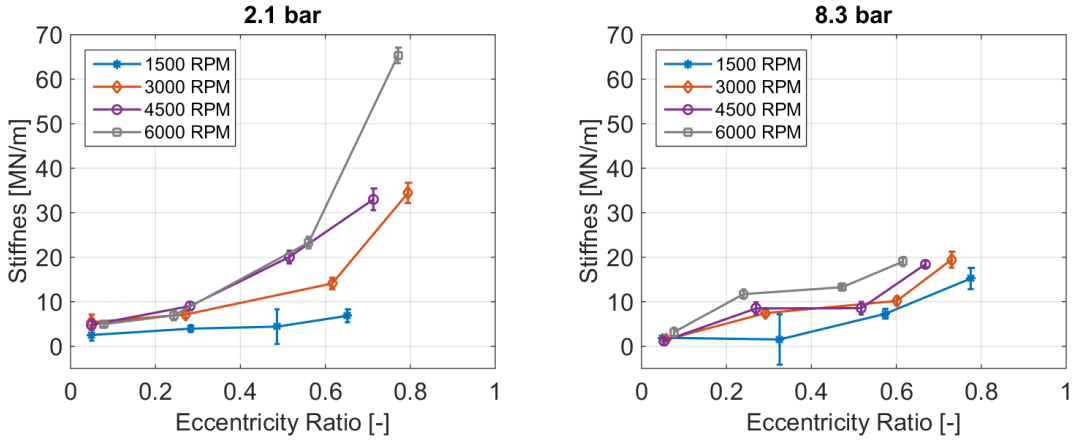

(a) **(b)**

Figure 26: K_{yy} (loaded direction) vs. ϵ_o of the LOD pressure-dam seal at (a) 2.1 bar and (b) 8.3 bar

Figure 27 shows K_{xx} of the LOL pressure-dam seal. As observed in the LOD orientation, K_{xx} at $\Delta P = 2.1$ bar is affected only slightly by increased ω. The effect is more pronounced at $\Delta P = 8.3$ bar, where increased ω results in increased K_{xx} at lower ϵ_o. Unlike the LOD orientation, the LOL pressure-dam seal also shows stronger influence of ΔP on K_{xx}, as shown in Figure 27c.

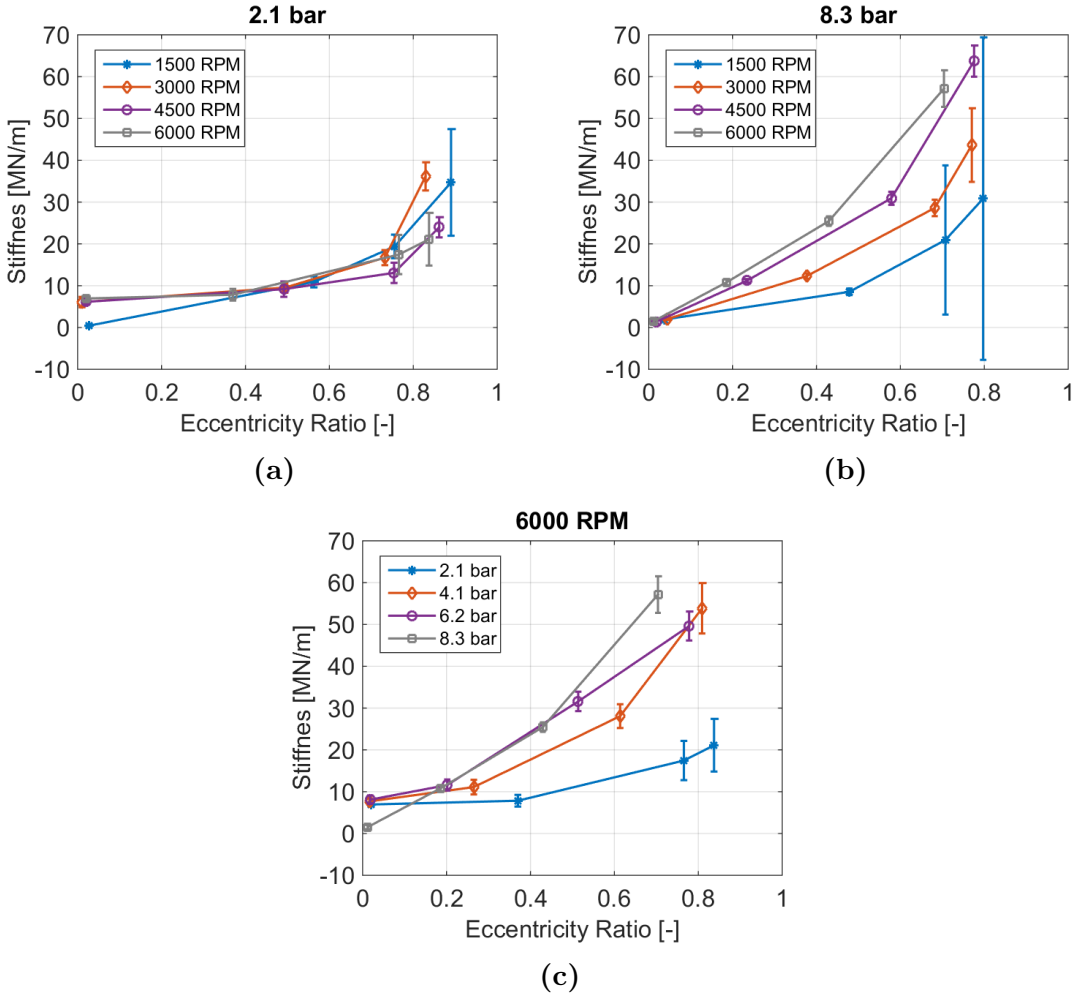

Figure 27: K_{xx} (unloaded direction) vs. ϵ_o of the LOL pressure-dam seal at (a) 2.1 bar, (b) 8.3 bar, and (c) 6000 RPM

43% of the K_{yy} values of the LOL pressure-dam seal are negative (versus 10% in the LOD orientation).

Figure 28 shows K_{yy} becoming negative as ΔP increases and ω is held constant. When ΔP is held constant, K_{yy} increases with increasing ω. These trends are seen across all speeds and pressure drops. The author theorized that the flow in the recess may have been transitional or turbulent, causing the rotor to be 'sucked' onto the seal wall. However, this was not confirmed and there is no indication that the flow Reynolds numbers are high enough to cause this.

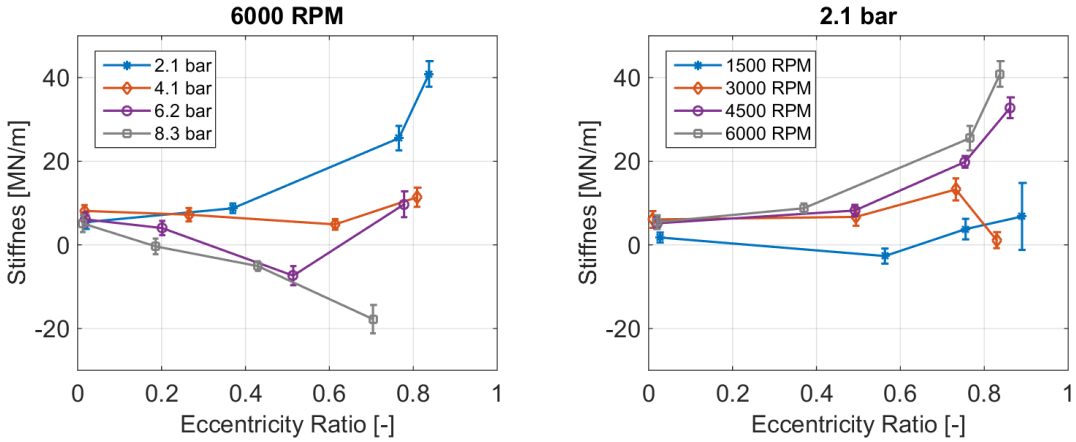

(a) (b)

Figure 28: K_{yy} (loaded direction) vs. ϵ_o of the LOL pressure-dam seal at (a) 4500 RPM and (b) 2.1 bar

Results for the pressure-dam seal do not exhibit K_{xx} and K_{yy} values that indicate whether the LOD or LOL orientation is superior; however, the significant number of negative stiffness coefficients show that the seal centering forces are in fact sensitive to load direction.

Figure 29 shows K_{xy} and K_{yx} of the LOD pressure dam seal at 6000 RPM and 2.1 bar. $|K_{xy}|$ and $|K_{yx}|$ do not change markedly for increases in ΔP or ω. At low ϵ_o, $K_{yx} = -K_{xy}$. For enhanced stability, they should have the same sign. This is consistently not the case, indicating that they are destabilizing.

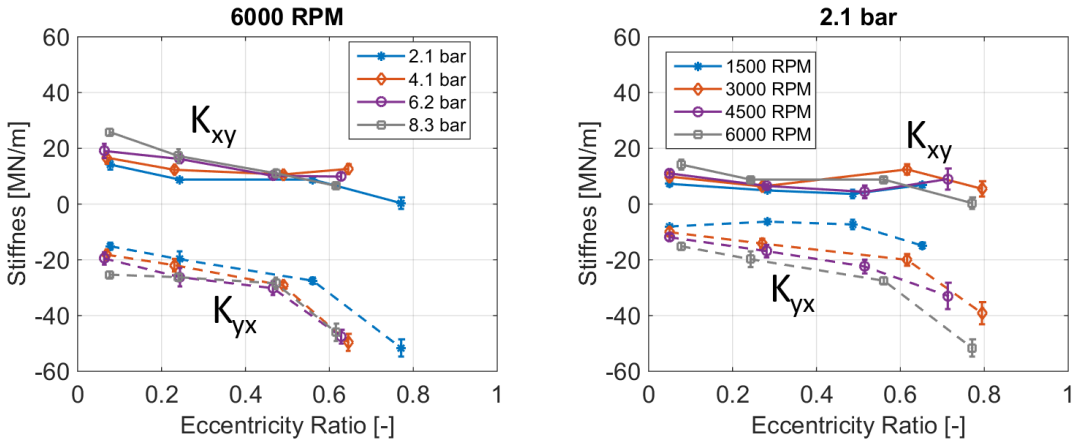

Figure 29: K_{yx} and K_{yx} vs. ϵ_o of the LOD pressure-dam seal at (a) 6000 RPM and (b) 2.1 bar

Figure 30 shows K_{xy} and K_{yx} of the LOL pressure-dam seal at 1500 and 6000 RPM. At 1500 RPM, changes in ΔP only change K_{xy} and K_{yx} at $\epsilon_o > 0.7$. At 6000 RPM, the changes take effect at lower ϵ_o values and are more pronounced as ϵ_o increases. Note that K_{xy} and K_{yx} are similar in magnitude and opposite in sign.

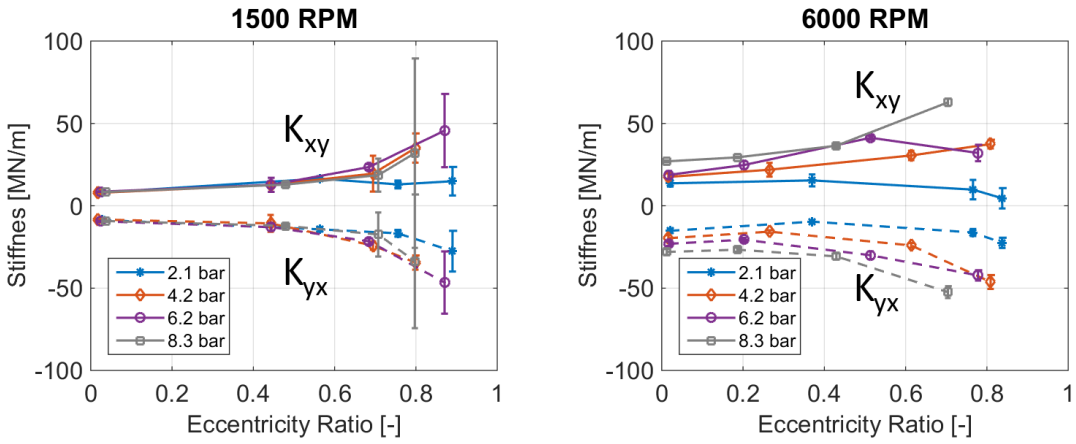

Figure 30: K_{xy} and K_{yx} vs. ϵ_o for the LOL pressure-dam seal at (a) 1500 RPM and (b) 6000 RPM

Note that K_{xy} and K_{yx} for both LOD and LOL pressure-dam seal are of the same magnitude as K_{xx} and K_{yy}.

Figure 31 shows C_{xx} of the LOD pressure-dam seal as a function of both ω and ΔP. At 1500 RPM, the trends are sporadic; at 8.3 bar, C_{xx} decreases with increases in ω.

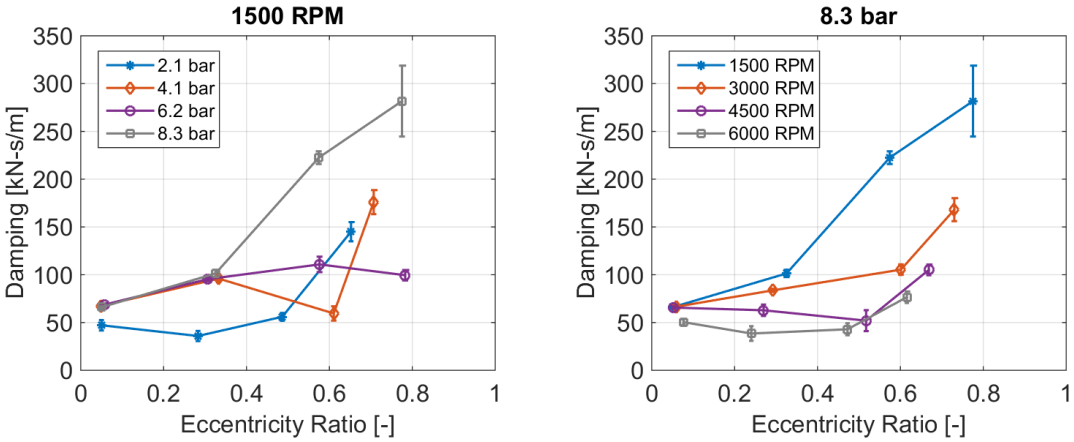

Figure 31: C_{xx} vs. ϵ_o for the LOD pressure-dam seal at (a) 1500 RPM and (b) 8.3 bar

As shown in Figure 32, C_{yy} exhibits no clear trends for varied ω or ΔP. At ΔP = 2.1 bar, C_{yy} varies slightly across ω values but is a strong function of ϵ_o. As ΔP increases, the trend is less apparent.

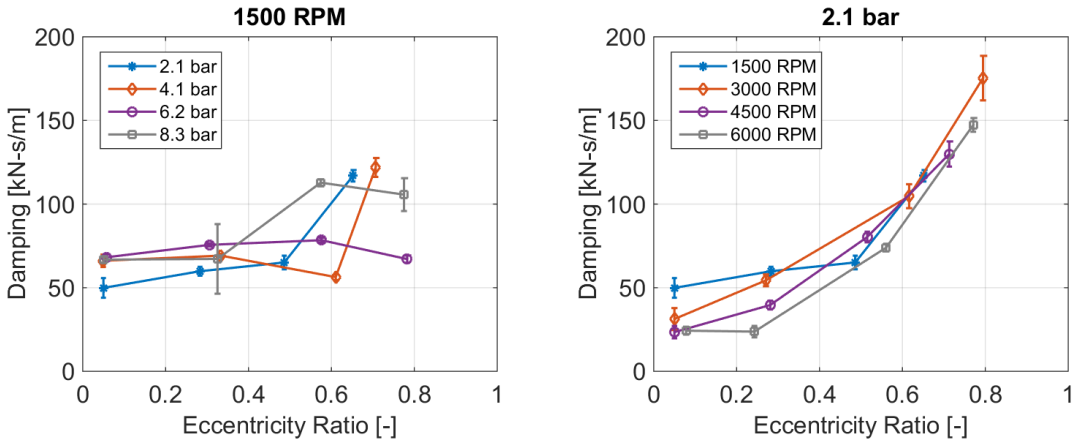

(a) (b)

Figure 32: C_{yy} vs. ϵ_o for the LOD pressure-dam seal at (a) 1500 RPM and (b) 2.1 bar

Figure 33 shows C_{xx} of the LOL pressure-dam seal at 6000 RPM and $\Delta P = 4.1$ bar. As in the LOD orientation, C_{xx} is influenced by both changes in ΔP and ω. Figure 33b shows that, at 1500 and 3000 RPM, C_{xx} is also a strong function of ϵ_o.

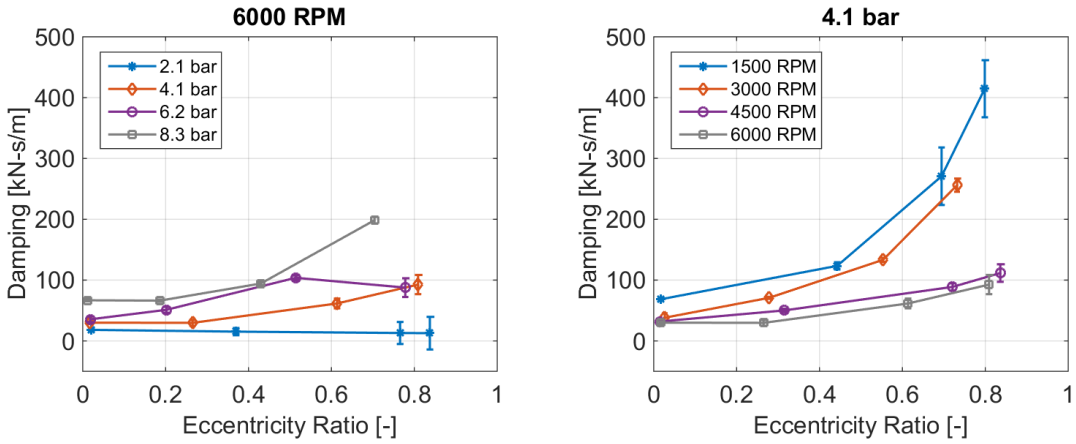

(a) (b)

Figure 33: C_{xx} vs. ϵ_o for the LOL pressure-dam seal at (a) 6000 RPM and (b) 4.2 bar

The same trends exist for C_{yy} of the LOL pressure-dam seal; these results are not

shown here but are included in Appendix B. As observed for stiffness coefficients, there is no clear advantage to either the LOD or LOL orientation for damping coefficients.

Nearly all C_{xy} and C_{yx} values of the LOD pressure-dam seal are found to be isotropic ($C_{xy} \approx C_{yx}$). Therefore, only C_{xy} is presented. As seen in Figure 34, C_{xy} is more strongly influenced by ΔP than by ω. At $\omega = 1500$ RPM, C_{xy} transitions from all negative at 2.1 bar to all positive at 8.3 bar.

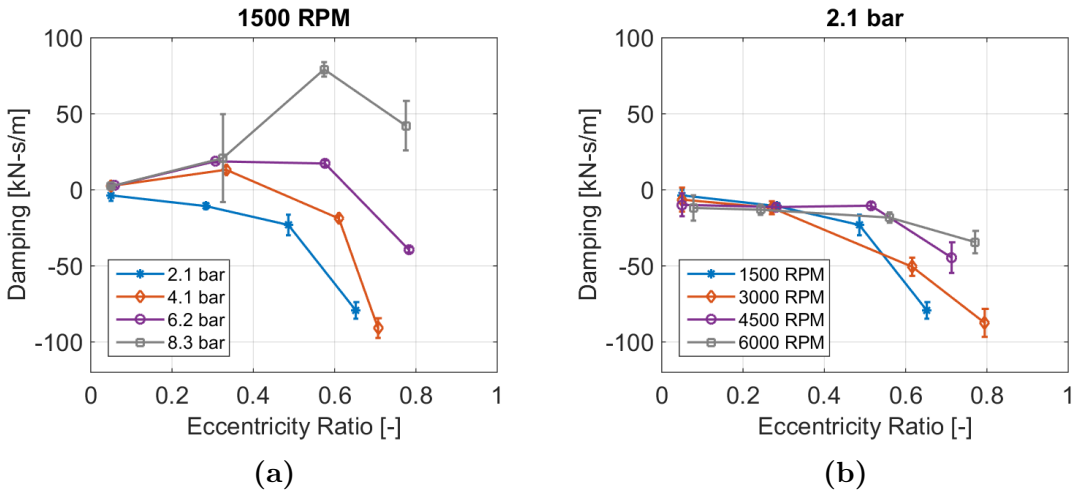

Figure 34: C_{xy} vs. ϵ_o for the LOD pressure-dam seal at (a) 1500 RPM and (b) 2.1 bar

C_{xy} and C_{yx} of the LOL pressure-dam seal had poor repeatability and are not shown. Trends are present in the data; however, when the error bars of the coefficients are considered, the data are inconclusive.

M_{xx} of the LOD pressure-dam seal exhibits poor repeatability and is excluded. Figure 35 shows M_{yy} of the LOD pressure-dam seal at 6000 RPM and 2.1 bar. Values range between -20 and 20 kilograms, regardless of speed or pressure drop. At ΔP = 2.1 bar, some M_{yy} values are negative in the centered position and become positive with increased ϵ_o. A negative virtual mass term indicates increasing dynamic stiffness

with excitation frequency. This occurs at all speeds except 6000 RPM. The author has no explanation for negative virtual mass terms.

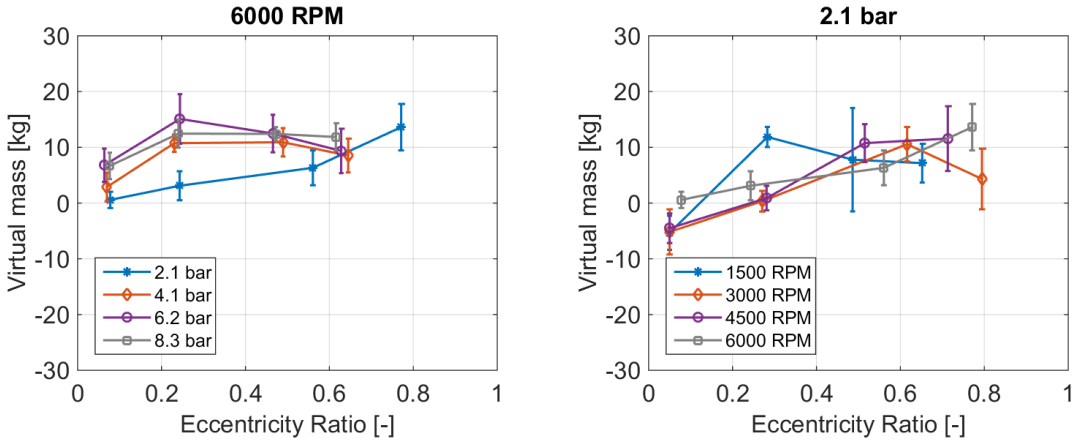

Figure 35: M_{yy} vs. ϵ_o for the LOD pressure-dam seal at (a) 6000 RPM and (b) 2.1 bar

Figures 36 and 37 show M_{xx} of the LOL pressure-dam seal at ΔP = 8.3 bar and ω = 6000 RPM, respectively. The call-out section of Figure 36 shows that, for eccentricities out to 0.6, virtual mass consistently decreases with increased ω. At low rotor speeds (1500, 3000 RPM), there is consistently an out-lying point at large eccentricity ratios. The data shows no consistent trend for fixed ω and varied ΔP.

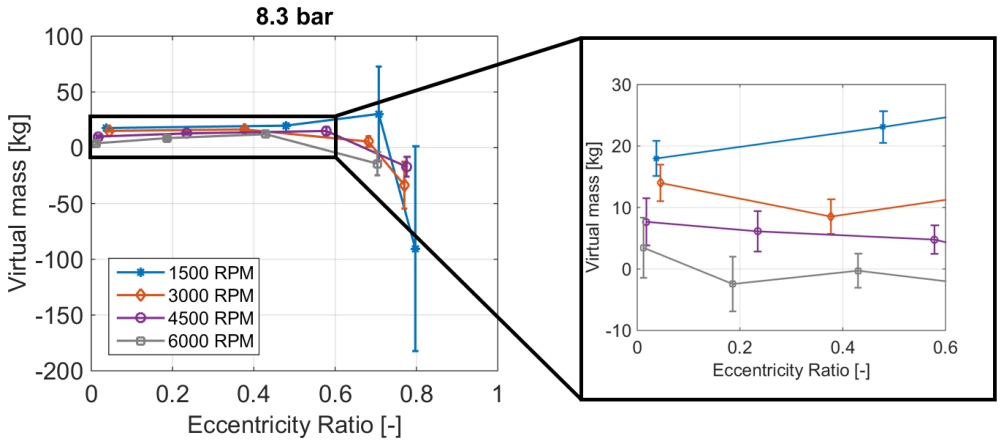

Figure 36: M_{xx} **vs.** ϵ_o **for the LOL pressure-dam seal at 8.3 bar**

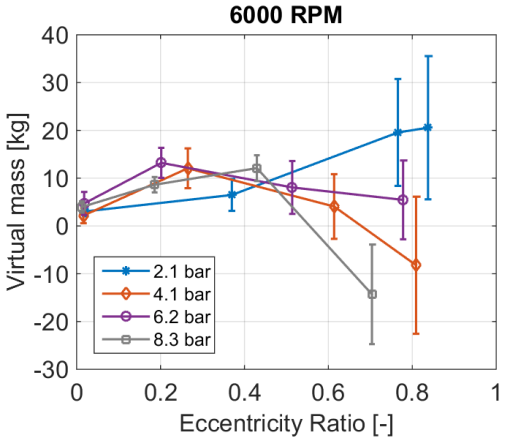

Figure 37: M_{xx} **vs.** ϵ_o **for the LOL pressure-dam seal at 6000 RPM**

The same trends are observed in M_{yy} as for M_{xx}, which are not shown here but can be found in Appendix B.

M_{xy} and M_{yx} of the LOD pressure-dam seal are shown in Figure 38. In the centered position, $M_{xy} \approx -M_{yx}$. Figures 38a and 38b show that, as ϵ_o increases, M_{xy} and M_{yx} sporadically have the same sign and, in some cases, differ by less than a kilogram. At the highest rotor speed, $M_{xy} = -M_{yx}$, implying that dynamic-stiffness is increasing with excitation frequency for one, decreasing with excitation frequency for the other, and overall stability is worsening.

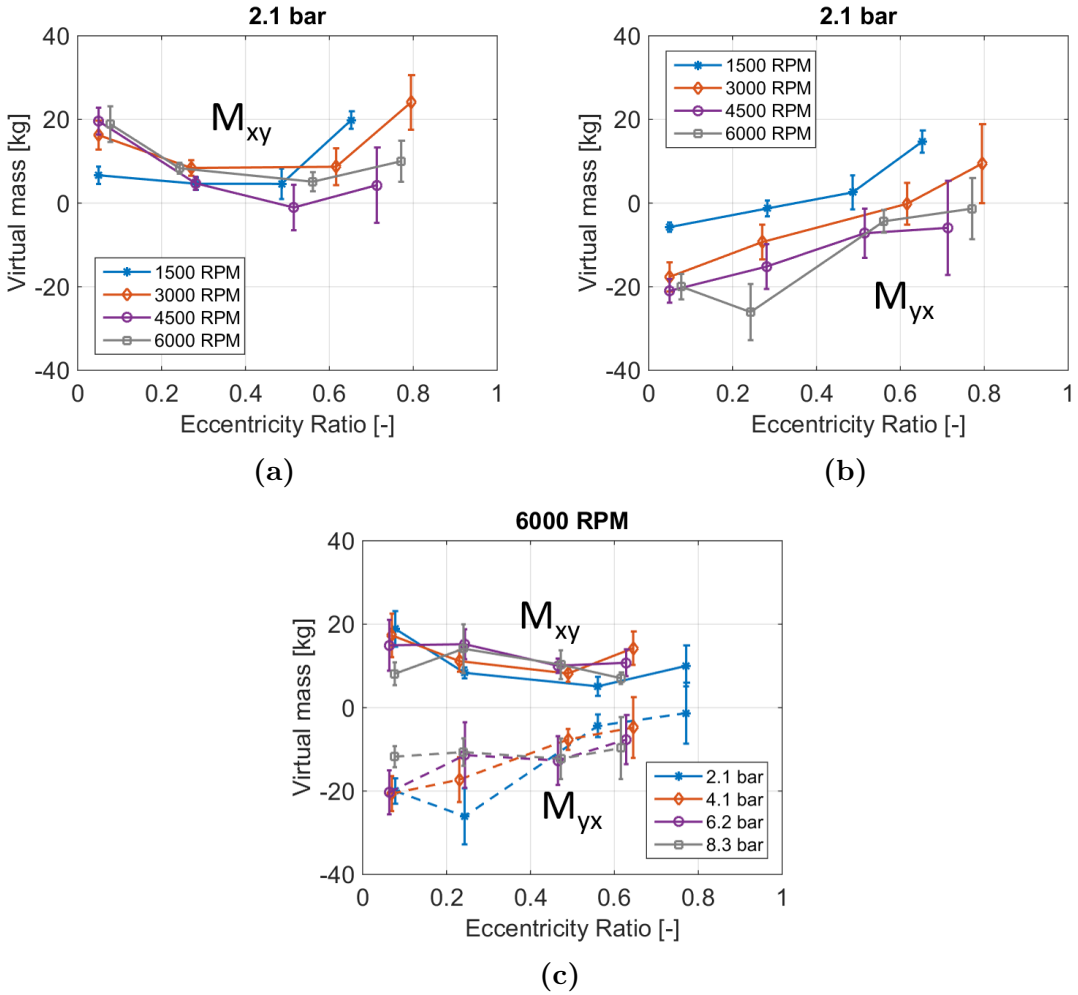

Figure 38: M_{xy} and M_{yx} vs. ϵ_o for the LOD pressure-dam seal at (a),(b) 2.1 bar and (c) 6000 RPM

Figure 39 shows the M_{xy} and M_{yx} values of the LOL pressure-dam seal at $\Delta P =$

2.1 bar. Like the M_{xy} and M_{yx} values of the LOD seal, $M_{xy} \approx -M_{yx}$ at low ϵ_o. At large ϵ_o values, the coefficients sporadically are the same sign, indicating enhanced stability.

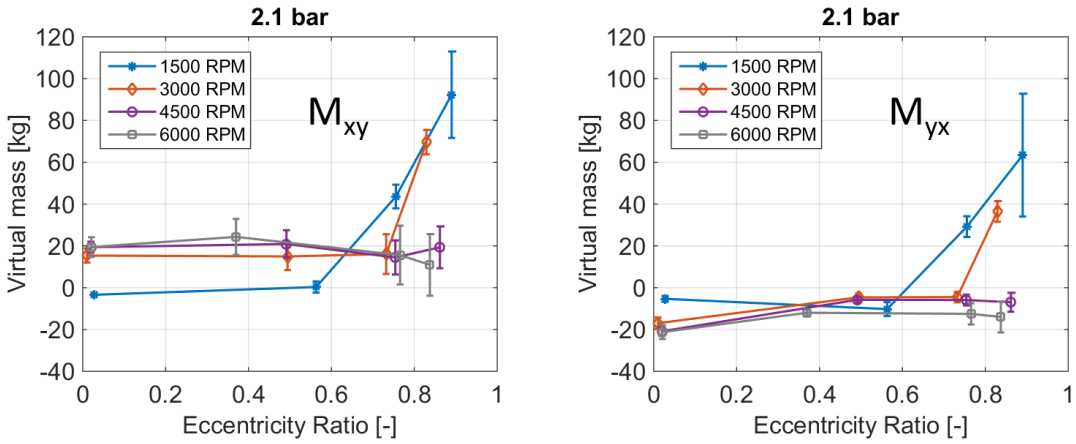

(a) (b)

Figure 39: (a) M_{xy} and (b) M_{yx} vs. ϵ_o for the LOL pressure-dam seal at 2.1 bar

Rotordynamic Coefficients: 2X-Clearance Pressure-dam Seal

A pair of pressure-dam seals with a 2X-clearance were also tested in the LOD and LOL orientations. This study aimed to assess the ability of the pressure-dam seals to provide centering forces when their clearance had been artificially worn.

The seal did not have a static equilibrium position under an applied static load. As a result, the presented data points were all taken about the 'centered' position. However, Figure 21 showed that, even with the ability to center the stator about the rotor manually, the seals tended to approach an off-center equilibrium position. The maximum ΔP across the 2X pressure-dam seal was 7.4 bar, which was limited by the oil supply system of the test rig.

The direct stiffness coefficients of the 2X pressure-dam seal are found not to exceed 2 MN/m for either load orientation. Additionally, the repeatability of the measurements is poor, with error bars indicating that the actual values could be positive or negative. The repeatability of the cross-coupled stiffness coefficients is also found to be poor. As a result, direct and cross-coupled stiffness coefficients of the 2X pressure-dam seal are not presented, but can be found in Appendix B.

The damping coefficients in the loaded (C_{yy}) and unloaded (C_{xx}) directions are nearly identical; as a result, only C_{xx} is shown. Figure 40 shows C_{xx} as a function of ΔP for the 1X and 2X pressure-dam seals in the LOD orientation. Note that the 2X pressure-dam seal exhibits C_{xx} that varies only slightly with both ω and ΔP.

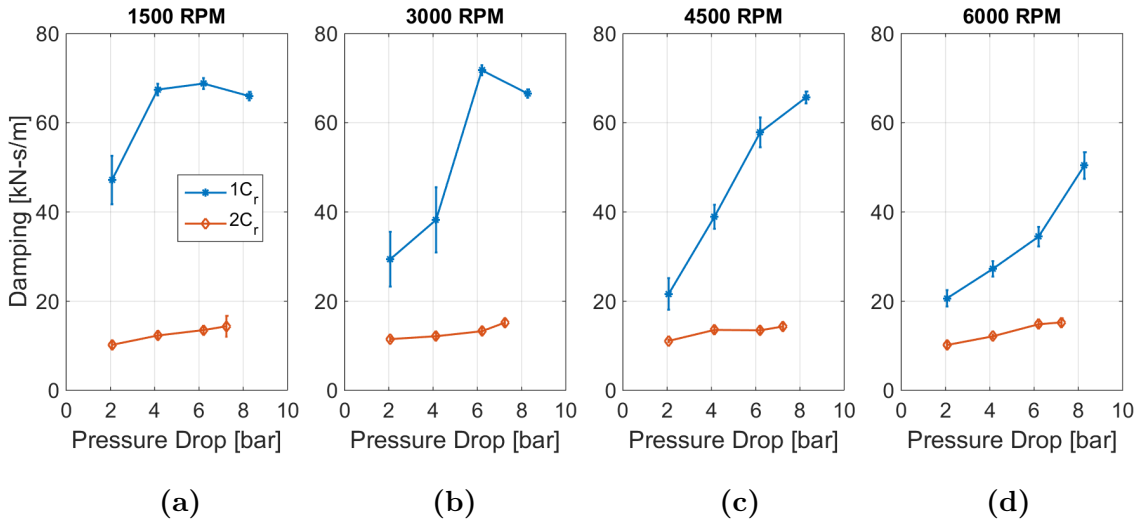

Figure 40: C_{xx} for the 1X and 2X pressure-dam seals in the LOD orientation with no applied static load (centered)

Figure 41 shows C_{xx} for the 1X and 2X pressure-dam seals in the LOL orientation. As ω increases, the differences between the 1X and 2X damping coefficients decreases. This reflects a decrease in the damping coefficients of the 1X pressure-dam seal. As observed in the LOD orientation, the damping coefficients of the 2X pressure-dam seal are nearly unchanged with increased ΔP and ω.

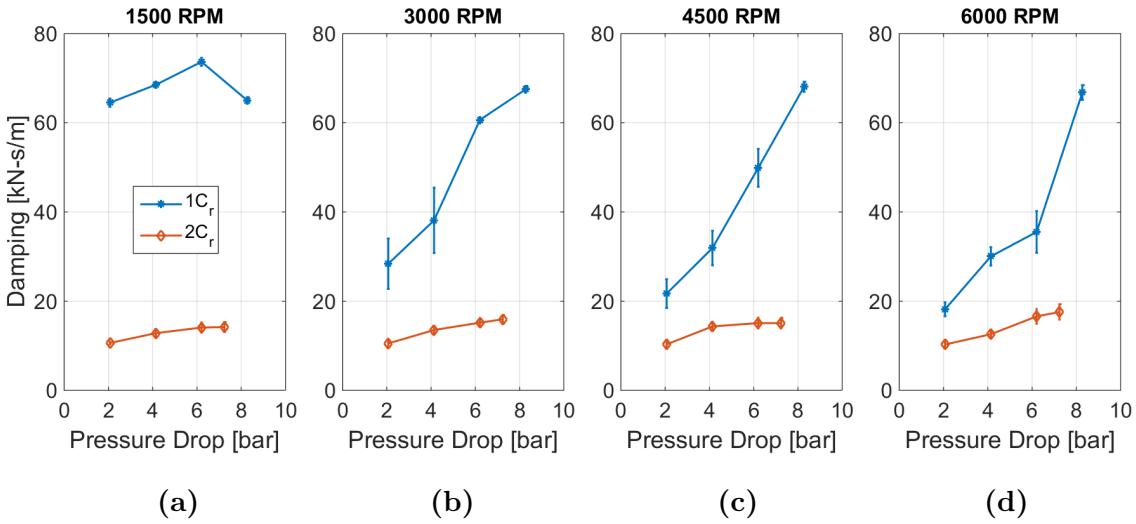

Figure 41: C_{xx} for the 1X and 2X pressure-dam seals in the LOL orientation with no applied static load (centered)

The initial finding that the 2X pressure-dam seal could not react a static load showed a significant disadvantage compared to smooth seals. Low stiffness coefficients and damping coefficients that are a fraction of the damping offered by the 1X pressure-dam seal shows that the seal does not retain its centering forces when its clearance is doubled.

Figure 42 shows M_{xx} versus ΔP for the 1X and 2X pressure-dam seals in the LOL orientation. M_{xx} for the 2X seal increases slightly with increasing ΔP, but overall becomes smaller with increased ω.

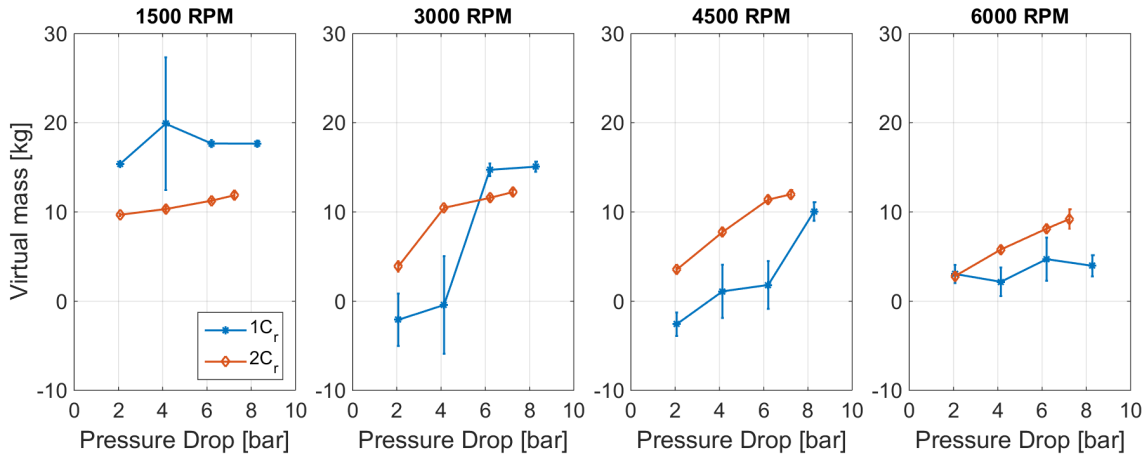

Figure 42: M_{xx} **versus axial pressure drop for the 1X and 2X pressure-dam seals in the LOL orientation with no applied static load**

Figure 43 shows that M_{yy} trends similarly to M_{xx} and is of the same magnitude. The values increase slightly with increased ΔP, but generally decrease as ω is increased.

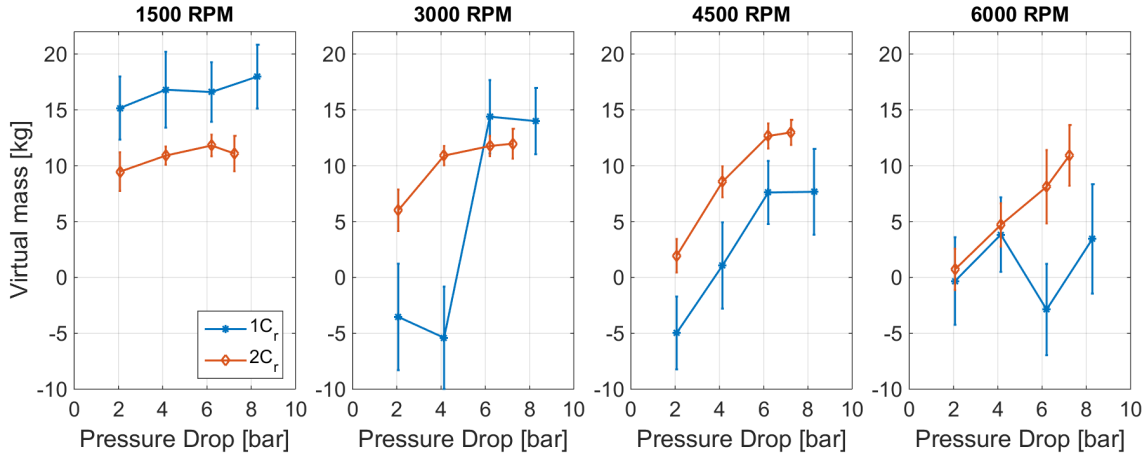

Figure 43: M_{yy} **versus axial pressure drop for the 1X and 2X-clearance pressure-dam seals in the LOL orientation with no applied static load**

M_{xx} and M_{yy} of the 2X LOD pressure-dam seal show very similar results to that of the 2X LOL pressure-dam seal. For brevity, those results are not presented here but are included in Appendix B.

Comparison of 1X Smooth and Pressure-dam Seals

This section compares WFR results for the 1X smooth and 1X pressure-dam seals of this test program. Recall that WFR is used to assess the stability characteristics of bearings and seals, and that a WFR at or close to zero is desirable. Literature has shown that smooth seals running on fluids with large viscosities in or near a centered position exhibit WFRs of 0.5 [1], [17]. To offer any improved stability, the pressure-dam seals should exhibit a WFR less than this. The means by which WFR is calculated is given by San Andrès [23] and accounts for significant cross-coupled virtual mass terms with similar magnitudes and opposite signs. This formulation is outlined in Appendix C.

Figure 44 shows the WFR for the smooth, LOD, and LOL pressure-dam seals at 1500 RPM. The smooth seal WFR varies little with changes in ΔP and consistently yield values of 0.5 out to $\epsilon_o \approx 0.7$. Both the LOD and LOL pressure-dam seals exhibit sporadic WFRs that are frequently greater than 0.5. The WFR of the smooth seal varies slightly with increased rotor speed and the LOD pressure-dam seal does not show any definite trends as rotor speed is increased.

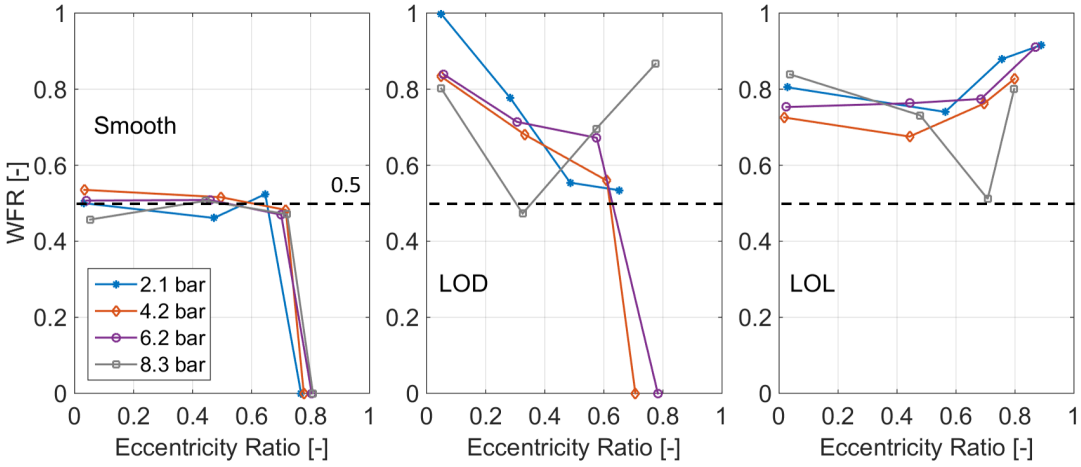

(a) (b) (c)

Figure 44: WFR versus ϵ_o for the smooth, LOD, and LOL pressure-dam seals at 1500 RPM

Figure 45 shows WFR of the LOL seal dropping slightly with increased ΔP and ω. These values are still consistently higher greater than 0.5.

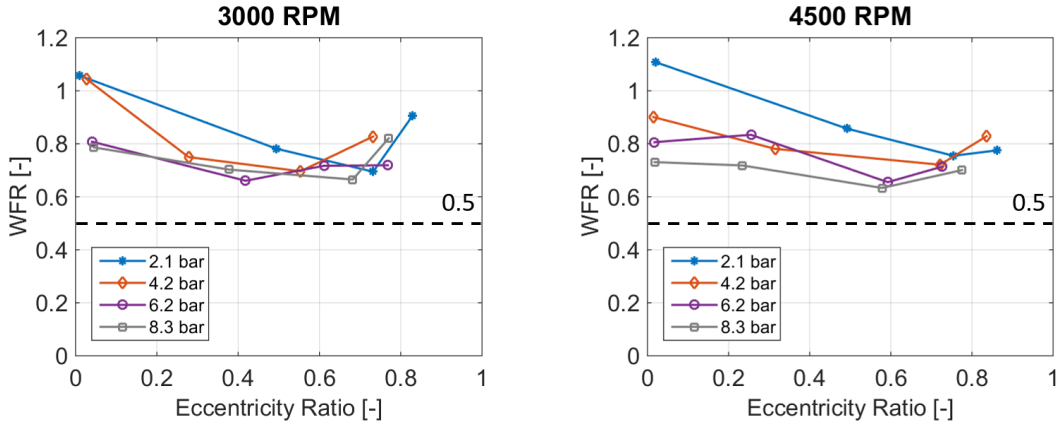

(a) (b)

Figure 45: WFR versus ϵ_o for the LOL pressure-dam seals at 3000 and 4500 RPM

Figure 46 shows the WFR of the smooth, LOD, and LOL pressure-dam seals at 6000 RPM. Again, the pressure-dam seal exhibits a WFR consistently greater than 0.5. Recall that the rotordynamic coefficients of the pressure-dam seal are load orientation-dependent. As a result, WFR is also load orientation-dependent.

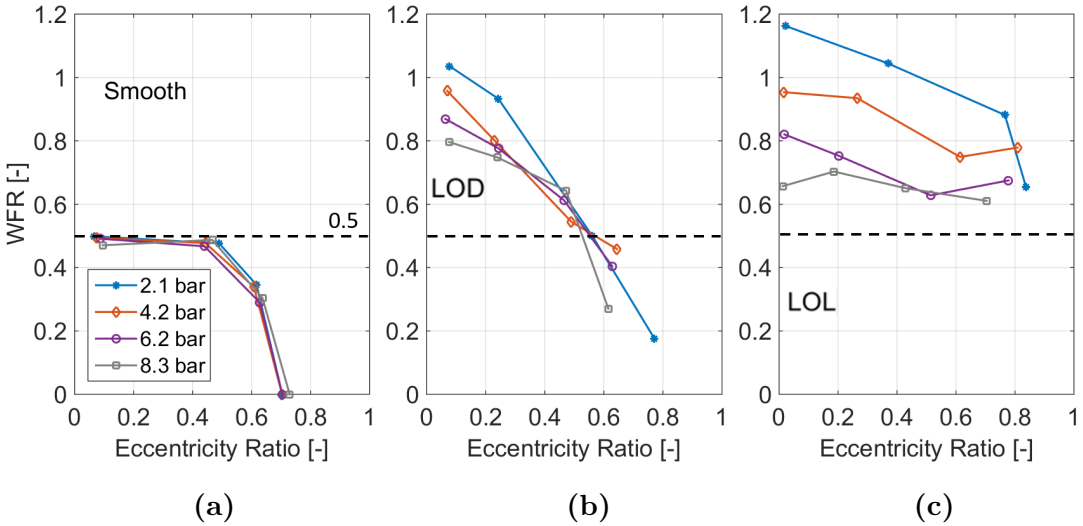

(a) **(b)** **(c)**

Figure 46: WFR versus ϵ_o for the smooth, LOD, and LOL pressure-dam seals at 6000 RPM

The WFR results show that the pressure-dam seal offers no advantage over the smooth seal and is a poor alternative, particularly for turbomachines where the load-direction is not fixed. In many cases, a rotor mounted on pressure-dam seals would become unstable very soon after crossing its first critical speed.

Comparison of Smooth Seal Results to XLAnSeal Predictions

Predictions for smooth seal $\dot{Q}$ and rotordynamic coefficients were made using XLAnSeal of the XLTRC^2 software suite. The code uses a bulk-flow version of the Navier-Stokes equations and accounts for convective and temporal acceleration terms. Hence, the code can predict not only stiffness and damping, also virtual mass. The code accepts seal static positions and performs a perturbation analysis that can be specified as either synchronous with rotor speed or non-synchronous, where excitation frequencies must be specified. The predictions from the synchronous solution agree well with the measured rotordynamic coefficients and are therefore presented in this section. The prescribed mesh density was set to 25x50 elements after a convergence study revealed only small deviations for larger mesh densities.

XLAnSeal outputs leakage in pounds per second. This value is converted to liters per minute using the fluid density, which is recalculated for each data point using the measured oil inlet temperature. Figure 47 shows the measured and predicted $\dot{Q}$ of the smooth seal at 1500 and 6000 RPM. The solid lines are measurements, and the dashed lines represent predictions. The software over-predicts leakage at 2.1 and 4.1 bar, and under-predicts at 6.2 and 8.3 bar. Overall agreement is good, as the predictions are within less than 1/2 liters per minute in all cases.

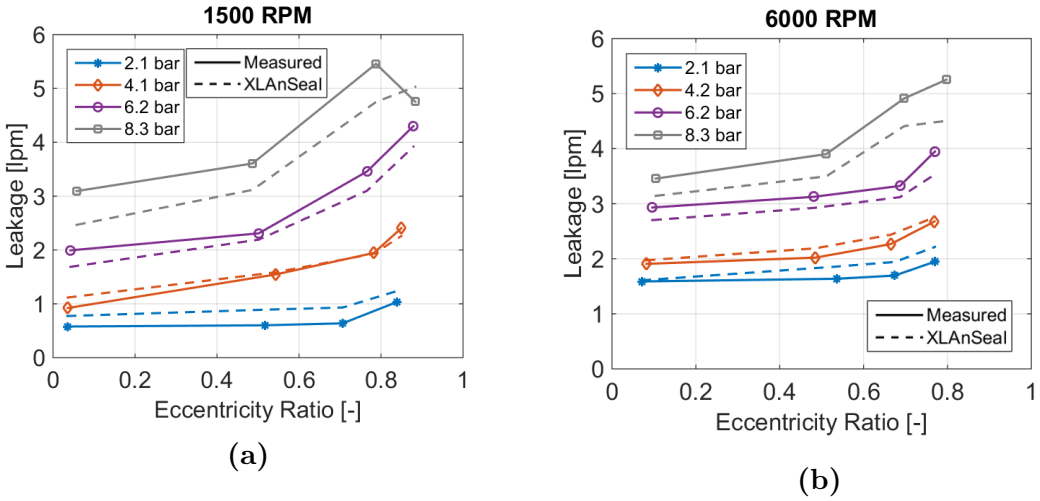

Figure 47: Smooth seal leakages at (a) 1500 RPM and (b) 6000 RPM

The following figures show measured and predicted rotordynamic coefficients of the smooth seal. All results are shown at $\omega = 3000$ RPM and $\Delta P = 2.1$ bar. These cases are the closest to operating conditions of pumps studied by Childs et al. [2]; the author has selected these cases to be concise. All measured rotordynamic coefficients are shown in Appendix B.

Before rotordynamic coefficients are presented, an incongruence in coordinate references is resolved. Figure 48 shows the transformation applied to XLAnSeal predictions that results in rotordynamic coefficients in the same coordinate system as the measured coefficients.

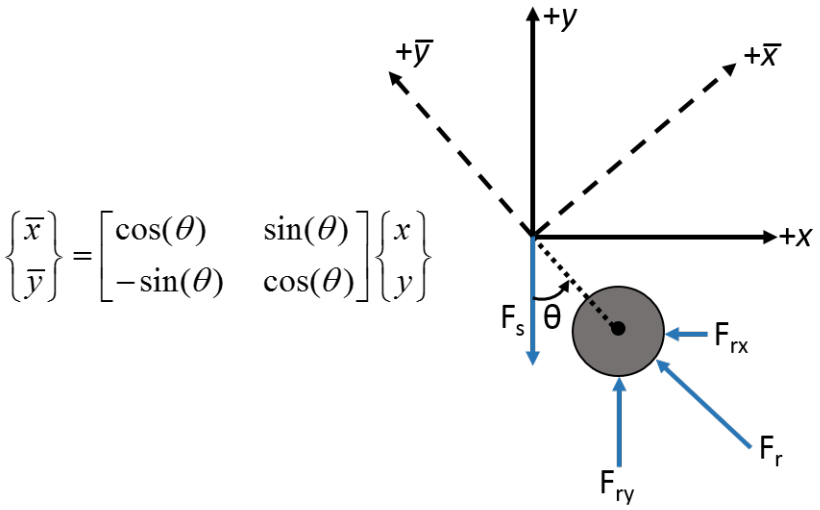

Figure 48: Coordinate transformation from presented coordinates to XLAnSeal coordinates

This incongruence arises because, in XLAnSeal, the rotor static position is user-specified, and the seal reaction forces in the $-x$ and y directions are predicted outputs. The angle between the resultant force, F_r, and the vertical y axis is used in a coordinate transformation from XLAnSeal into coordinates that match the test rig and the applied static load direction.

Figure 49 shows the measured and predicted stiffness coefficients of the smooth seal. Predicted values are all of the same magnitude as the measurements. K_{xx} is predicted well in the centered position; agreement gets poorer as eccentricity increases. K_{yx}, K_{xy}, and K_{yy} are well predicted through the eccentricity range. All predicted stiffness coefficients trend in the same manner as the measured values.

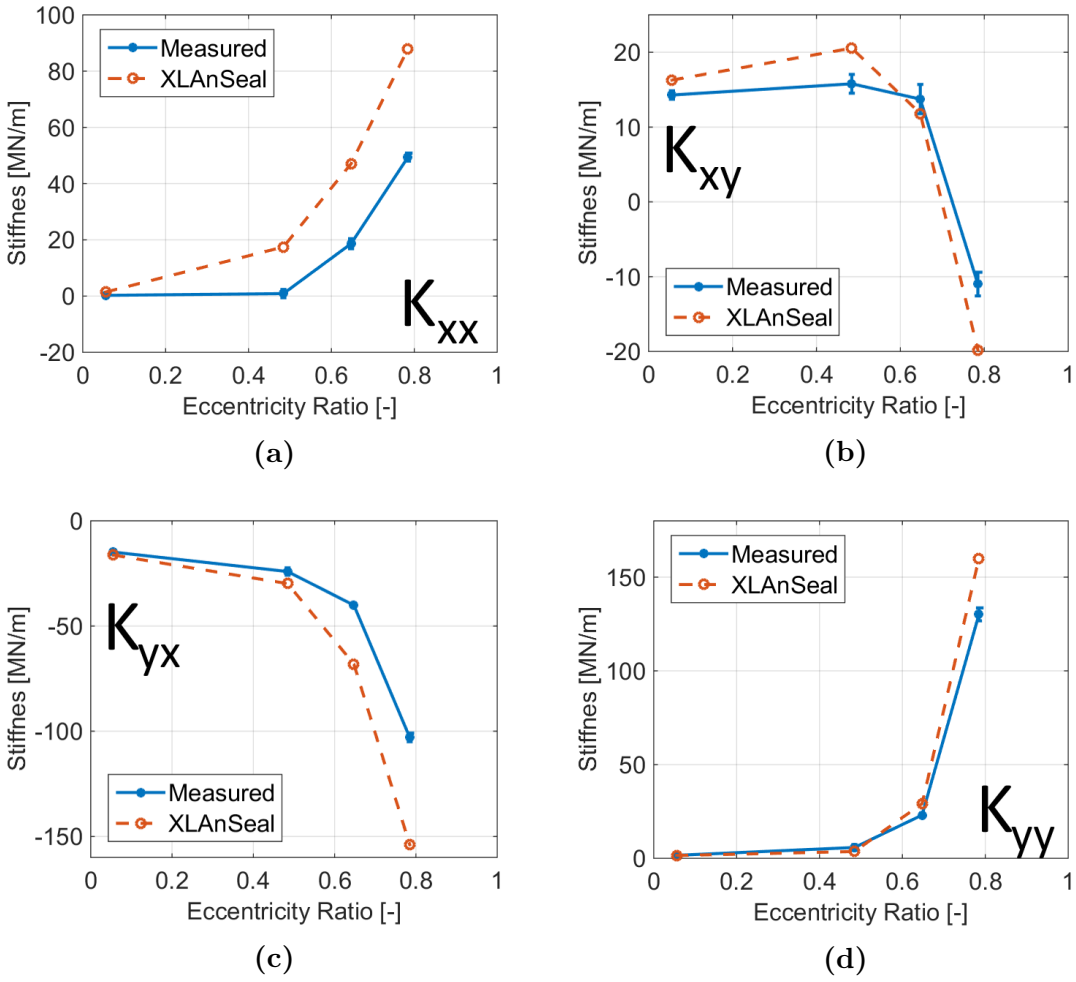

Figure 49: Stiffness coefficients vs. ϵ for the smooth seal at 3000 RPM and 2.1 bar

Figure 50 shows the measured and predicted damping coefficients. Predictions agree best with measurements out to eccentricity ratios of 0.5, after which predicted values are larger than the measurements. The trends of measurements and predictions are similar through the entire eccentricity range.

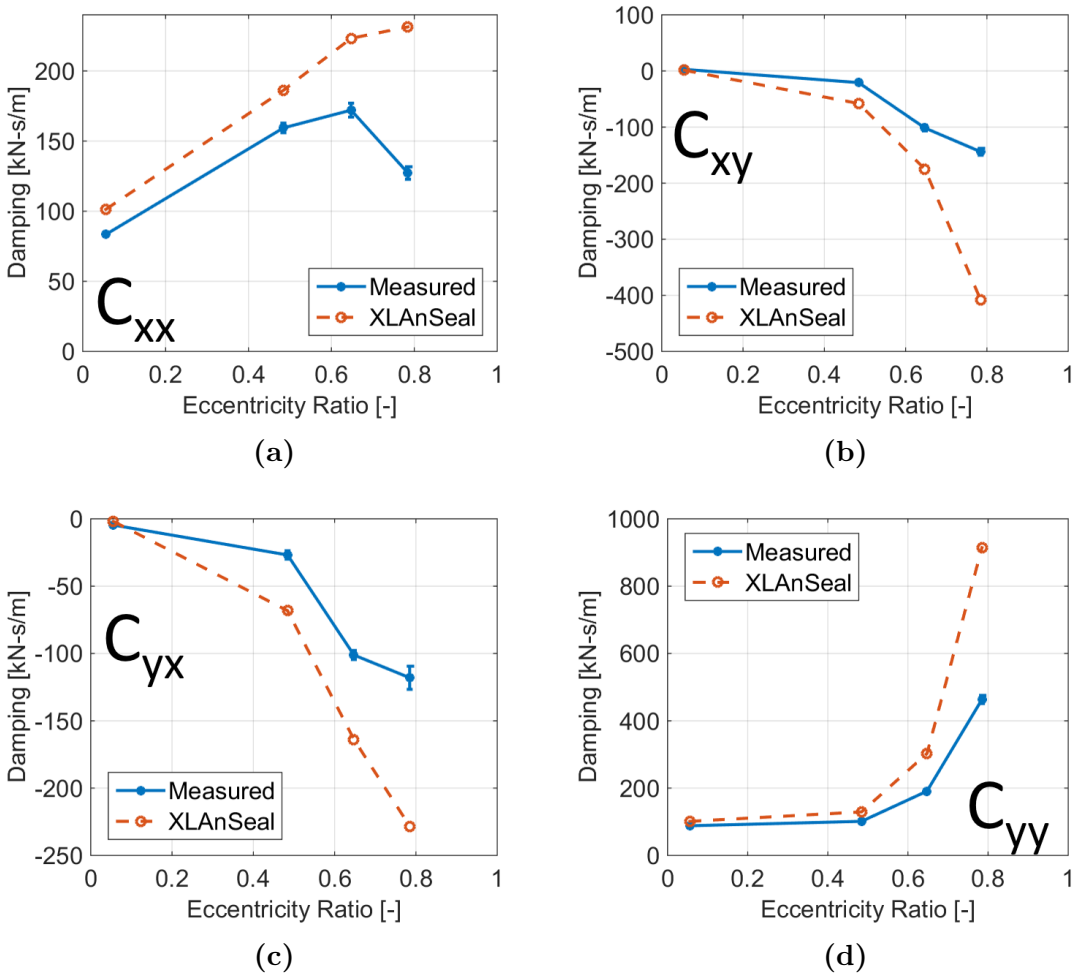

Figure 50: Damping coefficients vs. ϵ for the smooth seal at 3000 RPM and 2.1 bar

Figure 51 shows predicted and measured virtual mass coefficients. At low eccentricity ratios, direct and cross-coupled terms are well predicted. M_{xx} shows measurements that become negative with increased ϵ_o. While the predicted values are positive, their magnitudes are very close to the measured magnitudes of M_{xx}. M_{yx} exhibits a similar trend; however, the magnitude of M_{yx} is not predicted as well. M_{yy} is well predicted through the full range of eccentricity ratios.

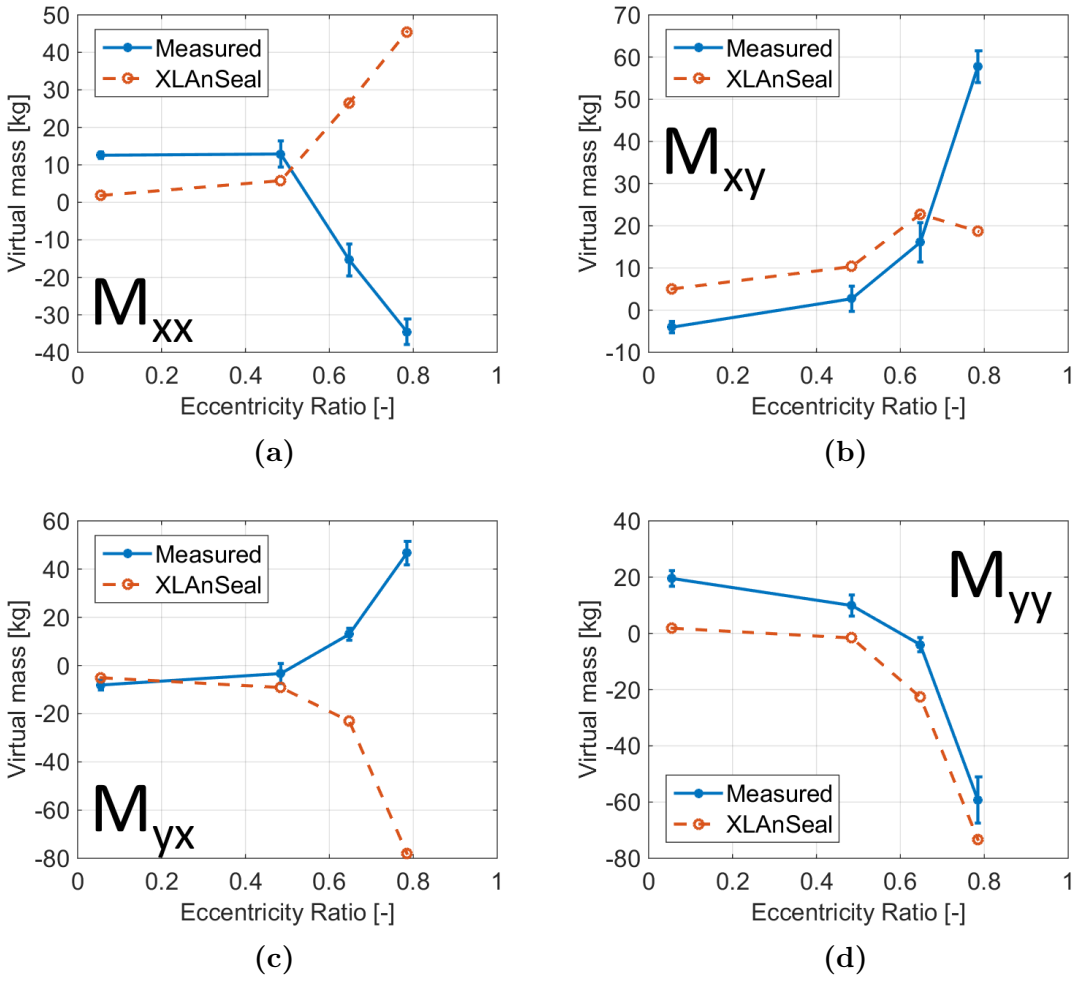

Figure 51: Virtual mass vs. ϵ for the smooth seal at 3000 RPM and 2.1 bar

San Andrés [34] provides a closed form solution for predicting M_{xx} in annular

seals and squeeze film dampers, given by Eq. (20).

$$M_{xx} = \frac{\rho \pi R^3 L}{C_r}(1 - \frac{tanh(L/D)}{L/D}) \tag{20}$$

Note that this expression is independent of rotor speed, pressure drop, and eccentricity ratio; it is strictly geometry and fluid dependent. The resulting predicted virtual mass coefficient, M_{xx}, is 4.32 kg, which agrees well with the predicted value for M_{xx} from XLAnSeal.

The smallest measured M_{xx} for the smooth seal in the centered ($\epsilon_o \cong 0.0$) position is 5.99 kg (38% larger than predicted). The largest measured M_{xx} for the smooth seal in the centered position is 16.86 kg, or nearly 4 times larger than the predicted value from Eq. (20).

Furthermore, the author provides solutions for predicting direct damping coefficients (C_{xx} and C_{yy}) and, as a result, cross-coupled stiffness (K_{xy} and K_{yx}), given by Eqs. (21) and (22).

$$C_{xx} = C_{yy} = \frac{12 \mu \pi R^3 L}{C_r^3}(1 - \frac{tanh(L/D)}{L/D}) \tag{21}$$

$$WFR = \frac{K_{xy}}{C_{xx}\omega} \tag{22}$$

The resulting direct damping coefficient is 112.3 kN-s/m, which correlates more strongly to measured values for C_{yy} than C_{xx}. Given that the smooth seal has a WFR of 0.5 in the centered position, the cross-coupled stiffness coefficient is calculated to be 17.61 MN/m, which correlates well to the measured values. Note that K_{xy} = -K_{yx}.

Recall that Figure 8 shows the seals, endcaps, and stator used during the con-

ducted experiments. The endcaps, which house the seals, include a single-tooth labyrinth seal outboard of the test seal. This is intended to prevent fluid cavitation by retaining the pressure of the fluid above ambient pressure. The author has no means of verifying that the fluid does not cavitate.

Zeidan et. al [35] discuss the difficulty in modeling squeeze film dampers (SFDs) with low lubricant supply pressures and the non-linearities that arise. The authors state that vapor cavitation can occur in SFD arrangments where oil is supplied at pressures as high as 5.5 bar (80 psi). This type of cavitation is similar to air entrainment, and involves the collapsing of bubbles in oil, leading to a nearly-instantaneous spike in fluid pressure. The authors state that the assumption of "homogeneous, incompressible fluids in the analysis of squeeze film dampers is grossly in error." As a result, the authors find that damping and virtual mass coefficients in real SFDs can vary largely with excitation (particularly at high frequencies) and that the damping coefficients be as low as 25% of the theoretical values. While the operation of annular seals is not identical to that of squeeze film dampers, the results for SFDs may be relevant in explaining the measured virtual mass coefficients for the smooth seals. The author investigated the potential of air-entrainment in the test lubricant; this was inconclusive.

Figure 52 illustrates the capacity of the test seals and the central plenum to accumulate a volume of fluid. Prior to exiting through the seal annulus, the fluid is allowed to accumulate in the plenum.

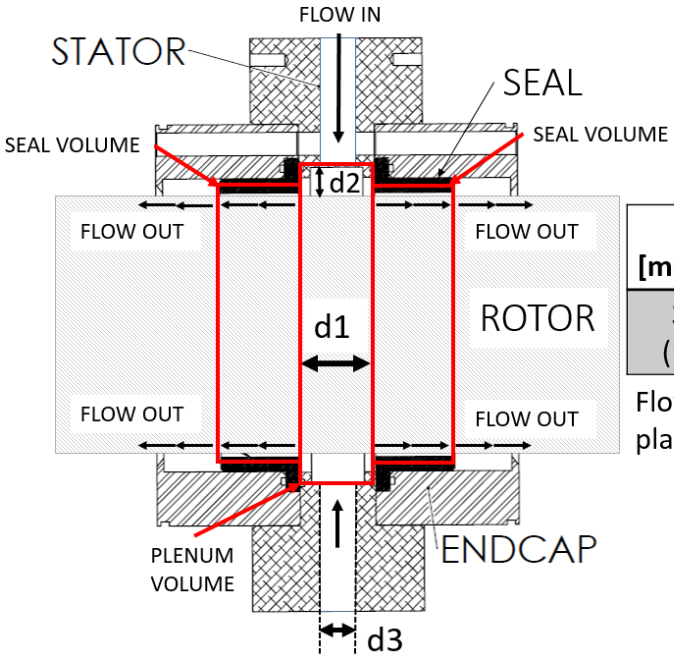

d1 [mm(in.)]	d2 [mm(in.)]	d3 [mm(in.)]
33.5 (1.32)	11.4 (.45)	23.4 (.92)

Flow is injected radially at two places, 90˚ from vertical

Figure 52: Illustration of fluid volume in the test seal annulus and the stator central plenum. Relevant plenum dimensions are also indicated.

The volume in the annulus between the test seal and rotor allows for less than .5 grams of fluid to accumulate. However, the predicted virtual mass coefficient is 4.32 kg. The central plenum of the stator has the volume to house 110 grams of fluid.

Childs et. al [17] used the same hardware as the current set of experiments to test smooth and grooved short, high-pressure (21-69 bar) liquid annular bushings with laminar flow for compressors. The authors found that the measured virtual mass of the smooth seals was consistently 5 to 8 times greater than the predicted value (in the centered position), which agrees moderately with the present results. The authors do not offer an analytical rationale for the discrepancy, but do state that the central plenum could be the source of the increased virtual mass coefficients. Their rationale is the fact that, when the test apparatus has been used for testing journal bearings, the stators of which do not include the plenums, the measured virtual mass coefficients tend agree with the predicted values.

Graviss [36] tested smooth and grooved short, high-pressure annular seals, also for compressors. The author measured significant virtual mass coefficients, roughly an order of magnitude greater than the values predicted by Eq. (20) from [34]. San Andrés et. al provide an analysis for direct comparison to the results of reference [36]. The developed FE model predicts virtual mass coefficients and accounts for the central plenum of the stator. The authors' results agree well with reference [36] (within 20%) out to eccentricity ratios of 0.5.

References [17, 36, 34] make a strong case for considering the central plenum of the stator as the source of the significant discrepancy between the predicted and measured virtual mass coefficients of the smooth seal in the centered position.

A negative virtual mass term signifies an increasing dynamic stiffness ($\mathrm{Re}(\boldsymbol{H_{ij}})$) with increased Ω. To the knowledge of the author, this phenomena has not been reported in the literature of liquid annular seals. Childs et al. [37] presents data in an annual report for short ($L/D = 0.21$), high-pressure liquid annular seals in which $\mathrm{Re}(\boldsymbol{H_{ij}})$ increased with increased Ω. An internal report by Childs et al. [38] shows the same phenomena on a set of plain annular seals, running on the same lubricant (ISO VG46), and with an L/D of 0.5. Neither of these results are publicly available.

Childs et al. [21] tested short smooth and grooved seals and measured only positive virtual mass terms. The author's results show smooth seal M_{xx} and M_{yy} converging to zero for $\epsilon_o \geq 0.7$. Childs et al. [21] do not provide predictions for virtual mass. The trends of this test program agree with the author's measurements out to eccentricities of 0.5.

To recreate these results in XLAnSeal, a non-synchronous study was also conducted. This involved setting excitation frequencies (as rotor speeds), predicting stiffness and virtual mass coefficients, and 'assembling' Re($\boldsymbol{H_{ij}}$). In Figure 53, Re($\boldsymbol{H_{ij}}$) represents the real part of the measured dynamic stiffness, and Re($\boldsymbol{H_{ij}}$)$_{pred}$ represents the real part of the predicted dynamic stiffness.

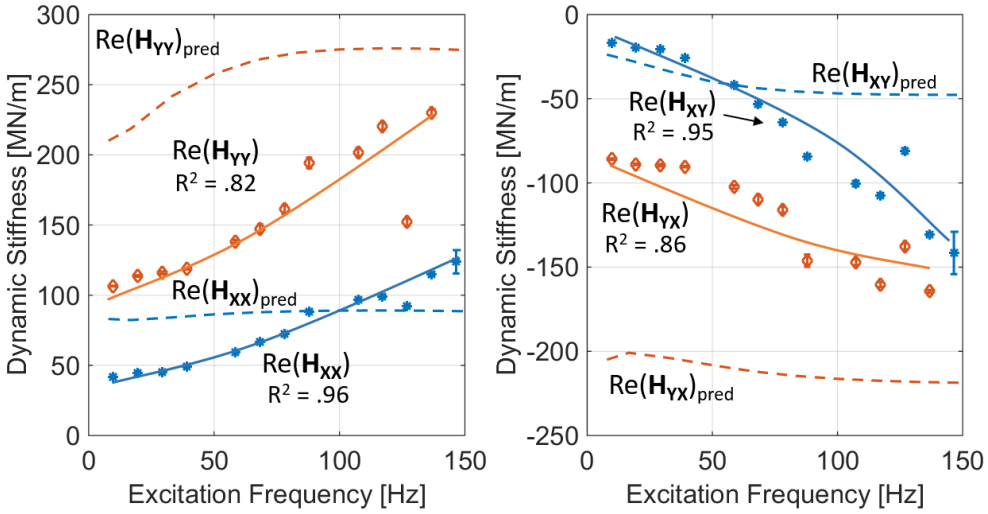

Figure 53: Measured and predicted Real part of $\boldsymbol{H_{ij}}$ for the smooth seal at 1500 RPM, 2.1 bar, and 0.83 eccentricity ratio

The predicted dynamic stiffness curves exhibit less frequency dependence, resulting in smaller virtual mass terms. However, M_{xx} and M_{yy} are both predicted to be negative. The resulting virtual mass coefficients of these dynamic stiffness curves are shown in Figure 54.

'XLAnSeal-1' represents the synchronous analysis and 'XLAnSeal-2' represents the non-synchronous, or 'assembled' dynamic stiffness model. The 'assembled' model agrees sporadically with M_{xx} and more poorly with M_{yy}. The synchronous model predicts the magnitude of the virtual mass coefficients well for nearly every test point.

The author has no explanation for the large negative virtual mass terms.

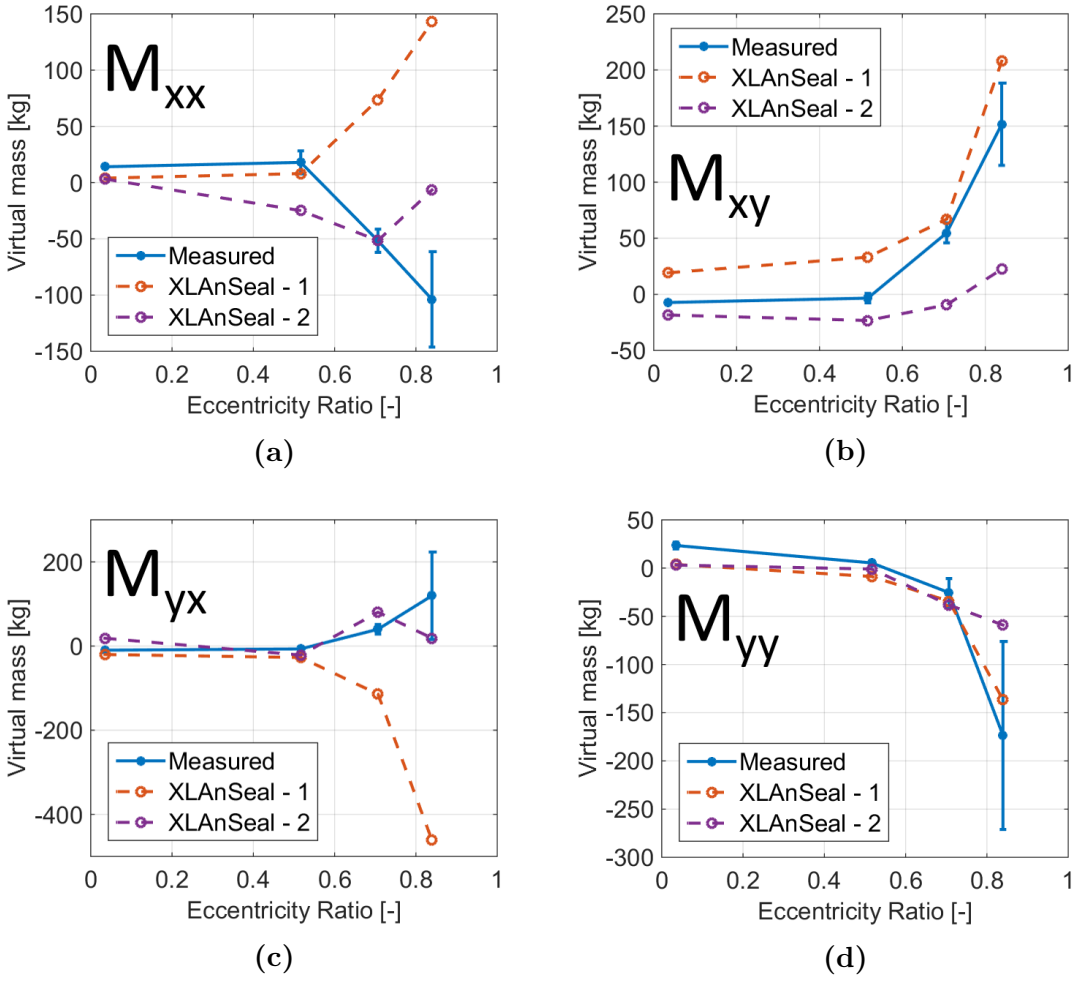

Figure 54: Virtual mass vs. ϵ for the smooth seal at 1500 RPM and 2.1 bar

CONCLUSIONS

This thesis has presented test results aimed at examining an alternative to plain annular seals for ESP applications. ESP seals have a history of being problematic for pump operators and manufacturers, as they often wear prematurely leading eventually to a pump failure. Tests were conducted on a set of smooth seals and a set of pressure-dam seals, each with a radial clearance of 0.109 mm. Another set of pressure-dam seals were manufactured with a double (2X) radial clearance of 0.221 mm. Tests were conducted at four speeds, four ΔPs, and four static eccentricity ratios. The pressure-dam seals were tested in load-on-land (LOL) and load-on-dam (LOD) orientation.

Static Results

The 1X pressure-dam seal leaks more than twice as much as the smooth seal in every static position tested. In the centered position, the 2X pressure-dam seal leaks nearly 5 times more than the 1X pressure-dam seal. In pumps, large seal leakage rates are undesirable and drive down pump efficiency. Pump manufacturers may have been willing to allow larger leakages for superior centering forces. However, this thesis has shown that pressure-dam seal fails to provide improved centering forces.

The LOD pressure-dam seal exhibits loci that vary with both ω and ΔP; in some cases, the seal attitude angles are greater than 90°. The smooth and LOL pressure-dam seals exhibit seal loci that vary only slightly between cases.

Pressure-dam Seal

The direct and cross-coupled stiffness coefficients of the 1X pressure-dam seal in the LOL and LOD orientations are comparable in magnitude. Stiffness and damping are found to be a function of ω, ΔP, and static eccentricity ratio. The LOL pressure-dam seal results exhibit negative K_{yy} (loaded direction) values, particularly at low

speeds and high pressure drops. The damping coefficients of the seals in the LOL and LOD orientations are also comparable. There is no clear-cut advantage to either load orientation. However, the stiffness and damping coefficients are shown to be load-orientation dependent, which makes these seals poorly suited to vertical operation. Additionally, when the clearance is doubled, load capacity is null.

Comparison of 1X Smooth and Pressure-dam Seals

Whirl frequency ratio (WFR) was used to assess the stability characteristics of the pressure-dam seal versus the smooth seal. In the LOD orientation, WFR is high (near 1) for the centered case and generally decreases with increased eccentricity ratio, but never consistently gets below 0.5. In the LOL orientation, WFR is consistently between 0.7 and 0.9. These stability results show the pressure-dam seal is inferior to the smooth seal.

Smooth Seal Comparison to XLAnSeal

Measurements of rotordynamic coefficients and leakage of the smooth seal compare well to predictions made in XLAnSeal of the XLTRC^2 software suite. Stiffness and damping coefficients are predicted well at moderate eccentricities (out to 0.5), and the measurements follow the predicted trends. Virtual mass is also predicted well at low eccentricities. $|M_{xx}|$ and $|M_{yx}|$ are well predicted; however, the sign of the predictions are opposite that of the measurements at large eccentricity ratios.

A non-synchronous analysis was also conducted to predict dynamic stiffness results using XLAnSeal. These results were used to extract virtual mass coefficients and compare them to the results of a synchronous analysis. The non-synchronous study was found not to be an improvement over the synchronous results. However, the measured negative M_{xx} and M_{yy} terms are found to be repeatable and predictable.

Table 4 shows the relevant smooth seal works, their test conditions, and the place of the current work within literature.

Table 4: Relevant smooth seal geometry and test results from literature

Work	C_r/R [-]	L/D[-]	ΔP [bar]	ϵ_o [-]	ω [rpm]	Re [-]
1X smooth seal	0.0021	0.3	2.1-8.3	0.0-0.85	1500-6000	112-719
Kanki et al.[13]	0.001	0.2-1	0.5-9.8	0.0-0.9	500-4000	100-10000
Falco et al.[15]	0.0023	0.25	10	0.0-0.7	4000	Turbulent[a]
Childs et al.[17]	0.0007	0.2	21-69	0.0-0.7	4000-10000	240-615

[a]Author does not give Reynolds number range

Recommendations

The pressure-dam seals leak significantly more than the smooth seals. WFR values are larger (worse) than for a plain smooth annular seals, indicating they would likely cause issues for ESPs if they were to be implemented. When their clearance is doubled, their centering capacity is gone. As a result, the author recommends a different alternative be sought.

REFERENCES

[1] Childs, D., *Turbomachinery Rotordynamics with Case Studies*. Minter Spring, 2013. pp. 323 - 365.

[2] Childs, D., Norrbin, C., and Phillips, S., "A lateral rotordynamics primer on electrical submersible pumps (esp's) for deep subsea applications," *Proceedings of the 30th Pump User's Symposia*, September 2014. Houston, TX.

[3] Wilson, B., "The effects of abrasives on electrical submersible pumps," SPE Itnl. Meeting on Petroleum Engineering, 1988. Tianjin, China.

[4] Takacs, G., *Electrical Sumbersible Pumps Manual*. Gulf Professional Publishing. pp. 72 - 83.

[5] Lea, J. and Nickens, H., "Selection of artifical lift," SPE Mid-Continent Operations Symposium, March 1999. Oklahoma City, OK.

[6] Bremner, C. and Harris, G., "Evolving technologies: Electrical submersible pumps," *Oilfield Review*, pp. 31–43, December 2006.

[7] Durham, M., "Effect of vibration on electric submersible pumps," *SPE Journal of Petroleum Engineering*, pp. 186–190, 1990.

[8] Salas, K., Delgado, A., and Van Dam, J., "Rotordynamic characterization of an electrical submersible pump motor," Society of Petroleum Engineers ESP Workshop, April 2013. Houston, TX.

[9] Valantas, R. and Bolleter, U., "Solutions to abrasive wear-related rotordynamic instability problems on prudhoe bay injection pumps," pp. 3–10, 5th International Pump User's Symposium, organized by the Turbomachinery Laboratory at Texas A&M University, September 1988. Houston, TX.

[10] Lomakin, A., "Calculation of the critical number of revolutions and the conditions necessary for dynamic stability of rotors in high-pressure hydraulic machines when taking into account forces originating in sealings," *Power and Mechanical Engineering (In Russian)*, April 1958.

[11] San Andrés, L., "Thermal analysis of finite length journal bearings including fluid inertia," *Modern Lubrication Theory*, Notes 8, 2009. Texas A&M University Digital Libraries, http://oaktrust.library.tamu.edu/handle/1969.1/93247 [web accessed October 2015].

[12] Childs, D., *Rotordynamics: Phenomena, Modeling, and Analysis*. Wiley-Interscience, 1993. pp. 230 - 247.

[13] Kanki, H. and Kawakami, T., "Experimental study on the dynamic characteristics of annular seals," *I. Mech. E C297/84*, pp. 159 – 166, 1984.

[14] Nelson, C. and Nguyen, D., "Analysis of eccentric annular incompressible seals: Part 2 - effects of eccentricity on rotordynamic coefficients," *ASME Journal of Tribology*, vol. 110, pp. 361 – 366, 1988.

[15] Falco, M., Mimmi, G., and Marenco, G., "Effects of seals on rotor dynamics," (Tokyo, Japan), pp. 655 – 661, IFToMM Proceedings, Sept. 1986.

[16] Marquette, O., Childs, D., and San Andrès, L., "Eccentricity effects on the rotordynamic coefficients of plain annular seals: Theory versus experiment," *ASME Journal of Tribology*, vol. 119, pp. 443 – 447, 1997.

[17] Childs, D., Rodriguez, L., Cullotta, V., Al-Ghasem, A., and Graviss, M., "Rotordynamic-coefficients and static (equilibrium loci and leakage) characteristics for short, laminar-flow annular seals," *ASME Journal of Tribology*, pp. 378–387, 2006.

[18] San Andrès, L. and Delgado, A., "A novel bulk flow model for improved predictions of force coefficients in grooved oil seals operating eccentrically," *American Society of Mechanical Engineers*, 2012.

[19] Semanate, J. and San Andrès, L., "Analysis of multi-land high pressure oil seals," *Tribology Transactions*, vol. 36, no. 4, pp. 661–669, 1993.

[20] Zirkleback, N. and San Andrès, L., "Bulk-flow model for the transition to turbulence regime in annular pressure seals," *Tribology Transactions*, vol. 39, no. 4, pp. 835–842, 1996.

[21] Childs, D., Graviss, M., and Rodriguez, L., "Influence of groove size on the static and rotordynamic characteristics of short, laminar-flow annular seals," *ASME Journal of Tribology*, vol. 129, pp. 398 – 406, 2007.

[22] Lund, J., *Self-Excited, Stationary Whirl Orbits of a Journal in a Sleeve Bearing*. PhD thesis, Rensselaer Polytechnic Institute, Troy, NY., 1996.

[23] San Andrès, L., "Effect of eccentricity on the force response of a hybrid bearing," *Tribology Transactions*, vol. 34, pp. 537–544, 1991.

[24] Nicholas, J., "Stabilizing turbomachinery with pressure dam bearings," *Encyclopedia of Fluid Mechanics*, vol. 2, 1994. pp. 1 - 18.

[25] Nicholas, J. and Allaire, P., "Analysis of step journal bearings - finite length stability," *ASLE Transaction*, pp. 197–207, 1980.

[26] Mehta, N. and Rattan, S., "Performance of three-lobe pressure-dam bearings," *Tribology International*, pp. 435–442, 1993.

[27] Mehta, N. and Rattan, S., "Effect of load orientation on the stability of a three-lobe pressure dam bearing with rigid and flexible rotors," *Journal of Engineering and Technology*, pp. 10–15, 2011.

[28] Kaul, A., "Design and development of a test setup for the experimental determination of the rotordynamic and leakage characteristics of annular bushing oil seals," Master's thesis, Texas A&M University, 1999.

[29] Glienicke, J., "Experimental investigation of the stiffness and damping coeffcients of turbine bearings and their application to instability prediction," pp. 116–129, 1966-67.

[30] Mitchell, L. and Elliot, K., "How to design stingers for vibration testing of structures," *Sound and Vibration*, 1984.

[31] Rouvass, C. and Childs, D., "A parameter identification method for the rotordynamic coefficients of a high reynolds number hydrostatic bearing," *Transactions of the ASME Journal of Vibrations and Acoustics*, pp. 264–270, 1993.

[32] Childs, D. and Hale, K., "A test apparatus and facility to identify the rotordynamic coefficients of high-speed hydrostatic bearings," *ASME Journal of Tribology*, pp. 337–343, 1994.

[33] Figliola, R. and Beasley, D., *Theory and Design for Mechanical Measurements*. John Wiley & Sons, 2011. pp. 139 - 141.

[34] San Andrés, L., "Squeeze film dampers: Operation, models, and technical issues," *Modern Lubrication Theory*, Notes 13, 2009. Texas A&M University Digital Libraries, http://oaktrust.library.tamu.edu/handle/1969.1/93253 [web accessed March 2016].

[35] Zeidan, F., San Andrés, L., and Vance, J., "Design and application of squeeze film dampers in rotating equipment," in *Proceedings of the 25th Turbomachinery Symposium*.

[36] Graviss, M., "The influence of a central groove on static and dynamic characteristics of an annular liquid seal with laminar flow," Master's thesis, Texas A&M University, 2005.

[37] Childs, D., Rodriguez, L., and Al-Ghasem, A., "Experimental rotordynamic coefficients and static characteristics for three laminar oil bushing seals," tech. rep., 2003. Annual TRC Report.

[38] Childs, D., Moreland, J., Torres, J., and Bullock, J., "Annular liquid seal tests - internal report." Unpublished internal report, January 2014.

[39] Vennard, J., *Elementary Fluid Mechanics*. Wiley & Sons, Inc., 1954. pp. 188 - 200.

APPENDIX A: STATIC TEST RESULTS

The following tables include the rotor speed, axial pressure drop, ϵ_x, ϵ_y, ϕ, static load, leakage, inlet temperature, outlet temperature, and whirl frequency ratio.

1X Clearance Smooth and Pressure-dam Seals

Table A.1: Static results of the 1X clearance smooth seals

Speed	ΔP	ε_{xo}	ε_{yo}	ϕ	F_s	Leakage	Tin	Tout (avg)	WFR
RPM	bar	-	-	deg	N	lpm	°C	°C	-
1500	2.07	-0.03	0.01	75.1	8.69	0.58	45.67	39.09	0.50
1500	2.07	0.57	-0.01	88.7	278.51	0.60	45.10	38.37	0.46
1500	2.07	0.67	-0.42	57.9	491.98	0.64	45.88	38.83	0.52
1500	2.07	0.58	-0.73	38.4	990.88	1.04	46.15	38.93	0.00
1500	4.14	-0.03	0.02	59.2	6.04	0.93	44.93	39.05	0.54
1500	4.14	0.60	0.01	90.8	319.42	1.55	45.19	38.31	0.52
1500	4.14	0.81	-0.32	68.2	687.42	1.95	45.79	38.34	0.48
1500	4.14	0.62	-0.71	41.0	1134.63	2.41	47.44	39.34	0.00
1500	6.21	-0.02	0.03	35.5	27.05	2.00	45.20	37.24	0.51
1500	6.21	0.56	0.01	91.5	302.49	2.32	45.07	37.98	0.51
1500	6.21	0.82	-0.23	74.4	655.92	3.47	46.48	38.27	0.47
1500	6.21	0.66	-0.72	42.8	1190.31	4.31	47.91	38.26	0.00
1500	8.28	-0.02	0.06	21.6	9.87	3.10	47.11	38.58	0.46
1500	8.28	0.54	0.02	92.9	283.46	3.62	46.77	37.67	0.51
1500	8.28	0.82	-0.30	69.6	721.21	5.47	48.15	40.59	0.47
1500	8.28	0.72	-0.67	47.1	1346.23	4.77	44.10	36.65	0.00
3000	2.07	0.04	-0.03	51.0	0.87	0.49	43.68	47.52	0.54
3000	2.07	0.53	-0.08	81.0	285.75	0.55	43.61	46.35	0.49
3000	2.07	0.63	-0.35	60.8	530.22	0.60	42.76	44.79	0.52
3000	2.07	0.51	-0.71	36.1	1219.33	0.65	45.15	45.77	0.00
3000	4.14	0.01	0.00	93.39	8.67	1.09	39.96	45.62	0.65
3000	4.14	0.52	0.00	88.9	408.52	1.59	44.63	48.41	0.51
3000	4.14	0.70	-0.37	62.0	818.95	1.67	44.96	47.24	0.49
3000	4.14	0.58	-0.70	39.6	1475.01	1.97	46.48	46.77	0.00
3000	6.21	0.02	0.02	44.3	6.95	2.26	47.63	47.42	0.56
3000	6.21	0.48	0.00	90.6	388.53	2.28	45.12	46.99	0.49
3000	6.21	0.75	-0.30	68.2	901.00	2.95	44.55	46.62	0.51
3000	6.21	0.64	-0.67	44.5	1596.12	3.77	47.29	48.75	0.00
3000	8.28	0.02	0.03	39.1	6.56	2.98	48.17	48.37	0.50
3000	8.28	0.49	0.01	91.2	396.10	3.56	46.64	48.04	0.43
3000	8.28	0.78	-0.30	68.7	999.12	4.29	45.98	48.29	0.48
3000	8.28	0.65	-0.68	43.4	1806.84	5.02	47.14	49.64	0.00

Table A.2: Static results of the 1X clearance smooth seals

Speed	ΔP	ε_{xo}	ε_{yo}	ϕ	F_s	Leakage	Tin	Tout (avg)	WFR
RPM	bar	-	-	deg	N	lpm	°C	°C	-
4500	2.07	-0.06	0.05	47.80	5.62	0.67	50.12	60.46	0.50
4500	2.07	0.54	0.00	89.62	381.02	0.67	49.52	58.85	0.46
4500	2.07	0.62	-0.38	58.84	683.57	0.70	50.40	57.83	0.42
4500	2.07	0.50	-0.69	36.32	1333.70	0.70	52.79	58.25	0.00
4500	4.14	-0.05	0.04	47.90	5.76	1.37	43.94	54.94	0.50
4500	4.14	0.53	0.01	91.23	511.12	1.41	43.82	55.30	0.46
4500	4.14	0.66	-0.42	57.25	1040.81	1.49	45.02	55.12	0.43
4500	4.14	0.56	-0.65	40.69	1701.76	1.71	45.05	54.30	0.00
4500	6.21	-0.01	0.04	10.94	8.77	1.99	43.82	54.89	0.49
4500	6.21	0.56	0.00	89.90	579.09	2.47	44.25	56.37	0.49
4500	6.21	0.73	-0.37	63.13	1172.11	3.56	46.33	57.99	0.41
4500	6.21	0.61	-0.67	42.11	2001.38	3.20	44.18	53.89	0.00
4500	8.28	-0.04	0.04	44.92	4.38	3.26	44.26	55.76	0.50
4500	8.28	0.52	0.01	90.98	593.54	3.29	43.88	56.92	0.49
4500	8.28	0.76	-0.32	67.22	1298.07	4.60	43.57	54.76	0.46
4500	8.28	0.62	-0.68	42.39	2203.81	4.91	45.18	54.89	0.00
6000	2.07	-0.05	0.05	45.85	-2.55	1.59	49.50	64.06	0.50
6000	2.07	0.59	0.07	83.06	499.02	1.64	53.04	66.91	0.48
6000	2.07	0.64	-0.40	58.07	851.34	1.70	54.16	66.44	0.35
6000	2.07	0.52	-0.68	37.21	1713.09	1.95	54.24	66.22	0.00
6000	4.14	-0.06	0.06	48.36	7.50	1.91	47.81	68.39	0.49
6000	4.14	0.54	0.01	90.91	590.66	2.03	47.93	67.77	0.48
6000	4.14	0.64	-0.37	59.49	1123.98	2.27	47.08	65.14	0.34
6000	4.14	0.48	-0.71	34.17	2394.52	2.68	46.76	63.61	0.00
6000	6.21	-0.08	0.06	50.30	7.00	2.94	47.37	67.02	0.49
6000	6.21	0.53	0.01	91.37	686.85	3.13	46.65	65.54	0.47
6000	6.21	0.65	-0.40	58.24	1346.76	3.33	46.95	63.22	0.29
6000	6.21	0.50	-0.70	35.49	2484.51	3.96	47.03	62.38	0.00
6000	8.28	-0.08	0.07	49.72	6.54	3.47	45.96	63.98	0.47
6000	8.28	0.57	0.01	90.99	798.82	3.91	45.90	63.97	0.49
6000	8.28	0.69	-0.34	63.45	1495.00	4.93	44.95	59.37	0.30
6000	8.28	0.50	-0.74	33.93	2905.63	5.27	46.09	59.15	0.00

Table A.3: Static results of the 1X clearance LOD pressure-dam seals

Speed	ΔP	ε_{xo}	ε_{yo}	ϕ	F_s	Leakage	Tin	Tout (avg)	WFR
RPM	bar	-	-	deg	N	lpm	°C	°C	-
1500	2.07	-0.08	0.04	63.0	-21.8	1.6	45.07	40.20	0.93
1500	2.07	0.31	0.02	94.0	737.9	1.6	45.09	40.30	0.68
1500	2.07	0.54	0.05	85.0	1260.3	1.9	45.01	40.49	0.52
1500	2.07	0.65	-0.32	63.0	1826.2	2.1	45.15	40.26	0.30
1500	4.14	-0.02	0.04	24.0	14.7	3.4	45.82	41.41	0.79
1500	4.14	0.35	0.12	109.0	644.0	4.0	46.60	42.84	0.38
1500	4.14	0.65	0.20	107.0	1312.2	5.2	47.31	45.00	0.33
1500	4.14	0.75	-0.24	72.0	2285.0	5.7	44.86	42.21	0.00
1500	6.21	-0.01	0.05	16.8	16.1	5.5	45.64	42.50	0.79
1500	6.21	0.32	0.11	109.0	607.9	6.1	45.88	43.78	0.72
1500	6.21	0.58	0.25	113.0	1066.9	7.4	45.73	45.49	0.57
1500	6.21	0.85	0.20	103.0	2196.7	9.1	46.31	47.48	0.00
1500	8.28	-0.01	0.05	16.1	16.8	8.4	46.97	46.22	0.75
1500	8.28	0.38	0.12	108.6	648.2	8.9	46.89	47.03	0.49
1500	8.28	0.64	0.30	115.5	1100.9	11.2	47.21	48.27	0.64
1500	8.28	0.89	0.36	112.1	2354.9	13.2	45.67	44.72	0.77
3000	2.07	-0.06	0.04	52.8	0.5	1.8	44.84	46.94	0.73
3000	2.07	0.29	-0.07	75.1	1375.4	1.8	44.40	46.52	0.58
3000	2.07	0.57	-0.39	55.8	2728.3	1.9	45.08	46.31	0.54
3000	2.07	0.63	-0.63	45.5	3913.5	2.3	45.74	47.58	0.40
3000	4.14	0.31	0.06	101.8	1191.9	3.9	46.19	47.69	0.70
3000	4.14	0.64	0.00	89.2	2565.8	4.9	46.11	47.92	0.20
3000	4.14	0.71	-0.32	65.8	3458.9	6.3	47.14	49.83	0.00
3000	6.21	-0.02	0.04	28.3	13.7	5.2	45.34	46.19	0.69
3000	6.21	0.26	0.09	109.0	998.4	6.4	45.75	48.52	0.74
3000	6.21	0.59	0.16	105.8	2262.7	7.9	46.94	50.06	0.53
3000	6.21	0.74	-0.26	70.1	3802.1	8.4	46.68	48.31	0.00
3000	8.28	0.02	0.05	28.8	14.4	7.9	46.66	49.31	0.77
3000	8.28	0.30	0.11	110.4	1057.5	8.3	47.03	49.69	0.70
3000	8.28	0.63	0.23	110.1	2278.7	10.7	47.67	49.94	0.67
3000	8.28	0.76	-0.30	63.3	4335.6	10.9	45.92	48.61	0.00

Table A.4: Static results of the 1X clearance LOD pressure-dam seals

Speed	ΔP	ε_{xo}	ε_{yo}	ϕ	F_s	Leakage	Tin	Tout (avg)	WFR
RPM	bar	-	-	deg	N	lpm	°C	°C	-
4500	2.07	-0.08	0.02	70.56	-6.61	1.54	46.68	54.08	0.78
4500	2.07	0.22	-0.22	44.42	1449.91	1.53	46.98	54.11	0.61
4500	2.07	0.40	-0.41	44.74	2539.40	1.54	47.44	53.68	0.34
4500	2.07	0.58	-0.55	46.36	4166.89	2.16	45.84	51.66	0.43
4500	4.14	0.03	0.03	47.55	6.62	4.24	46.35	52.35	0.83
4500	4.14	0.25	0.01	93.90	1369.19	4.16	45.50	51.46	0.70
4500	4.14	0.49	-0.09	78.80	2845.22	4.25	44.74	51.23	0.51
4500	4.14	0.64	-0.36	60.76	4228.77	4.59	44.95	50.98	0.44
4500	6.21	0.03	0.03	44.06	5.53	6.16	46.77	51.59	0.71
4500	6.21	0.25	0.05	102.95	1246.95	6.33	45.68	51.16	0.79
4500	6.21	0.52	0.05	95.87	2796.62	6.44	45.60	50.81	0.45
4500	6.21	0.68	-0.26	68.79	4625.06	7.44	45.41	50.51	0.16
4500	8.28	0.03	0.03	44.90	-9.33	6.87	46.11	51.34	0.71
4500	8.28	0.29	0.07	104.46	1376.89	7.67	45.99	50.65	0.68
4500	8.28	0.56	0.13	103.34	2804.66	9.04	46.01	50.03	0.58
4500	8.28	0.72	-0.20	74.04	4911.71	9.95	46.10	50.07	0.00
6000	2.07	-0.06	0.05	49.88	-0.93	2.55	48.49	60.45	0.86
6000	2.07	0.21	-0.17	50.25	1588.92	2.57	49.06	60.81	0.72
6000	2.07	0.48	-0.41	49.52	3354.37	2.63	50.32	60.58	0.44
6000	2.07	0.52	-0.68	37.60	5537.68	2.68	50.64	59.43	0.08
6000	4.14	-0.05	0.04	50.26	-0.32	3.70	47.17	59.30	0.83
6000	4.14	0.25	-0.04	80.72	1780.14	3.97	46.98	57.90	0.70
6000	4.14	0.51	-0.20	68.31	3594.19	4.46	46.46	55.74	0.48
6000	4.14	0.62	-0.36	59.42	5138.87	5.45	45.35	53.68	0.41
6000	6.21	-0.05	0.03	55.77	-2.62	5.21	46.11	57.09	0.76
6000	6.21	0.27	0.03	97.14	1962.48	5.82	45.41	54.70	0.72
6000	6.21	0.52	-0.02	86.99	3683.17	6.54	45.00	53.13	0.52
6000	6.21	0.64	-0.29	65.71	5275.25	7.08	45.54	53.24	0.32
6000	8.28	-0.06	0.05	50.40	-32.60	7.35	45.59	55.07	0.73
6000	8.28	0.26	0.05	102.34	1748.81	7.52	46.10	54.47	0.70
6000	8.28	0.52	0.06	96.64	3554.51	8.34	46.10	53.42	0.56
6000	8.28	0.66	-0.18	74.69	5336.89	9.42	46.13	53.27	0.00

Table A.5: Static results of the 1X clearance LOL pressure-dam seals

Speed	ΔP	ε_{xo}	ε_{yo}	ϕ	F_s	Leakage	Tin	Tout (avg)	WFR
RPM	bar	-	-	deg	N	lpm	°C	°C	-
1500	2.07	0.02	0.01	53.2	**27.18**	1.95	46.11	35.76	0.74
1500	2.07	0.61	0.25	67.2	216.18	2.10	43.90	35.09	0.52
1500	2.07	0.80	-0.40	63.0	292.33	2.26	45.67	36.72	0.56
1500	2.07	0.92	-0.51	60.8	341.49	2.26	46.35	36.59	0.27
1500	4.14	0.00	0.01	163.7	29.07	3.52	45.89	37.01	0.66
1500	4.14	0.50	-0.15	72.4	202.58	4.07	44.79	37.24	0.60
1500	4.14	0.75	-0.33	65.8	294.74	5.31	46.12	37.70	1.04
1500	4.14	0.85	-0.41	64.3	375.17	6.51	46.28	39.05	0.46
1500	6.21	0.01	0.02	159.8	28.83	4.32	44.23	37.27	0.68
1500	6.21	0.50	-0.16	71.8	204.53	6.89	44.87	38.13	0.72
1500	6.21	0.74	-0.33	65.7	297.07	8.22	45.80	42.04	0.60
1500	6.21	0.91	-0.47	62.6	398.08	10.04	46.35	46.39	0.87
1500	8.28	0.01	0.04	155.2	30.80	7.78	46.41	39.50	0.73
1500	8.28	0.53	-0.20	69.3	198.26	9.21	46.60	45.14	0.61
1500	8.28	0.76	-0.36	64.6	282.35	11.51	47.49	48.43	1.04
1500	8.28	0.84	-0.42	63.1	345.29	12.40	46.56	45.15	1.03
3000	2.07	0.00	0.01	153.4	23.60	1.77	45.18	42.03	0.75
3000	2.07	0.53	-0.23	66.5	257.94	1.86	45.41	43.00	0.64
3000	2.07	0.77	-0.40	62.4	351.09	1.88	45.98	43.00	0.18
3000	2.07	0.86	-0.47	61.5	442.93	2.39	46.45	43.75	0.77
3000	4.14	0.00	0.03	166.0	28.58	3.24	45.54	44.84	0.97
3000	4.14	0.32	-0.06	75.0	193.67	3.73	47.24	45.78	0.72
3000	4.14	0.61	-0.23	69.4	366.18	5.44	46.66	46.78	0.63
3000	4.14	0.78	-0.37	64.5	505.06	5.45	45.36	45.90	0.77
3000	6.21	0.01	0.04	164.1	27.88	5.87	47.24	49.35	0.77
3000	6.21	0.48	-0.12	75.3	302.63	6.59	45.65	46.82	0.64
3000	6.21	0.67	-0.26	68.6	445.82	6.91	45.69	48.61	0.69
3000	6.21	0.82	-0.39	64.5	589.19	8.51	44.45	46.45	0.65
3000	8.28	0.02	0.04	148.4	28.87	7.59	45.36	47.57	0.77
3000	8.28	0.43	-0.09	77.8	292.79	8.26	45.77	48.43	0.73
3000	8.28	0.74	-0.31	67.3	503.60	10.82	46.93	48.66	0.62
3000	8.28	0.83	-0.38	65.09	627.90	11.48	44.88	45.69	0.00

Table A.6: Static results of the 1X clearance LOL pressure-dam seals

Speed	ΔP	ε_{xo}	ε_{yo}	ϕ	F_s	Leakage	Tin	Tout (avg)	WFR
RPM	bar	-	-	deg	N	lpm	°C	°C	-
4500	2.07	0.00	0.02	11.03	15.32	1.74	45.89	44.65	0.89
4500	2.07	0.53	-0.23	65.77	296.06	1.84	45.77	45.03	0.69
4500	2.07	0.79	-0.41	62.10	452.38	1.91	46.12	45.50	0.48
4500	2.07	0.89	-0.49	61.09	568.38	2.00	46.93	46.66	0.06
4500	4.14	0.01	0.00	64.71	28.76	3.30	44.95	48.33	0.79
4500	4.14	0.35	-0.12	69.73	302.25	3.43	43.39	47.84	0.77
4500	4.14	0.77	-0.37	64.04	616.52	4.99	46.43	52.75	0.74
4500	4.14	0.88	-0.45	62.58	743.16	5.53	46.97	51.07	0.77
4500	6.21	0.01	0.01	58.70	27.43	5.13	45.13	48.50	0.77
4500	6.21	0.29	-0.07	75.99	297.22	5.56	45.84	51.93	0.81
4500	6.21	0.65	-0.25	68.67	596.25	8.00	46.13	51.11	0.63
4500	6.21	0.78	-0.36	65.19	742.75	7.71	45.07	48.49	0.63
4500	8.28	0.01	0.01	29.42	27.30	7.15	45.10	49.97	0.72
4500	8.28	0.27	-0.04	80.94	289.68	7.31	45.31	49.14	0.70
4500	8.28	0.64	-0.23	69.78	607.50	9.56	46.64	50.69	0.65
4500	8.28	0.83	-0.39	64.93	858.76	11.35	45.90	50.04	0.69
6000	2.07	0.01	0.01	42.48	28.73	2.25	47.76	55.87	0.87
6000	2.07	0.40	-0.17	67.02	296.92	2.28	48.37	56.97	0.72
6000	2.07	0.79	-0.43	61.39	593.14	2.35	48.08	55.40	0.55
6000	2.07	0.86	-0.49	60.32	688.44	2.34	48.43	56.26	0.00
6000	4.14	0.01	-0.01	61.45	29.12	4.20	46.55	58.36	0.84
6000	4.14	0.29	-0.10	70.52	305.25	4.27	46.40	59.27	0.85
6000	4.14	0.66	-0.30	65.43	596.21	5.13	46.40	57.40	0.73
6000	4.14	0.85	-0.44	62.78	859.83	6.15	46.22	54.94	0.79
6000	6.21	0.01	0.00	68.41	30.38	5.71	46.66	56.19	0.78
6000	6.21	0.23	-0.05	76.24	292.90	6.23	46.41	55.31	0.76
6000	6.21	0.57	-0.21	68.98	605.00	7.33	45.95	54.02	0.65
6000	6.21	0.82	-0.41	63.59	887.50	8.71	45.99	52.62	0.68
6000	8.28	0.01	0.00	87.72	22.48	7.79	45.85	52.42	0.63
6000	8.28	0.21	-0.04	78.84	284.63	7.67	45.83	53.39	0.72
6000	8.28	0.48	-0.14	73.25	590.98	9.32	45.66	52.46	0.67
6000	8.28	0.76	-0.35	65.97	904.37	11.50	45.32	50.59	0.61

2X Clearance Pressure-dam Seals

Table A.7: Static results of the 2X clearance LOD pressure-dam seals

Speed	ΔP	ε_{xo}	ε_{yo}	ϕ	Leakage	Tin	Tout (avg)
RPM	bar	-	-	deg	lpm	°C	°C
1500	2.07	0.03	-0.02	48.43	11.22	45.21	45.81
1500	4.14	0.03	-0.03	44.00	23.58	45.64	46.29
1500	6.21	0.03	-0.03	42.00	34.28	45.50	46.23
1500	7.24	0.03	0.03	140.00	34.80	42.45	42.80
3000	2.07	0.04	0.02	114.00	13.15	46.10	47.62
3000	4.14	0.05	0.02	116.11	23.66	46.35	47.63
3000	6.21	0.07	0.02	107.48	33.29	46.86	47.59
3000	7.24	0.01	0.05	168.85	35.28	43.28	43.85
4500	2.07	0.01	0.01	127.46	11.81	45.20	48.28
4500	4.14	0.05	0.04	134.50	22.55	45.22	47.75
4500	6.21	0.10	0.05	117.04	32.74	46.72	47.43
4500	7.24	-0.01	0.07	-167.71	36.12	47.37	45.76
6000	2.07	0.04	0.00	93.89	11.29	46.13	50.72
6000	4.14	-0.07	0.06	-134.02	21.47	45.77	49.49
6000	6.21	0.03	0.07	-157.05	31.43	47.24	47.78
6000	7.24	0.01	0.05	162.10	34.71	48.36	44.79

Table A.8: Static results of the 2X clearance LOL pressure-dam seals

Speed	ΔP	ε_{xo}	ε_{yo}	ϕ	Leakage	Tin	Tout (avg)
RPM	bar	-	-	deg	lpm	°C	°C
1500	2.07	-0.01	-0.08	-176.20	11.34	46.04	45.10
1500	4.14	0.07	-0.05	126.44	23.13	45.71	45.98
1500	6.21	0.06	-0.02	113.33	33.00	45.37	45.08
1500	7.24	0.07	-0.01	102.66	38.76	46.09	46.91
3000	2.07	0.31	-0.15	116.25	10.85	46.11	46.26
3000	4.14	0.17	-0.13	127.77	24.52	46.81	47.84
3000	6.21	0.17	-0.07	113.20	31.79	45.79	45.28
3000	7.24	0.20	-0.06	109.00	36.10	45.60	45.12
4500	2.07	-0.04	-0.07	-148.30	8.66	46.92	47.31
4500	4.14	-0.01	-0.11	-172.91	22.16	45.25	47.62
4500	6.21	0.12	-0.09	128.00	31.06	46.27	45.98
4500	7.24	0.12	-0.09	128.31	35.04	47.14	46.17
6000	2.07	-0.08	-0.07	-134.01	11.52	47.05	50.93
6000	4.14	0.07	-0.11	-147.34	22.05	46.57	49.69
6000	6.21	-0.08	-0.11	-142.49	30.14	45.70	46.30
6000	7.24	-0.05	-0.09	-149.57	31.86	44.69	44.83

APPENDIX B: TABULATED ROTORDYNAMIC COEFFICIENTS

The following tables include the KCM values for both smooth and pressure-dam seals. The speeds, pressure drops, and eccentricity ratios of the test points accompany the KCM values and their uncertainties.

1X Smooth and Pressure-dam Seals

Table B.1: Speed, pressure drop, eccentricity ratio, and stiffness coefficients of the 1X clearance smooth seals

Speed	ΔP	ε_o	Kxx	Kxy	Kyx	Kyy	eKxx	eKxy	eKyx	eKyy
RPM	bar	-	MN/m	MN/m	MN/m	MN/m	MN/m	MN/m	MN/m	MN/m
1500	2.07	0.03	0.45	7.71	-8.63	1.50	0.39	0.31	0.82	1.48
1500	2.07	0.47	2.17	9.88	-18.07	2.06	4.29	1.76	0.98	1.07
1500	2.07	0.65	19.93	4.47	-34.69	26.16	4.33	3.71	4.77	6.13
1500	2.07	0.76	35.49	-15.08	-66.59	97.75	17.81	15.40	43.58	40.95
1500	4.14	0.03	1.48	8.28	-10.34	1.34	6.01	0.58	7.22	2.17
1500	4.14	0.49	2.90	12.00	-21.77	1.66	4.29	1.07	0.84	0.92
1500	4.14	0.71	34.38	5.87	-57.00	26.79	13.69	5.42	3.66	3.55
1500	4.14	0.77	63.58	-31.12	-108.88	122.37	8.44	9.51	9.60	13.70
1500	6.21	0.03	0.28	8.54	-9.31	1.38	0.32	0.30	0.72	1.03
1500	6.21	0.45	1.03	11.69	-19.11	1.64	3.34	1.26	0.59	1.01
1500	6.21	0.7	29.93	6.85	-51.17	20.99	29.63	42.45	13.97	22.23
1500	6.21	0.8	79.55	-49.77	-125.13	140.33	8.92	10.99	8.09	9.21
1500	8.28	0.05	0.15	6.74	-8.12	2.10	0.24	2.49	0.57	2.54
1500	8.28	0.44	-0.09	10.74	-15.71	1.35	8.54	1.85	13.98	0.79
1500	8.28	0.72	42.85	2.88	-56.60	26.43	14.88	6.31	3.84	2.20
1500	8.28	0.8	88.28	-44.18	-118.73	115.72	21.88	23.25	32.17	37.33
3000	2.07	0.05	0.26	14.28	-14.87	1.61	0.36	0.56	0.86	1.17
3000	2.07	0.44	0.88	15.78	-24.11	5.78	1.47	1.25	1.75	1.58
3000	2.07	0.59	18.63	13.73	-40.11	23.06	1.79	1.96	1.05	1.06
3000	2.07	0.71	49.42	-10.99	-102.91	130.13	1.43	1.58	2.05	3.45
3000	4.14	0.006	1.79	17.59	-22.43	1.75	6.59	5.64	21.36	3.53
3000	4.14	0.42	0.05	18.66	-27.52	2.80	1.48	0.87	0.97	1.03
3000	4.14	0.64	33.25	8.97	-57.21	33.98	2.76	2.73	2.31	1.94
3000	4.14	0.75	68.55	-23.76	-122.42	141.22	1.01	1.64	4.47	7.65
3000	6.21	0.03	-0.78	13.36	-18.04	1.31	3.33	1.97	7.43	2.15
3000	6.21	0.39	1.02	17.99	-26.49	2.64	1.16	0.51	0.70	0.64
3000	6.21	0.66	37.99	14.15	-59.92	28.29	2.74	2.34	2.16	1.80
3000	6.21	0.76	82.35	-31.88	-133.52	140.84	1.44	2.25	4.76	5.99
3000	8.28	0.03	0.56	13.62	-14.93	1.72	0.31	0.58	0.93	1.38
3000	8.28	0.4	0.10	14.29	-24.05	-0.43	4.78	14.32	4.97	8.42
3000	8.28	0.67	49.70	10.86	-68.01	30.08	3.32	2.31	2.95	1.99
3000	8.28	0.78	98.28	-41.15	-155.30	164.13	3.50	3.35	4.95	5.40

Table B.2: Speed, pressure drop, eccentricity ratio, and stiffness coefficients of the 1X clearance smooth seals

Speed	ΔP	ε_o	Kxx	Kxy	Kyx	Kyy	eKxx	eKxy	eKyx	eKyy
RPM	bar	-	MN/m	MN/m	MN/m	MN/m	MN/m	MN/m	MN/m	MN/m
4500	2.07	0.07	0.78	14.40	-16.01	1.57	0.44	0.23	0.97	1.45
4500	2.07	0.44	2.50	15.65	-25.12	2.81	1.68	0.41	1.62	0.83
4500	2.07	0.6	24.85	6.43	-50.20	32.33	1.97	2.17	1.26	1.48
4500	2.07	0.71	57.27	-14.97	-111.02	135.07	1.59	2.20	2.44	3.97
4500	4.14	0.05	1.78	18.91	-21.58	2.89	0.55	0.30	1.37	1.89
4500	4.14	0.44	3.88	21.40	-32.10	2.74	1.76	0.68	2.15	0.89
4500	4.14	0.65	50.59	6.11	-79.78	52.89	3.27	3.74	2.73	3.00
4500	4.14	0.71	82.28	-26.55	-143.32	153.79	2.49	1.75	4.59	4.66
4500	6.21	0.03	1.84	20.37	-23.60	3.49	0.74	1.04	1.67	1.37
4500	6.21	0.45	4.40	25.26	-38.11	3.73	1.53	0.86	1.74	1.57
4500	6.21	0.66	61.09	5.21	-85.22	46.36	3.36	2.61	3.37	3.00
4500	6.21	0.75	103.89	-36.00	-161.66	170.87	2.65	1.69	6.41	5.40
4500	8.28	0.04	2.93	21.92	-23.85	3.05	1.59	1.03	1.36	2.05
4500	8.28	0.43	3.31	27.01	-39.24	3.68	1.44	0.58	1.07	0.98
4500	8.28	0.67	66.54	12.72	-90.59	41.97	4.19	3.38	4.08	2.58
4500	8.28	0.75	114.97	-45.23	-182.86	194.12	3.56	1.76	4.13	4.34
6000	2.07	0.06	1.12	17.53	-19.45	2.03	0.51	0.38	1.37	1.71
6000	2.07	0.49	11.35	17.35	-31.04	6.07	1.38	1.06	1.08	0.82
6000	2.07	0.61	36.42	2.40	-65.62	42.68	2.84	2.38	2.01	1.57
6000	2.07	0.71	77.66	-28.76	-143.61	176.29	2.09	2.12	3.42	4.60
6000	4.14	0.07	2.28	20.68	-23.11	2.21	0.66	0.39	1.49	1.43
6000	4.14	0.44	8.22	25.14	-37.51	2.19	2.53	1.77	2.52	0.93
6000	4.14	0.6	52.34	2.80	-82.21	50.27	2.91	2.24	3.17	2.42
6000	4.14	0.71	115.83	-52.19	-203.21	257.85	2.27	2.63	5.00	6.64
6000	6.21	0.08	2.77	22.67	-25.10	3.36	0.61	0.70	1.88	2.07
6000	6.21	0.44	8.84	28.95	-41.37	3.65	2.43	1.02	2.16	1.21
6000	6.21	0.62	72.77	-0.73	-97.63	61.23	2.68	1.93	7.50	4.63
6000	6.21	0.71	122.46	-57.21	-203.03	250.21	1.77	2.13	3.94	6.56
6000	8.28	0.09	3.12	23.75	-26.85	3.86	0.48	0.78	2.46	2.80
6000	8.28	0.46	11.47	32.27	-48.89	4.48	3.22	1.22	1.70	1.24
6000	8.28	0.63	88.60	1.39	-111.01	59.04	19.95	11.11	18.49	14.17
6000	8.28	0.73	140.72	-71.41	-233.14	303.70	2.97	1.54	7.81	5.87

Table B.3: Speed, pressure drop, eccentricity ratio, and damping coefficients of the 1X clearance smooth seals

Speed	ΔP	ε_o	Cxx	Cxy	Cyx	Cyy	eCxx	eCxy	eCyx	eCyy
RPM	bar	-	kN-s/m	kN-s/m	kN-s/m	kN-s/m	kN-s/m	kN-s/m	kN-s/m	kN-s/m
1500	2.07	0.03	99.87	1.28	-1.35	107.54	1.35	0.65	1.18	3.49
1500	2.07	0.47	234.37	-9.53	-9.52	145.50	12.48	3.63	1.46	2.74
1500	2.07	0.65	215.43	-145.70	-140.98	258.46	17.87	15.31	12.82	19.37
1500	2.07	0.76	163.65	-178.20	-156.10	556.79	54.66	97.63	114.79	197.46
1500	4.14	0.03	105.08	2.02	5.88	115.42	7.16	2.90	23.16	7.12
1500	4.14	0.49	261.85	-7.37	-4.28	151.90	8.12	2.89	1.38	1.83
1500	4.14	0.71	466.82	-200.51	-170.86	276.79	73.16	35.31	35.26	17.76
1500	4.14	0.77	200.53	-227.29	-188.45	597.80	25.37	32.49	29.47	42.02
1500	6.21	0.03	107.54	1.09	-1.76	116.08	1.04	1.02	1.02	1.68
1500	6.21	0.45	235.57	-3.82	-2.73	148.69	8.01	3.46	1.67	2.15
1500	6.21	0.7	480.17	-146.83	-136.13	215.56	64.53	59.74	43.46	47.74
1500	6.21	0.8	214.01	-223.85	-178.98	604.93	42.32	59.46	49.03	71.60
1500	8.28	0.05	99.26	1.33	-1.25	105.01	1.20	4.02	1.63	4.80
1500	8.28	0.44	194.01	-1.80	-5.76	137.12	52.91	1.57	12.61	3.16
1500	8.28	0.72	411.28	-194.75	-183.17	263.22	34.09	18.19	11.84	12.18
1500	8.28	0.8	263.98	-239.16	-208.83	610.54	105.41	97.42	186.60	152.55
3000	2.07	0.05	83.42	2.78	-4.66	88.19	1.37	2.91	1.56	4.59
3000	2.07	0.44	159.38	-20.83	-26.85	101.38	3.39	2.81	3.10	4.03
3000	2.07	0.59	172.05	-101.67	-101.13	190.97	4.97	5.13	3.32	3.92
3000	2.07	0.71	127.21	-144.10	-118.03	463.43	4.46	6.18	8.60	12.18
3000	4.14	0.006	86.17	0.56	-7.97	108.76	56.76	4.54	35.89	13.51
3000	4.14	0.42	174.16	-6.50	-8.75	113.86	4.11	2.21	2.86	2.73
3000	4.14	0.64	211.33	-130.99	-123.25	223.51	4.74	5.71	6.83	6.85
3000	4.14	0.75	151.89	-170.14	-133.13	477.31	8.32	9.46	18.27	22.08
3000	6.21	0.03	80.60	2.28	-4.80	94.83	17.77	1.47	17.71	4.62
3000	6.21	0.39	165.07	-3.11	-5.51	121.81	2.54	1.38	1.70	2.64
3000	6.21	0.66	270.78	-138.48	-126.97	211.61	6.28	5.31	9.08	8.09
3000	6.21	0.76	178.91	-188.61	-144.31	464.10	8.04	9.92	15.24	16.94
3000	8.28	0.03	89.02	1.92	-2.17	93.54	1.00	1.09	1.42	1.59
3000	8.28	0.4	164.85	-8.99	-1.21	112.11	7.00	19.68	10.21	39.11
3000	8.28	0.67	288.73	-147.18	-136.70	218.63	6.71	4.70	9.21	8.82
3000	8.28	0.78	181.69	-191.99	-136.11	471.44	13.63	18.28	14.86	20.58

Table B.4: Speed, pressure drop, eccentricity ratio, and damping coefficients of the 1X clearance smooth seals

Speed	ΔP	ε_o	Cxx	Cxy	Cyx	Cyy	eCxx	eCxy	eCyx	eCyy
RPM	bar	-	kN-s/m	kN-s/m	kN-s/m	kN-s/m	kN-s/m	kN-s/m	kN-s/m	kN-s/m
4500	2.07	0.07	63.11	3.79	-6.58	65.31	0.95	1.03	1.64	2.00
4500	2.07	0.44	119.73	-7.38	-16.21	71.95	4.33	1.68	3.87	2.13
4500	2.07	0.6	113.83	-72.27	-75.78	151.65	5.58	5.90	4.32	4.34
4500	2.07	0.71	99.72	-109.43	-94.10	342.48	3.07	3.44	10.65	9.38
4500	4.14	0.05	84.98	3.22	-6.39	86.30	2.14	1.10	2.73	2.23
4500	4.14	0.44	155.09	-7.11	-15.69	96.04	5.65	1.44	5.79	2.64
4500	4.14	0.65	158.60	-109.40	-102.69	215.79	32.01	6.06	20.56	7.46
4500	4.14	0.71	127.08	-128.60	-99.20	373.12	4.95	5.00	12.20	16.61
4500	6.21	0.03	91.85	2.48	-3.79	97.03	5.14	2.17	2.54	2.60
4500	6.21	0.45	172.25	-7.06	-12.38	106.24	5.12	2.33	5.47	3.91
4500	6.21	0.66	183.25	-114.02	-103.52	199.84	6.78	5.58	7.75	5.25
4500	6.21	0.75	152.39	-157.09	-110.61	435.14	8.73	17.67	17.95	47.95
4500	8.28	0.04	92.13	2.72	-7.78	103.37	8.39	1.86	9.74	2.82
4500	8.28	0.43	169.63	-3.24	-8.79	116.26	3.21	1.82	3.15	2.08
4500	8.28	0.67	239.87	-128.39	-112.30	203.21	7.97	7.46	10.99	7.10
4500	8.28	0.75	148.63	-153.83	-99.62	409.45	9.24	9.82	12.21	14.57
6000	2.07	0.06	58.39	5.25	-8.60	59.45	1.86	1.21	2.35	1.73
6000	2.07	0.49	97.73	-21.79	-30.78	67.83	4.82	4.23	4.04	3.75
6000	2.07	0.61	97.47	-63.67	-68.15	142.02	9.47	8.17	4.62	5.50
6000	2.07	0.71	91.07	-98.11	-77.33	314.31	4.74	2.74	10.43	11.99
6000	4.14	0.07	69.09	4.87	-9.70	71.82	2.37	1.10	2.67	1.57
6000	4.14	0.44	133.52	-10.06	-19.38	79.17	7.65	4.00	7.51	4.30
6000	4.14	0.6	120.90	-77.38	-78.64	171.28	11.23	5.27	10.29	6.56
6000	4.14	0.71	104.53	-111.43	-65.50	387.87	9.13	8.68	17.58	20.55
6000	6.21	0.08	76.37	4.72	-8.68	78.28	2.25	2.06	3.67	7.39
6000	6.21	0.44	150.82	-7.84	-19.20	92.61	4.69	1.74	5.41	3.28
6000	6.21	0.62	144.85	-100.63	-90.93	200.95	6.85	5.24	8.45	9.46
6000	6.21	0.71	103.27	-108.27	-63.79	376.35	5.42	7.43	13.17	16.12
6000	8.28	0.09	83.68	2.57	-9.07	87.29	2.62	0.86	3.48	2.63
6000	8.28	0.46	168.92	-11.95	-22.81	100.45	6.11	2.77	7.48	3.26
6000	8.28	0.63	168.60	-105.48	-76.60	193.94	33.63	4.22	69.90	13.41
6000	8.28	0.73	109.65	-117.23	-61.47	436.46	10.69	12.89	24.59	24.96

Table B.5: Speed, pressure drop, eccentricity ratio, and virtual mass coefficients of the 1X clearance smooth seals

Speed	ΔP	ε_o	Mxx	Mxy	Myx	Myy	eMxx	eMxy	eMyx	eMyy
RPM	bar	-	kg	kg	kg	kg	kg	kg	kg	kg
1500	2.07	0.03	13.18	-5.91	-6.33	21.84	0.67	1.10	1.90	1.79
1500	2.07	0.47	6.13	-1.68	4.71	6.07	5.48	1.45	6.51	1.56
1500	2.07	0.65	-38.26	45.39	38.14	-21.93	5.96	4.35	4.98	6.19
1500	2.07	0.76	-50.15	81.85	75.68	-97.14	14.71	20.21	27.59	31.87
1500	4.14	0.03	8.88	-13.23	12.50	31.67	5.24	16.73	21.22	22.72
1500	4.14	0.49	9.48	-3.00	1.37	3.78	3.50	1.73	4.35	1.95
1500	4.14	0.71	-94.97	76.28	61.66	-40.18	19.54	10.58	9.79	8.30
1500	4.14	0.77	-53.50	96.75	67.64	-94.10	11.27	15.35	12.26	20.71
1500	6.21	0.03	13.42	-4.44	-11.63	21.65	0.54	4.04	2.40	6.21
1500	6.21	0.45	12.15	-2.66	-4.72	5.94	6.93	6.93	8.16	3.86
1500	6.21	0.7	-42.27	35.34	38.01	-13.26	29.11	27.40	32.01	16.77
1500	6.21	0.8	-59.92	102.21	73.88	-96.96	15.05	20.74	15.96	26.27
1500	8.28	0.05	14.29	-8.07	-8.38	20.47	0.71	2.37	1.42	3.58
1500	8.28	0.44	15.15	-3.10	-3.75	9.80	5.27	1.46	8.15	1.39
1500	8.28	0.72	-81.25	70.70	61.52	-33.19	11.18	6.01	4.13	4.61
1500	8.28	0.8	-70.53	115.63	92.43	-115.76	23.05	30.10	25.50	36.44
3000	2.07	0.05	12.72	-1.97	-4.87	18.74	0.61	0.99	1.39	1.95
3000	2.07	0.44	12.22	3.02	1.66	10.69	1.17	1.05	1.62	1.67
3000	2.07	0.59	-12.62	20.22	12.97	0.46	12.32	7.16	13.42	8.72
3000	2.07	0.71	-26.48	52.59	37.18	-41.94	2.65	3.09	4.14	8.72
3000	4.14	0.006	5.99	-0.11	17.02	17.79	5.50	5.37	24.11	5.33
3000	4.14	0.42	14.45	0.14	-0.32	11.74	1.14	1.31	1.37	2.49
3000	4.14	0.64	-13.58	29.53	12.76	-6.99	21.59	8.22	25.58	10.41
3000	4.14	0.75	-31.15	62.58	41.72	-52.47	3.93	4.26	5.10	9.99
3000	6.21	0.03	15.05	0.25	14.20	18.43	3.82	2.94	20.93	1.81
3000	6.21	0.39	14.13	-1.61	-1.01	11.79	1.28	1.10	1.33	1.69
3000	6.21	0.66	-33.40	36.05	30.00	-13.90	4.72	2.38	2.26	2.51
3000	6.21	0.76	-39.98	69.85	46.86	-56.94	5.73	6.25	6.47	10.07
3000	8.28	0.03	11.37	-4.09	-5.91	19.94	0.47	0.49	1.46	1.70
3000	8.28	0.4	15.70	-39.05	-2.60	2.45	5.36	35.25	5.51	9.42
3000	8.28	0.67	-28.87	36.85	29.27	-11.38	5.84	2.66	3.37	3.82
3000	8.28	0.78	-39.28	74.85	47.57	-55.00	6.30	7.92	8.05	12.36

Table B.6: Speed, pressure drop, eccentricity ratio, and virtual mass coefficients of the 1X clearance smooth seals

Speed	ΔP	ε_o	Mxx	Mxy	Myx	Myy	eMxx	eMxy	eMyx	eMyy
RPM	bar	-	kg	kg	kg	kg	kg	kg	kg	kg
4500	2.07	0.07	13.66	-3.79	-9.34	32.64	1.02	0.56	2.77	3.55
4500	2.07	0.44	14.96	0.88	1.14	11.24	2.00	0.74	1.14	1.33
4500	2.07	0.6	-3.51	7.63	6.97	6.00	1.88	1.79	1.44	1.91
4500	2.07	0.71	-13.92	29.63	19.72	-13.53	1.47	1.70	2.87	4.06
4500	4.14	0.05	14.77	-8.06	-9.77	40.66	1.44	1.59	5.62	6.31
4500	4.14	0.44	16.84	0.40	2.82	10.23	2.01	0.88	1.38	1.17
4500	4.14	0.65	-14.67	25.49	19.36	-8.24	2.04	2.35	1.95	2.37
4500	4.14	0.71	-17.24	39.16	20.74	-22.22	2.07	1.46	3.50	6.54
4500	6.21	0.03	12.55	-5.63	-5.38	21.43	3.01	1.71	5.27	2.57
4500	6.21	0.45	17.62	0.28	2.08	9.71	1.45	0.61	1.20	1.41
4500	6.21	0.66	-6.51	24.31	2.30	4.40	7.88	2.04	18.06	16.51
4500	6.21	0.75	-18.14	43.46	2.10	-10.58	11.27	9.58	36.80	31.82
4500	8.28	0.04	11.08	-1.36	-5.49	19.35	1.17	4.59	1.72	1.34
4500	8.28	0.43	14.94	-1.15	0.46	12.49	2.38	1.10	1.41	1.63
4500	8.28	0.67	-17.32	27.60	15.24	-5.24	4.18	2.40	9.24	7.82
4500	8.28	0.75	-26.65	52.85	26.44	-32.63	4.09	3.85	3.54	6.47
6000	2.07	0.06	12.97	-0.81	-2.58	30.93	2.05	4.73	4.90	5.54
6000	2.07	0.49	9.82	2.67	-2.54	10.68	1.98	3.66	2.99	3.33
6000	2.07	0.61	-1.97	7.04	4.58	5.84	1.85	2.20	2.52	2.85
6000	2.07	0.71	-7.92	24.02	12.62	-4.43	1.70	1.38	3.54	6.13
6000	4.14	0.07	16.20	-8.11	8.93	31.84	1.78	1.95	14.15	6.39
6000	4.14	0.44	18.16	0.67	1.79	8.11	3.18	1.48	1.87	1.43
6000	4.14	0.6	-2.68	10.67	5.95	3.36	1.88	1.78	3.01	3.72
6000	4.14	0.71	-10.01	31.86	8.18	-7.44	1.95	1.89	4.75	10.12
6000	6.21	0.08	15.72	-8.12	-2.58	46.94	2.67	1.81	7.95	13.49
6000	6.21	0.44	27.43	0.78	11.43	11.84	8.85	1.02	7.61	1.80
6000	6.21	0.62	-8.34	17.65	11.96	-1.30	1.99	2.34	5.95	7.07
6000	6.21	0.71	-9.90	30.13	7.15	-3.94	2.02	1.88	4.95	9.38
6000	8.28	0.09	16.86	-10.23	-3.69	42.89	2.98	3.24	7.23	13.42
6000	8.28	0.46	18.74	1.13	2.83	9.24	3.95	1.41	1.31	1.37
6000	8.28	0.63	0.35	15.63	-12.38	9.16	15.79	7.63	47.39	24.40
6000	8.28	0.73	-11.75	36.07	6.51	-12.31	2.85	2.87	6.18	8.37

Table B.7: Speed, pressure drop, eccentricity ratio, and stiffness coefficients of the 1X clearance LOD pressure-dam seals

Speed	ΔP	ε_o	Kxx	Kxy	Kyx	Kyy	eKxx	eKxy	eKyx	eKyy
RPM	bar	-	MN/m	MN/m	MN/m	MN/m	MN/m	MN/m	MN/m	MN/m
1500	2.07	0.05	4.11	7.26	-8.04	2.53	1.42	0.87	0.47	1.28
1500	2.07	0.28	5.23	4.89	-6.31	3.95	1.42	0.62	0.79	0.76
1500	2.07	0.48	8.35	3.63	-7.32	4.40	0.95	1.53	1.71	3.90
1500	2.07	0.65	19.02	6.86	-14.90	6.84	2.11	0.88	1.11	1.46
1500	4.14	0.049	-0.04	8.42	-9.09	1.03	0.62	1.40	0.82	0.53
1500	4.14	0.33	-4.60	9.04	-10.29	4.41	1.21	0.77	0.61	0.66
1500	4.14	0.61	11.99	5.89	-6.48	4.24	2.09	0.41	1.32	0.56
1500	4.14	0.7	38.62	1.01	-23.56	8.88	2.78	3.18	2.29	3.46
1500	6.21	0.057	0.14	8.99	-9.10	1.32	0.24	0.16	0.34	0.50
1500	6.21	0.3	-4.38	10.02	-10.60	4.54	1.10	0.50	0.55	0.55
1500	6.21	0.57	3.17	10.92	-8.68	5.48	1.68	1.11	0.90	1.05
1500	6.21	0.78	34.03	-2.87	-15.65	6.92	2.08	0.67	1.92	1.31
1500	8.28	0.04	0.41	8.34	-8.45	1.90	1.22	0.22	0.39	0.37
1500	8.28	0.32	-4.97	4.53	-9.74	1.53	3.34	6.98	2.60	5.68
1500	8.28	0.57	-10.26	15.42	-18.61	7.29	3.38	1.47	1.58	1.08
1500	8.28	0.77	17.62	20.50	-24.67	15.21	6.64	3.74	3.11	2.38
3000	2.07	0.05	6.23	9.84	-10.09	5.42	1.59	1.45	1.46	1.70
3000	2.07	0.27	6.05	6.31	-14.17	7.13	1.71	0.78	1.74	0.78
3000	2.07	0.61	14.70	12.44	-20.03	14.10	3.10	1.85	2.10	1.30
3000	2.07	0.79	40.25	5.47	-39.14	34.44	4.93	2.74	3.97	2.28
3000	4.14	0.28	6.11	9.19	-13.22	6.33	2.54	1.40	1.47	0.62
3000	4.14	0.57	19.26	3.21	-16.71	6.11	1.97	0.48	2.04	1.53
3000	4.14	0.69	43.25	6.53	-36.23	12.89	1.94	1.49	3.40	0.73
3000	6.21	0.04	1.08	16.72	-16.25	1.20	0.45	0.30	0.60	0.65
3000	6.21	0.25	0.85	15.82	-15.05	6.16	1.34	0.76	1.08	0.66
3000	6.21	0.55	13.87	9.62	-12.86	6.25	4.24	2.67	7.41	1.45
3000	6.21	0.7	54.37	2.67	-39.95	14.49	1.39	0.85	2.04	0.79
3000	8.28	0.05	1.30	17.08	-16.52	1.51	0.31	0.25	0.50	0.42
3000	8.28	0.29	-6.30	18.78	-18.18	7.44	0.74	0.56	0.47	0.71
3000	8.28	0.6	3.81	18.09	-19.50	10.18	1.31	0.60	1.53	0.95
3000	8.28	0.73	69.52	1.71	-54.22	19.46	4.30	0.80	2.50	1.81

Table B.8: Speed, pressure drop, eccentricity ratio, and stiffness coefficients of the 1X clearance LOD pressure-dam seals

Speed	ΔP	ε_o	Kxx	Kxy	Kyx	Kyy	eKxx	eKxy	eKyx	eKyy
RPM	bar	-	MN/m	MN/m	MN/m	MN/m	MN/m	MN/m	MN/m	MN/m
4500	2.07	0.05	5.94	10.99	-11.89	4.82	0.86	1.35	1.19	1.12
4500	2.07	0.28	3.75	6.50	-16.88	9.02	1.34	0.66	2.25	0.92
4500	2.07	0.51	1.78	4.36	-22.41	20.04	5.47	2.29	2.47	1.43
4500	2.07	0.71	26.33	8.97	-32.94	33.00	6.84	3.78	4.73	2.44
4500	4.14	0.05	5.34	14.84	-17.58	6.51	0.65	2.02	1.23	1.76
4500	4.14	0.23	5.56	11.17	-20.36	9.22	1.51	1.62	1.61	0.77
4500	4.14	0.45	14.20	7.57	-23.23	12.23	0.75	1.06	1.86	1.01
4500	4.14	0.66	44.63	13.06	-40.18	19.12	2.74	1.34	2.41	0.85
4500	6.21	0.05	3.00	20.63	-21.31	-0.26	1.12	1.15	0.52	3.89
4500	6.21	0.23	1.66	18.66	-21.83	8.14	1.58	0.63	1.08	0.59
4500	6.21	0.46	15.62	6.88	-19.34	10.60	8.00	2.35	13.06	3.75
4500	6.21	0.65	52.45	7.20	-43.73	18.03	2.19	0.79	2.70	0.86
4500	8.28	0.05	2.45	22.36	-23.18	1.15	0.41	0.56	0.73	0.81
4500	8.28	0.26	1.40	20.54	-21.00	8.50	1.80	1.09	1.44	1.36
4500	8.28	0.51	14.16	12.90	-21.30	8.55	2.68	1.49	2.31	1.41
4500	8.28	0.66	56.78	2.60	-45.44	18.43	2.58	0.77	2.52	0.74
6000	2.07	0.07	6.84	14.16	-15.13	4.96	0.72	1.79	1.28	0.61
6000	2.07	0.24	8.43	8.78	-19.79	6.93	1.04	0.55	2.82	1.09
6000	2.07	0.56	12.79	8.78	-27.49	23.30	2.27	0.96	1.14	1.31
6000	2.07	0.77	46.02	0.32	-51.61	65.36	3.77	2.06	3.07	1.75
6000	4.14	0.06	7.69	16.64	-18.18	6.24	0.87	2.19	1.77	1.08
6000	4.14	0.23	6.87	12.30	-21.92	10.04	0.92	1.06	2.26	0.65
6000	4.14	0.48	20.69	10.62	-29.19	15.83	1.70	0.84	1.06	1.07
6000	4.14	0.64	50.51	12.61	-49.60	25.55	3.70	1.69	3.06	1.28
6000	6.21	0.06	8.01	19.05	-19.52	7.40	0.64	2.56	2.21	1.26
6000	6.21	0.24	7.13	16.16	-26.22	12.87	2.16	1.50	3.30	1.87
6000	6.21	0.46	18.20	10.14	-30.17	14.57	1.26	0.73	2.45	1.42
6000	6.21	0.62	50.89	9.86	-47.55	22.34	2.37	1.35	2.48	1.67
6000	8.28	0.07	7.49	25.84	-25.32	3.18	0.86	1.15	1.06	1.00
6000	8.28	0.24	5.94	17.23	-26.24	11.71	2.18	2.46	1.38	1.06
6000	8.28	0.47	16.96	11.03	-28.43	13.26	1.39	1.44	2.04	0.52
6000	8.28	0.61	52.63	6.56	-46.00	19.02	0.82	0.58	3.12	1.04

Table B.9: Speed, pressure drop, eccentricity ratio, and damping coefficients of the 1X clearance LOD pressure-dam seals

Speed	ΔP	ε_o	Cxx	Cxy	Cyx	Cyy	eCxx	eCxy	eCyx	eCyy
RPM	bar	-	kN-s/m	kN-s/m	kN-s/m	kN-s/m	kN-s/m	kN-s/m	kN-s/m	kN-s/m
1500	2.07	0.05	47.15	-3.62	4.08	49.88	5.43	3.61	1.12	5.89
1500	2.07	0.28	35.94	-10.67	-10.22	59.85	5.32	2.06	2.82	2.65
1500	2.07	0.48	56.00	-23.09	-27.22	65.08	4.08	6.78	3.21	4.05
1500	2.07	0.65	145.03	-79.28	-80.23	116.90	10.07	5.46	6.14	3.41
1500	4.14	0.049	67.44	2.51	0.28	66.09	1.30	0.57	0.59	3.73
1500	4.14	0.33	95.98	13.24	18.24	69.18	2.71	2.29	0.96	1.09
1500	4.14	0.61	59.52	-18.82	-18.46	56.34	7.48	1.93	5.08	1.77
1500	4.14	0.7	176.00	-90.91	-93.41	121.89	12.60	6.50	6.70	5.64
1500	6.21	0.057	68.79	2.82	0.50	68.20	1.22	0.78	0.77	1.69
1500	6.21	0.3	95.37	18.75	16.49	75.62	1.85	0.72	0.79	0.97
1500	6.21	0.57	110.83	17.33	17.51	78.40	8.10	2.09	5.25	1.46
1500	6.21	0.78	99.52	-39.40	-44.43	67.09	5.46	1.76	5.29	2.19
1500	8.28	0.04	65.97	2.33	-0.85	66.76	0.95	0.76	3.33	1.74
1500	8.28	0.32	101.38	20.88	18.79	67.19	3.76	28.88	3.13	20.80
1500	8.28	0.57	222.48	79.24	82.12	112.81	6.67	4.75	3.68	1.90
1500	8.28	0.77	281.70	42.21	59.30	105.65	37.10	16.25	20.25	9.80
3000	2.07	0.05	29.41	-6.43	6.56	31.26	6.13	7.88	6.86	6.55
3000	2.07	0.27	30.21	-11.78	-7.45	54.41	6.39	4.27	5.67	3.54
3000	2.07	0.61	93.60	-50.60	-49.89	104.69	10.66	5.98	6.88	7.17
3000	2.07	0.79	123.73	-87.47	-78.31	175.32	13.75	9.20	11.74	13.31
3000	4.14	0.28	34.88	-9.78	-4.63	55.30	8.92	5.85	5.86	1.76
3000	4.14	0.57	58.52	-26.94	-29.37	61.50	5.10	2.75	8.38	2.56
3000	4.14	0.69	135.57	-75.21	-77.62	114.16	5.79	4.82	6.84	3.25
3000	6.21	0.04	71.77	1.12	-1.85	72.79	1.13	1.11	1.54	1.29
3000	6.21	0.25	63.01	1.37	1.47	62.90	4.52	1.98	2.88	2.07
3000	6.21	0.55	48.85	-15.99	-15.99	51.66	14.26	3.51	10.38	7.92
3000	6.21	0.7	146.92	-77.04	-77.17	110.92	7.29	3.93	8.18	2.85
3000	8.28	0.05	66.54	1.93	-2.62	66.12	0.93	0.90	0.91	1.37
3000	8.28	0.29	83.67	15.69	11.41	68.31	1.66	1.07	1.68	1.32
3000	8.28	0.6	105.39	13.08	13.93	69.56	5.41	1.70	6.65	1.57
3000	8.28	0.73	168.08	-89.25	-81.54	121.63	12.07	4.53	11.25	4.79

Table B.10: Speed, pressure drop, eccentricity ratio, and damping coefficients of the 1X clearance LOD pressure-dam seals

Speed	ΔP	ε_o	Cxx	Cxy	Cyx	Cyy	eCxx	eCxy	eCyx	eCyy
RPM	bar	-	kN-s/m	kN-s/m	kN-s/m	kN-s/m	kN-s/m	kN-s/m	kN-s/m	kN-s/m
4500	2.07	0.05	21.62	-9.83	9.00	23.43	3.54	7.53	6.87	3.71
4500	2.07	0.28	25.63	-11.30	-2.37	39.65	3.51	2.75	10.00	2.62
4500	2.07	0.51	27.23	-10.42	-12.83	80.31	11.91	2.15	5.80	3.19
4500	2.07	0.71	74.57	-44.55	-44.66	129.93	14.78	10.06	11.48	7.53
4500	4.14	0.05	38.92	-6.07	10.51	39.09	2.70	6.98	5.86	6.13
4500	4.14	0.23	33.25	-10.74	-1.64	54.17	6.57	6.12	6.68	1.69
4500	4.14	0.45	43.84	-19.47	-18.46	60.60	3.56	3.84	6.75	2.29
4500	4.14	0.66	111.41	-61.15	-56.63	103.33	7.09	6.50	5.81	4.64
4500	6.21	0.05	57.85	-9.56	-3.37	59.58	3.34	10.11	4.31	6.44
4500	6.21	0.23	50.04	-6.70	2.20	61.05	7.52	4.30	4.13	2.65
4500	6.21	0.46	41.04	-17.17	-3.12	50.54	16.42	9.81	45.33	14.40
4500	6.21	0.65	110.19	-54.50	-52.59	90.40	6.42	4.58	8.15	4.17
4500	8.28	0.05	65.67	-1.90	-4.27	63.55	1.33	1.15	1.12	1.30
4500	8.28	0.26	62.83	-1.56	0.19	61.48	5.95	2.52	7.18	2.53
4500	8.28	0.51	52.00	-17.60	-16.96	55.81	10.93	4.91	14.02	4.54
4500	8.28	0.66	105.10	-50.26	-51.13	88.04	5.59	3.71	11.30	3.63
6000	2.07	0.07	20.64	-11.92	11.48	24.30	1.83	8.34	6.38	2.35
6000	2.07	0.24	23.63	-13.07	4.38	23.75	2.92	3.39	11.32	3.43
6000	2.07	0.56	37.08	-18.23	-19.21	73.96	7.34	3.40	3.59	2.31
6000	2.07	0.77	57.38	-34.36	-36.41	147.35	11.78	7.37	6.26	4.09
6000	4.14	0.06	27.24	-12.49	12.00	30.55	1.72	8.84	7.37	3.02
6000	4.14	0.23	29.74	-14.05	0.46	38.34	4.04	4.68	9.93	3.55
6000	4.14	0.48	49.37	-24.16	-22.16	65.80	5.02	3.75	4.59	3.24
6000	4.14	0.64	88.87	-50.07	-46.58	101.40	7.26	5.81	6.15	3.76
6000	6.21	0.06	34.47	-11.18	8.16	36.23	2.19	9.21	9.05	2.93
6000	6.21	0.24	36.16	-13.57	0.96	50.60	7.03	7.35	12.30	4.54
6000	6.21	0.46	43.97	-20.49	-13.36	56.02	5.02	4.45	10.43	3.17
6000	6.21	0.62	85.02	-45.33	-41.81	88.07	6.22	4.09	7.72	4.53
6000	8.28	0.07	50.41	-9.21	-0.41	51.93	2.98	4.53	5.09	2.02
6000	8.28	0.24	38.51	-10.34	-0.37	53.64	7.65	9.45	6.45	2.24
6000	8.28	0.47	42.95	-17.61	-9.07	50.48	6.27	6.40	8.19	2.30
6000	8.28	0.61	76.54	-37.45	-36.28	73.65	6.04	3.70	8.28	2.30

Table B.11: Speed, pressure drop, eccentricity ratio, and virtual mass coefficients of the 1X clearance LOD pressure-dam seals

Speed	ΔP	ε_o	Mxx	Mxy	Myx	Myy	eMxx	eMxy	eMyx	eMyy
RPM	bar	-	kg	kg	kg	kg	kg	kg	kg	kg
1500	2.07	0.05	6.57	1.33	-3.08	3.51	1.71	1.01	0.64	1.83
1500	2.07	0.28	10.02	2.78	1.27	12.72	1.23	0.52	0.61	1.16
1500	2.07	0.48	6.80	1.98	0.64	12.97	1.38	1.10	1.38	2.85
1500	2.07	0.65	-7.82	14.18	12.72	7.95	7.18	4.33	4.08	4.14
1500	4.14	0.049	15.65	-2.27	-0.07	16.95	0.54	1.40	0.83	1.29
1500	4.14	0.33	12.40	-18.28	-1.57	11.81	4.43	15.72	1.33	5.07
1500	4.14	0.61	10.41	0.45	-1.35	18.90	1.82	0.57	1.38	1.17
1500	4.14	0.7	-17.34	17.91	16.16	8.43	4.97	3.53	3.14	4.53
1500	6.21	0.057	16.21	-0.77	-0.69	18.09	0.55	0.26	0.47	0.96
1500	6.21	0.3	16.01	-0.66	-2.62	16.13	0.84	2.39	0.90	2.13
1500	6.21	0.57	2.85	-10.61	-7.21	12.59	2.02	0.99	1.78	1.19
1500	6.21	0.78	6.94	1.43	2.47	15.07	3.65	1.52	2.91	2.30
1500	8.28	0.04	16.18	-0.49	-0.72	18.85	0.75	0.78	0.50	1.10
1500	8.28	0.32	16.16	-12.55	-2.08	7.50	1.90	8.48	1.92	8.76
1500	8.28	0.57	-7.22	-20.93	-19.59	4.01	3.41	1.14	3.27	1.39
1500	8.28	0.77	-43.28	-34.68	-35.86	-3.84	14.75	9.12	9.58	3.49
3000	2.07	0.05	7.92	3.35	-4.09	5.83	2.02	2.24	2.30	2.05
3000	2.07	0.27	6.78	0.10	-1.41	3.90	2.12	1.51	3.04	1.67
3000	2.07	0.61	-3.44	6.65	4.41	10.19	4.92	2.82	3.43	2.31
3000	2.07	0.79	-19.60	23.18	18.06	3.97	4.64	3.59	4.76	4.72
3000	4.14	0.28	8.40	3.98	-0.04	13.40	2.27	1.16	1.59	3.68
3000	4.14	0.57	10.53	1.67	-0.04	12.07	4.64	4.24	5.79	5.08
3000	4.14	0.69	-2.75	8.93	8.17	8.23	3.50	3.09	2.51	1.99
3000	6.21	0.04	14.38	-1.16	0.13	16.57	0.54	0.39	0.90	1.14
3000	6.21	0.25	10.94	-1.25	-1.70	17.05	1.21	0.61	1.08	1.02
3000	6.21	0.55	9.23	1.11	0.03	16.34	3.66	2.07	4.87	1.86
3000	6.21	0.7	-3.73	8.79	6.05	9.26	4.88	3.25	3.00	2.15
3000	8.28	0.05	13.90	-1.39	-0.24	16.19	0.52	0.36	0.41	0.90
3000	8.28	0.29	14.37	-2.08	-1.17	15.66	1.10	0.50	0.58	0.99
3000	8.28	0.6	5.36	-9.96	-8.46	10.97	2.08	1.05	2.23	1.87
3000	8.28	0.73	-9.18	13.25	9.58	7.19	5.46	2.73	3.29	1.92

Table B.12: Speed, pressure drop, eccentricity ratio, and virtual mass coefficients of the 1X clearance LOD pressure-dam seals

Speed	ΔP	ε_o	Mxx	Mxy	Myx	Myy	eMxx	eMxy	eMyx	eMyy
RPM	bar	-	kg	kg	kg	kg	kg	kg	kg	kg
4500	2.07	0.05	4.78	5.33	-5.55	2.32	1.31	2.60	2.81	1.51
4500	2.07	0.28	4.25	-0.51	-6.44	0.33	1.48	1.01	2.08	2.05
4500	2.07	0.51	3.46	-1.83	-2.62	9.75	3.27	1.30	1.70	3.08
4500	2.07	0.71	-2.94	6.77	3.90	11.14	4.67	2.43	3.80	2.96
4500	4.14	0.05	5.58	3.56	-7.35	6.35	1.10	1.38	1.85	1.75
4500	4.14	0.23	6.25	5.53	-1.99	10.27	1.94	1.31	1.73	1.36
4500	4.14	0.45	6.58	1.84	-0.78	8.34	1.32	0.96	2.19	1.61
4500	4.14	0.66	-2.90	8.11	4.19	9.01	4.40	3.66	3.03	2.98
4500	6.21	0.05	6.61	0.65	-0.21	13.33	1.52	0.77	1.29	2.74
4500	6.21	0.23	2.00	4.08	-4.06	9.20	2.72	0.93	1.23	1.38
4500	6.21	0.46	7.08	1.90	-1.21	9.27	4.63	1.46	7.59	2.43
4500	6.21	0.65	2.31	1.70	-1.54	11.71	6.35	4.21	4.93	2.39
4500	8.28	0.05	7.03	-2.54	-1.80	13.43	0.67	0.61	1.70	1.19
4500	8.28	0.26	7.46	-0.87	-3.25	15.94	1.63	0.64	1.27	1.81
4500	8.28	0.51	7.20	1.80	-1.11	14.91	2.52	0.97	2.56	2.03
4500	8.28	0.66	0.62	1.65	1.03	11.79	1.97	1.71	2.84	1.72
6000	2.07	0.07	3.91	8.05	-9.63	0.78	0.73	2.23	2.03	1.47
6000	2.07	0.24	5.61	2.16	-9.80	4.48	1.12	1.18	4.45	1.32
6000	2.07	0.56	5.42	-0.93	-2.74	10.52	1.58	1.18	1.12	1.98
6000	2.07	0.77	0.96	2.79	1.22	13.54	2.36	2.40	2.36	2.67
6000	4.14	0.06	5.78	8.10	-9.58	1.71	0.89	2.01	2.05	1.76
6000	4.14	0.23	4.11	5.40	-6.00	7.44	1.23	1.17	2.26	1.84
6000	4.14	0.48	5.50	2.56	-3.24	10.56	1.27	1.26	2.00	1.86
6000	4.14	0.64	1.95	5.87	0.59	8.02	2.45	2.15	2.79	2.46
6000	6.21	0.06	6.87	7.70	-6.96	4.02	0.94	1.92	2.41	1.77
6000	6.21	0.24	4.55	7.25	-8.08	10.96	2.71	1.58	6.02	1.93
6000	6.21	0.46	6.88	3.28	-3.57	9.64	2.09	1.31	2.11	1.79
6000	6.21	0.62	4.49	3.40	-0.46	8.19	2.16	1.83	2.21	1.85
6000	8.28	0.07	6.20	4.26	-3.72	5.87	1.12	1.05	1.98	1.40
6000	8.28	0.24	6.04	5.84	-2.97	10.92	2.01	1.93	1.54	1.24
6000	8.28	0.47	6.06	3.99	-3.17	9.10	1.84	1.38	3.81	1.37
6000	8.28	0.61	4.90	1.06	-0.63	9.33	2.45	1.12	3.55	1.84

Table B.13: Speed, pressure drop, eccentricity ratio, and stiffness coefficients of the 1X clearance LOL pressure-dam seals

Speed	ΔP	ε_o	Kxx	Kxy	Kyx	Kyy	eKxx	eKxy	eKyx	eKyy
RPM	bar	-	MN/m	MN/m	MN/m	MN/m	MN/m	MN/m	MN/m	MN/m
1500	2.07	0.02	0.44	8.06	-8.62	1.76	0.11	0.11	0.59	1.19
1500	2.07	0.56	10.91	16.48	-14.29	-2.67	1.32	1.12	1.39	1.81
1500	2.07	0.75	19.39	12.97	-16.71	3.77	2.83	2.38	2.09	2.47
1500	2.07	0.89	34.70	14.91	-27.55	6.80	12.75	8.68	12.33	8.01
1500	4.14	0.01	0.71	7.84	-8.32	2.06	3.12	0.17	0.55	1.42
1500	4.14	0.44	8.13	12.63	-10.69	-2.85	4.33	1.52	5.14	1.76
1500	4.14	0.69	18.74	19.51	-24.16	-4.94	9.52	10.89	2.48	4.31
1500	4.14	0.79	31.18	35.05	-34.46	-13.74	5.41	8.88	4.33	6.94
1500	6.21	0.02	1.21	8.58	-9.44	2.05	0.16	0.13	0.40	1.12
1500	6.21	0.44	8.91	12.71	-12.95	-2.56	3.06	4.26	2.18	3.15
1500	6.21	0.68	17.34	23.52	-21.60	-7.65	1.38	1.80	1.79	1.78
1500	6.21	0.87	52.77	45.64	-46.61	-15.61	57.87	22.24	18.89	11.60
1500	8.28	0.03	1.92	8.37	-9.24	2.46	0.14	0.13	0.48	1.20
1500	8.28	0.47	8.54	12.85	-12.18	-2.10	0.79	0.74	0.95	1.08
1500	8.28	0.7	20.94	18.62	-17.42	-5.90	17.84	10.03	13.38	7.42
1500	8.28	0.79	30.83	31.96	-33.74	-9.44	38.55	57.51	40.59	47.42
3000	2.07	0.01	6.08	9.36	-9.43	6.07	1.23	1.42	1.16	2.00
3000	2.07	0.49	9.55	7.77	-8.44	6.69	1.22	2.75	0.81	2.11
3000	2.07	0.73	16.71	4.03	-12.19	13.26	1.81	4.00	1.04	2.63
3000	2.07	0.82	36.14	31.89	-27.38	1.12	3.36	2.46	2.07	1.92
3000	4.14	0.02	6.81	13.16	-13.33	4.64	2.30	1.27	1.13	1.92
3000	4.14	0.27	8.90	17.00	-12.81	-1.32	1.06	0.31	0.84	1.52
3000	4.14	0.55	22.29	25.84	-21.85	-6.22	1.08	0.80	1.61	1.31
3000	4.14	0.73	38.72	50.52	-38.20	-17.90	5.93	3.23	2.25	2.11
3000	6.21	0.04	1.40	14.77	-16.66	1.60	0.30	0.19	0.72	1.38
3000	6.21	0.41	12.84	20.31	-19.43	-4.02	1.79	0.69	0.80	0.99
3000	6.21	0.61	23.82	30.85	-27.33	-8.68	4.78	2.22	1.41	1.11
3000	6.21	0.76	46.21	53.42	-44.86	-19.87	4.41	2.32	2.06	1.80
3000	8.28	0.04	2.05	16.11	-18.10	1.59	0.24	0.23	0.54	1.25
3000	8.28	0.37	12.30	19.67	-19.39	-4.24	0.64	0.58	0.38	1.18
3000	8.28	0.68	28.60	33.51	-35.61	-11.93	1.98	1.38	1.40	1.41
3000	8.28	0.77	43.63	52.66	-48.88	-21.19	8.81	27.81	15.06	9.88

Table B.14: Speed, pressure drop, eccentricity ratio, and stiffness coefficients of the 1X clearance LOL pressure-dam seals

Speed	ΔP	ε_o	Kxx	Kxy	Kyx	Kyy	eKxx	eKxy	eKyx	eKyy
RPM	bar	-	MN/m	MN/m	MN/m	MN/m	MN/m	MN/m	MN/m	MN/m
4500	2.07	0.01	6.14	11.95	-12.23	5.16	0.55	1.11	0.92	1.37
4500	2.07	0.49	9.17	10.79	-7.73	8.22	1.83	2.77	0.68	1.36
4500	2.07	0.75	13.07	7.65	-10.37	19.85	2.42	3.43	1.08	1.40
4500	2.07	0.86	23.97	4.49	-21.37	32.80	2.42	4.19	1.90	2.49
4500	4.14	0.01	7.32	13.59	-14.07	7.91	1.25	2.38	2.09	1.62
4500	4.14	0.31	12.49	21.37	-14.97	3.08	1.33	1.89	1.28	1.51
4500	4.14	0.72	33.29	26.61	-27.92	4.67	1.94	1.36	1.64	0.98
4500	4.14	0.83	47.41	35.11	-41.28	6.35	3.32	1.59	2.23	1.30
4500	6.21	0.17	5.30	18.51	-19.62	7.38	1.12	1.67	1.59	1.19
4500	6.21	0.25	12.70	22.16	-18.59	2.06	0.72	1.67	0.88	2.00
4500	6.21	0.59	32.88	38.62	-31.18	-9.22	1.88	0.82	1.75	0.81
4500	6.21	0.72	53.65	60.36	-48.62	-17.86	2.72	1.59	3.77	1.46
4500	8.28	0.01	1.38	23.01	-24.64	3.89	0.44	0.23	0.64	1.61
4500	8.28	0.23	11.20	24.92	-22.51	-0.81	0.40	0.37	0.86	1.38
4500	8.28	0.57	30.91	35.72	-33.08	-8.31	1.57	0.91	1.83	0.97
4500	8.28	0.77	63.71	68.51	-58.71	-23.14	3.73	2.31	4.14	1.34
6000	2.07	0.02	6.94	13.64	-15.19	5.45	0.43	1.99	1.37	1.64
6000	2.07	0.37	7.84	15.41	-9.63	8.76	1.40	3.62	0.58	1.15
6000	2.07	0.76	17.45	9.82	-16.21	25.52	4.70	5.91	2.14	2.93
6000	2.07	0.83	21.12	4.56	-22.49	40.88	6.29	6.20	3.10	3.06
6000	4.14	0.01	7.68	17.55	-19.69	8.12	0.67	2.17	1.85	1.40
6000	4.14	0.26	11.11	21.89	-15.70	7.22	1.75	4.18	0.82	1.59
6000	4.14	0.61	28.07	30.56	-24.08	4.90	2.84	2.83	1.49	1.27
6000	4.14	0.8	53.86	37.47	-46.26	11.40	6.02	2.65	4.22	2.29
6000	6.21	0.01	8.09	18.78	-23.09	6.10	1.01	2.37	1.30	1.72
6000	6.21	0.2	11.59	24.71	-20.57	4.02	1.32	2.44	1.10	1.71
6000	6.21	0.51	31.59	41.30	-30.03	-7.36	2.32	1.24	2.38	2.29
6000	6.21	0.77	49.62	32.06	-42.26	9.71	3.46	5.00	3.12	3.08
6000	8.28	0.01	1.55	26.98	-28.04	5.13	0.50	0.53	1.75	2.06
6000	8.28	0.018	10.82	29.40	-26.66	-0.36	0.68	0.48	1.20	1.87
6000	8.28	0.42	25.45	36.49	-30.72	-5.07	1.13	0.91	1.87	1.17
6000	8.28	0.7	57.13	62.79	-52.42	-17.76	4.37	2.17	3.62	3.40

Table B.15: Speed, pressure drop, eccentricity ratio, and damping coefficients of the 1X clearance LOL pressure-dam seals

Speed	ΔP	ε_o	Cxx	Cxy	Cyx	Cyy	eCxx	eCxy	eCyx	eCyy
RPM	bar	-	kN-s/m	kN-s/m	kN-s/m	kN-s/m	kN-s/m	kN-s/m	kN-s/m	kN-s/m
1500	2.07	0.02	64.50	1.26	-0.73	66.96	0.93	0.48	1.23	2.07
1500	2.07	0.56	187.31	-69.75	-75.03	103.25	2.07	2.64	1.88	3.47
1500	2.07	0.75	128.73	-64.49	-62.74	97.00	15.03	14.73	6.55	7.47
1500	2.07	0.89	154.79	-99.82	-92.75	136.83	51.02	41.02	35.01	30.20
1500	4.14	0.01	68.51	0.93	0.85	72.78	0.68	1.64	8.35	2.24
1500	4.14	0.44	123.40	-34.80	-37.01	86.17	5.91	1.55	6.44	4.28
1500	4.14	0.69	270.73	-116.93	-125.83	144.95	47.32	51.76	36.80	38.80
1500	4.14	0.79	414.59	-209.35	-224.71	218.84	46.86	33.71	35.74	24.33
1500	6.21	0.02	73.66	0.50	-1.40	78.41	0.90	0.67	1.69	2.30
1500	6.21	0.44	122.89	-32.25	-36.08	84.51	13.01	10.78	11.23	8.72
1500	6.21	0.68	269.83	-119.76	-126.40	146.16	10.70	5.37	6.17	4.77
1500	6.21	0.87	481.05	-278.20	-283.99	270.84	305.33	198.23	207.24	126.47
1500	8.28	0.03	65.00	0.45	-1.94	68.50	0.75	0.55	1.37	1.74
1500	8.28	0.47	131.15	-40.64	-44.29	88.15	1.75	2.51	0.85	2.28
1500	8.28	0.7	257.76	-120.36	-138.72	154.39	86.63	33.42	64.12	27.78
1500	8.28	0.79	376.82	-174.47	-214.23	214.69	224.23	177.15	112.88	75.28
3000	2.07	0.01	28.39	-6.61	6.30	28.21	5.65	7.20	6.37	6.67
3000	2.07	0.49	34.10	-1.21	7.77	31.28	5.23	12.92	3.60	7.49
3000	2.07	0.73	23.49	-4.67	3.93	40.94	10.53	20.09	5.38	10.43
3000	2.07	0.82	124.82	-92.14	-69.47	107.99	18.78	22.08	8.37	10.56
3000	4.14	0.02	38.12	-8.90	5.51	42.45	7.32	5.94	4.76	6.81
3000	4.14	0.27	70.82	-14.90	-10.81	51.23	1.74	1.68	2.05	4.18
3000	4.14	0.55	133.35	-52.18	-56.98	79.62	3.19	1.73	2.88	3.20
3000	4.14	0.73	256.11	-136.64	-137.43	139.44	10.85	6.75	7.84	5.61
3000	6.21	0.04	60.62	1.76	-1.61	63.03	0.67	0.57	1.38	1.61
3000	6.21	0.41	111.18	-26.84	-29.31	75.02	2.37	1.56	1.78	3.40
3000	6.21	0.61	173.97	-68.90	-71.13	95.26	3.51	3.72	4.10	4.14
3000	6.21	0.76	318.74	-170.16	-170.48	174.01	6.62	5.31	6.15	5.66
3000	8.28	0.04	67.50	1.25	-1.55	70.77	0.76	0.50	1.51	1.46
3000	8.28	0.37	97.60	-19.22	-22.90	70.49	2.64	1.23	1.41	3.07
3000	8.28	0.68	222.40	-92.24	-96.14	124.11	5.17	3.99	3.66	4.51
3000	8.28	0.77	278.32	-117.61	-123.10	138.87	113.24	90.66	85.29	86.42

Table B.16: Speed, pressure drop, eccentricity ratio, and damping coefficients of the 1X clearance LOL pressure-dam seals

Speed	ΔP	ε_o	Cxx	Cxy	Cyx	Cyy	eCxx	eCxy	eCyx	eCyy
RPM	bar	-	kN-s/m	kN-s/m	kN-s/m	kN-s/m	kN-s/m	kN-s/m	kN-s/m	kN-s/m
4500	2.07	0.01	21.70	-10.35	10.05	24.60	3.22	6.57	7.14	3.71
4500	2.07	0.49	19.44	-8.76	6.61	26.03	7.57	15.64	3.69	5.27
4500	2.07	0.75	16.40	-9.25	2.43	37.09	13.33	21.41	7.07	8.17
4500	2.07	0.86	19.53	-18.16	-2.63	52.00	17.73	28.50	12.06	15.30
4500	4.14	0.01	31.92	-9.08	9.53	33.23	3.87	8.17	7.93	4.57
4500	4.14	0.31	50.12	-11.52	3.25	44.32	2.81	9.72	4.17	7.24
4500	4.14	0.72	88.83	-51.58	-38.46	76.11	5.89	10.52	4.07	6.75
4500	4.14	0.83	111.61	-80.22	-58.13	104.71	14.43	16.88	6.60	9.36
4500	6.21	0.17	49.89	-4.67	2.96	50.31	4.25	5.33	5.48	3.87
4500	6.21	0.25	54.48	-5.81	2.76	45.88	1.27	7.03	3.74	8.85
4500	6.21	0.59	140.59	-59.25	-60.88	83.19	3.39	2.77	4.70	4.62
4500	6.21	0.72	223.13	-120.63	-121.91	132.50	17.49	7.67	9.82	8.10
4500	8.28	0.01	68.05	2.72	0.02	70.09	1.13	1.24	1.36	1.99
4500	8.28	0.23	75.94	-8.68	-10.46	61.56	1.28	1.09	2.69	4.49
4500	8.28	0.57	140.83	-52.11	-53.85	84.76	4.18	3.26	4.56	4.51
4500	8.28	0.77	278.22	-151.81	-150.28	155.17	7.30	6.45	7.24	5.65
6000	2.07	0.02	18.18	-10.82	11.34	21.21	1.56	8.84	7.36	3.26
6000	2.07	0.37	15.28	-9.39	9.28	22.74	5.99	15.35	4.07	3.38
6000	2.07	0.76	13.03	-9.00	3.33	40.73	18.09	22.62	10.31	11.44
6000	2.07	0.83	12.75	-11.85	0.97	49.53	26.80	28.22	15.38	16.74
6000	4.14	0.01	30.04	-12.64	11.54	32.08	2.08	8.86	8.09	3.79
6000	4.14	0.26	29.71	-8.65	14.11	33.70	4.83	15.14	4.90	6.97
6000	4.14	0.61	61.56	-32.31	-20.52	55.12	8.07	14.86	5.37	6.58
6000	4.14	0.8	92.63	-67.97	-43.75	92.87	15.76	21.29	10.72	13.18
6000	6.21	0.01	35.51	-9.12	9.49	45.71	4.66	10.27	5.24	4.42
6000	6.21	0.2	51.12	-4.96	5.39	43.32	4.83	6.99	4.32	7.63
6000	6.21	0.51	103.80	-39.77	-39.06	68.40	3.76	3.80	6.44	5.51
6000	6.21	0.77	87.68	-54.34	-36.20	85.95	15.42	27.60	12.14	14.89
6000	8.28	0.01	66.78	-0.55	-1.68	66.23	1.65	1.33	2.16	4.38
6000	8.28	0.018	66.22	-6.58	-2.73	58.59	1.80	1.67	3.48	4.57
6000	8.28	0.42	94.35	-24.49	-24.98	63.09	2.85	2.13	3.55	6.56
6000	8.28	0.7	198.45	-102.10	-99.30	117.36	5.34	8.70	7.03	6.23

Table B.17: Speed, pressure drop, eccentricity ratio, and virtual mass coefficients of the 1X clearance LOL pressure-dam seals

Speed	ΔP	ε_o	Mxx	Mxy	Myx	Myy	eMxx	eMxy	eMyx	eMyy
RPM	bar	-	kg	kg	kg	kg	kg	kg	kg	kg
1500	2.07	0.02	14.63	-2.09	-1.03	13.32	0.25	0.67	0.99	2.81
1500	2.07	0.56	13.10	4.08	13.19	9.40	3.16	2.17	11.61	5.07
1500	2.07	0.75	-6.07	15.60	12.67	1.91	8.01	6.57	5.15	4.31
1500	2.07	0.89	-32.04	33.31	17.94	-3.31	16.99	13.96	12.69	8.91
1500	4.14	0.01	16.43	-1.93	-0.29	15.18	1.82	0.77	1.77	3.25
1500	4.14	0.44	14.38	3.98	4.30	16.08	10.87	8.74	3.05	6.35
1500	4.14	0.69	-26.87	47.84	12.30	15.20	26.68	30.12	16.39	8.52
1500	4.14	0.79	-80.79	78.58	84.00	-39.15	9.93	21.16	12.48	9.47
1500	6.21	0.02	17.13	-2.92	-0.77	15.17	0.44	1.03	1.35	2.09
1500	6.21	0.44	16.10	5.39	3.06	20.70	3.31	6.19	2.31	2.05
1500	6.21	0.68	7.70	13.85	12.85	10.17	25.38	12.46	26.57	12.66
1500	6.21	0.87	-141.14	121.61	107.72	-57.96	45.34	24.32	22.92	17.14
1500	8.28	0.03	17.49	-3.40	-0.35	8.84	0.33	1.63	1.76	7.14
1500	8.28	0.47	17.27	1.27	3.23	17.86	1.50	1.03	2.34	1.23
1500	8.28	0.7	-32.06	45.03	11.93	11.24	29.66	24.98	15.78	6.95
1500	8.28	0.79	-79.52	86.00	52.48	-13.88	36.07	46.91	28.95	28.58
3000	2.07	0.01	7.61	3.92	-3.52	7.35	1.74	2.03	2.23	3.20
3000	2.07	0.49	11.17	4.18	-0.42	5.64	1.02	2.33	0.86	1.98
3000	2.07	0.73	14.69	2.19	-2.11	6.69	1.09	3.11	0.79	2.32
3000	2.07	0.82	-14.83	26.73	15.96	-7.45	8.74	7.99	5.17	5.03
3000	4.14	0.02	7.55	5.14	-3.41	4.01	1.86	1.44	1.62	3.78
3000	4.14	0.27	7.83	1.98	-0.39	7.46	1.19	0.43	1.64	2.02
3000	4.14	0.55	12.69	1.45	-0.44	10.52	1.05	1.04	2.56	1.73
3000	4.14	0.73	-15.93	20.09	17.12	-0.02	4.56	3.00	4.18	2.66
3000	6.21	0.04	15.01	-1.84	-1.18	14.04	0.37	0.46	1.35	3.48
3000	6.21	0.41	15.04	-0.92	1.75	13.75	2.28	1.30	7.09	1.85
3000	6.21	0.61	5.67	5.47	4.80	7.24	9.98	4.31	7.23	3.63
3000	6.21	0.76	-27.46	31.72	34.21	-8.09	5.29	4.63	5.45	4.52
3000	8.28	0.04	16.63	-2.00	-3.48	13.80	2.56	0.59	4.05	2.09
3000	8.28	0.37	13.90	2.18	-1.42	11.24	2.13	5.50	2.18	3.94
3000	8.28	0.68	6.43	6.63	10.39	7.18	2.30	2.46	3.85	2.36
3000	8.28	0.77	50.22	-2.94	8.59	-3.93	52.67	34.83	24.32	7.97

Table B.18: Speed, pressure drop, eccentricity ratio, and virtual mass coefficients of the 1X clearance LOL pressure-dam seals

Speed	ΔP	ε_o	Mxx	Mxy	Myx	Myy	eMxx	eMxy	eMyx	eMyy
RPM	bar	-	kg	kg	kg	kg	kg	kg	kg	kg
4500	2.07	0.01	5.11	5.98	-7.80	4.08	1.38	2.49	2.54	2.72
4500	2.07	0.49	5.93	7.54	-0.16	5.68	1.26	2.75	1.13	1.66
4500	2.07	0.75	8.05	6.50	-0.68	5.63	2.07	2.34	1.15	1.20
4500	2.07	0.86	11.61	5.12	-3.32	6.33	1.59	3.25	1.47	2.16
4500	4.14	0.01	6.71	6.03	-6.49	6.27	1.21	1.87	2.16	3.05
4500	4.14	0.31	7.22	9.43	0.88	1.69	2.09	2.35	1.78	2.59
4500	4.14	0.72	2.13	12.00	3.86	-0.10	3.27	2.58	2.38	2.36
4500	4.14	0.83	-6.59	21.68	9.80	-5.80	7.18	5.91	4.01	4.01
4500	6.21	0.17	5.04	1.85	-4.21	10.40	1.05	1.09	1.86	3.16
4500	6.21	0.25	14.63	0.85	-6.16	5.45	0.48	1.73	1.12	2.52
4500	6.21	0.59	8.08	1.68	-0.77	5.62	1.48	0.99	2.28	1.41
4500	6.21	0.72	-9.66	15.92	12.52	-1.03	3.10	1.96	4.18	2.11
4500	8.28	0.01	11.30	-2.63	-2.31	7.22	0.42	0.35	1.15	3.21
4500	8.28	0.23	12.67	-1.15	-3.00	10.31	0.58	0.32	1.31	1.27
4500	8.28	0.57	10.40	0.07	-2.78	4.83	2.67	1.56	2.17	1.90
4500	8.28	0.77	-17.77	21.24	21.16	-5.00	5.35	3.62	4.24	3.19
6000	2.07	0.02	4.17	7.34	-10.68	3.02	0.57	2.27	2.34	3.47
6000	2.07	0.37	4.49	8.52	-1.82	4.60	0.85	3.28	1.91	1.59
6000	2.07	0.76	10.17	4.38	-3.39	5.10	3.05	3.73	1.91	2.39
6000	2.07	0.83	9.65	2.97	-3.88	5.96	3.98	3.67	2.51	2.49
6000	4.14	0.01	5.83	7.47	-11.20	8.53	0.81	1.93	1.96	3.65
6000	4.14	0.26	9.67	9.65	-6.33	2.37	1.15	3.07	1.61	2.00
6000	4.14	0.61	5.10	8.00	-0.04	3.44	1.68	2.09	1.38	1.30
6000	4.14	0.8	-5.08	18.55	6.58	-3.29	3.45	2.41	3.19	2.64
6000	6.21	0.01	8.05	5.42	-8.33	7.48	0.98	2.01	1.35	4.12
6000	6.21	0.2	10.15	1.80	-7.02	5.20	0.97	1.43	1.27	2.02
6000	6.21	0.51	10.47	0.86	-3.04	6.02	1.61	0.84	1.69	1.56
6000	6.21	0.77	0.92	11.79	3.61	-1.05	3.53	3.72	3.32	2.57
6000	8.28	0.01	7.02	-2.92	-3.63	14.28	1.14	0.48	1.61	3.18
6000	8.28	0.018	10.24	-0.10	-4.13	6.05	1.06	0.39	1.12	1.86
6000	8.28	0.42	12.78	-0.80	-5.40	7.03	1.10	0.64	1.37	1.47
6000	8.28	0.7	-0.91	6.69	4.62	2.04	8.08	4.49	3.63	4.25

2X Pressure-dam Seals

Table B.19: Speed, pressure drop, eccentricity ratio, and stiffness coefficients of the 2X clearance LOD pressure-dam seals

Speed	ΔP	ε_o	Kxx	Kxy	Kyx	Kyy	eKxx	eKxy	eKyx	eKyy
RPM	bar	-	MN/m	MN/m	MN/m	MN/m	MN/m	MN/m	MN/m	MN/m
1500	2.07	0.04	-0.82	1.42	-1.29	-0.39	0.54	0.75	1.07	1.20
1500	4.14	0.04	-0.38	1.16	-0.89	-0.44	0.38	0.25	0.67	1.10
1500	6.21	0.05	-0.11	1.18	-0.89	-0.12	0.33	0.18	0.63	1.07
1500	7.24	0.05	-0.67	1.35	-0.39	0.27	1.31	0.17	1.72	0.97
3000	2.07	0.05	-0.60	2.33	-1.99	-0.81	0.23	0.17	0.92	0.95
3000	4.14	0.06	-0.59	2.57	-1.87	-0.36	0.32	0.19	0.72	1.01
3000	6.21	0.08	-0.42	2.59	-2.03	-0.15	0.38	0.33	0.80	1.16
3000	7.24	0.05	0.04	3.12	-2.34	0.21	0.33	0.23	0.60	0.94
4500	2.07	0.02	-0.05	3.19	-2.79	-1.03	0.28	0.16	0.73	1.04
4500	4.14	0.07	-0.72	4.22	-2.75	-0.95	0.31	0.19	0.77	1.15
4500	6.21	0.11	-0.78	4.10	-3.26	0.53	0.29	0.21	0.78	0.82
4500	7.24	0.08	0.08	4.78	-3.37	0.05	0.24	0.30	0.76	1.03
6000	2.07	0.03	0.78	4.10	-4.29	1.63	0.72	0.38	0.99	1.19
6000	4.14	0.09	0.38	4.60	-3.74	0.16	0.22	0.23	0.81	0.92
6000	6.21	0.08	-0.20	6.01	-3.87	-0.44	0.37	0.33	0.92	1.11
6000	7.24	0.05	-0.14	5.76	-4.46	0.48	0.35	0.31	0.81	1.22

Table B.20: Speed, pressure drop, eccentricity ratio, and damping coefficients of the 2X clearance LOD pressure-dam seals

Speed	ΔP	ε_o	Cxx	Cxy	Cyx	Cyy	eCxx	eCxy	eCyx	eCyy
RPM	bar	-	kN-s/m	kN-s/m	kN-s/m	kN-s/m	kN-s/m	kN-s/m	kN-s/m	kN-s/m
1500	2.07	0.04	10.20	0.87	-1.63	12.11	0.69	0.32	1.21	1.10
1500	4.14	0.04	12.30	1.08	-1.52	14.10	0.63	0.14	1.23	1.31
1500	6.21	0.05	13.52	1.28	-1.53	15.55	0.85	0.35	1.26	1.71
1500	7.24	0.05	14.36	1.23	-1.72	16.59	2.34	0.16	2.92	1.59
3000	2.07	0.05	11.49	1.62	-2.70	13.40	0.42	0.37	1.23	1.28
3000	4.14	0.06	12.14	2.28	-2.81	13.85	0.68	0.18	1.17	1.34
3000	6.21	0.08	13.26	2.32	-2.67	15.13	0.78	0.20	1.12	1.56
3000	7.24	0.05	15.18	2.31	-3.02	16.78	0.72	0.18	0.73	1.55
4500	2.07	0.02	11.09	1.77	-2.04	13.45	0.29	0.26	0.76	0.95
4500	4.14	0.07	13.56	2.56	-3.52	16.09	0.60	0.28	1.07	1.63
4500	6.21	0.11	13.46	3.31	-3.80	14.93	0.58	1.08	0.91	1.34
4500	7.24	0.08	14.33	3.52	-5.12	16.44	0.67	0.30	1.04	1.56
6000	2.07	0.03	10.17	-1.07	-1.10	10.30	0.72	3.78	1.11	4.27
6000	4.14	0.09	12.12	2.85	-2.69	14.56	0.39	0.56	0.93	0.76
6000	6.21	0.08	14.83	2.90	-5.75	17.23	0.59	0.40	1.32	1.99
6000	7.24	0.05	15.24	3.76	-6.93	17.82	0.90	0.30	1.84	1.90

Table B.21: Speed, pressure drop, eccentricity ratio, and virtual mass coefficients of the 2X clearance LOD pressure-dam seals

Speed	ΔP	ε_o	Mxx	Mxy	Myx	Myy	eMxx	eMxy	eMyx	eMyy
RPM	bar	-	kg	kg	kg	kg	kg	kg	kg	kg
1500	2.07	0.04	8.57	1.11	-0.08	9.12	0.50	0.70	0.99	1.11
1500	4.14	0.04	9.88	0.43	0.36	9.62	0.35	0.24	0.62	1.02
1500	6.21	0.05	11.03	0.35	0.57	10.58	0.31	0.16	0.59	0.99
1500	7.24	0.05	9.58	0.26	0.19	11.18	1.22	0.16	1.59	0.90
3000	2.07	0.05	7.61	0.13	0.23	6.92	0.22	0.16	0.85	0.88
3000	4.14	0.06	9.83	0.22	0.30	9.68	0.30	0.17	0.66	0.94
3000	6.21	0.08	10.53	0.36	0.30	10.50	0.36	0.31	0.74	1.07
3000	7.24	0.05	11.09	0.09	0.15	11.79	0.31	0.22	0.56	0.88
4500	2.07	0.02	5.13	0.68	0.86	3.44	0.26	0.15	0.68	0.97
4500	4.14	0.07	8.28	0.12	0.63	7.93	0.29	0.18	0.71	1.07
4500	6.21	0.11	10.59	-0.11	0.09	10.94	0.27	0.20	0.72	0.76
4500	7.24	0.08	10.98	-0.08	-0.57	12.63	0.22	0.28	0.70	0.95
6000	2.07	0.03	2.38	1.50	-0.90	2.58	0.67	0.35	0.92	1.10
6000	4.14	0.09	6.16	0.93	1.10	4.75	0.21	0.21	0.75	0.86
6000	6.21	0.08	7.73	-0.07	-0.03	10.10	0.34	0.30	0.85	1.03
6000	7.24	0.05	10.29	-0.39	-0.69	13.73	0.33	0.29	0.75	1.13

Table B.22: Speed, pressure drop, eccentricity ratio, and stiffness coefficients of the 2X clearance LOL pressure-dam seals

Speed	ΔP	ε_o	Kxx	Kxy	Kyx	Kyy	eKxx	eKxy	eKyx	eKyy
RPM	bar	-	MN/m	MN/m	MN/m	MN/m	MN/m	MN/m	MN/m	MN/m
1500	2.07	0.08	-0.21	1.28	-0.29	-1.04	0.15	0.13	1.23	1.86
1500	4.14	0.08	-0.60	1.27	-0.72	0.24	0.27	0.29	0.71	0.87
1500	6.21	0.06	-0.21	1.26	-0.64	0.39	0.23	0.27	1.01	1.04
1500	7.24	0.08	-0.08	0.98	-0.60	-0.03	0.35	0.61	0.90	1.71
3000	2.07	0.34	0.09	2.35	-1.33	0.84	0.63	0.76	0.90	2.00
3000	4.14	0.21	-1.21	2.85	-1.75	0.87	0.24	0.18	0.69	0.93
3000	6.21	0.19	-0.97	2.91	-1.56	0.95	0.26	0.18	0.82	0.98
3000	7.24	0.21	-0.97	3.03	-1.69	0.82	0.30	0.47	0.81	1.44
4500	2.07	0.08	0.26	3.08	-1.30	-0.18	0.26	0.30	1.88	1.61
4500	4.14	0.11	-0.80	4.43	-1.23	-0.81	0.48	0.21	2.59	1.49
4500	6.21	0.15	-1.04	4.36	-1.45	0.95	0.39	0.22	2.96	1.21
4500	7.24	0.15	-0.81	4.47	-1.55	0.86	0.50	0.26	3.03	1.21
6000	2.07	0.11	0.85	4.61	-2.89	-0.01	0.46	0.18	2.42	1.99
6000	4.14	0.13	-0.08	4.86	-2.22	-0.36	0.35	0.15	3.37	2.09
6000	6.21	0.13	-0.19	6.33	-2.47	-1.96	0.52	0.63	3.38	3.54
6000	7.24	0.11	-0.04	6.48	-2.66	-1.34	1.17	0.38	3.01	2.92

Table B.23: Speed, pressure drop, eccentricity ratio, and damping coefficients of the 2X clearance LOL pressure-dam seals

Speed	ΔP	ε_o	Cxx	Cxy	Cyx	Cyy	eCxx	eCxy	eCyx	eCyy
RPM	bar	-	kN-s/m	kN-s/m	kN-s/m	kN-s/m	kN-s/m	kN-s/m	kN-s/m	kN-s/m
1500	2.07	0.08	10.62	1.16	-3.62	13.90	0.34	0.14	2.97	3.61
1500	4.14	0.08	12.82	1.48	-2.36	15.17	0.70	0.33	2.91	1.54
1500	6.21	0.06	14.09	1.23	-3.63	17.56	1.14	0.22	3.57	2.22
1500	7.24	0.08	14.19	2.46	-3.57	16.85	1.11	2.70	3.52	2.57
3000	2.07	0.34	10.52	0.58	-2.15	14.29	1.03	0.87	1.97	2.60
3000	4.14	0.21	13.54	3.06	-3.01	15.04	0.74	0.17	2.71	1.47
3000	6.21	0.19	15.18	2.99	-4.53	17.53	0.94	0.26	3.34	2.24
3000	7.24	0.21	15.93	3.55	-4.32	17.90	0.95	1.04	3.36	2.20
4500	2.07	0.08	10.33	0.70	-2.63	14.10	0.64	0.44	3.54	2.23
4500	4.14	0.11	14.34	2.30	-6.54	18.28	1.03	0.33	5.33	3.03
4500	6.21	0.15	15.09	4.05	-7.83	18.08	1.19	0.27	5.76	2.72
4500	7.24	0.15	15.08	4.12	-8.18	18.49	1.19	0.34	6.28	3.07
6000	2.07	0.11	10.28	0.59	-1.47	14.46	0.67	0.51	5.40	2.42
6000	4.14	0.13	12.59	2.65	-4.45	16.77	0.83	0.40	5.47	2.56
6000	6.21	0.13	16.58	1.93	-6.25	21.14	1.65	1.81	6.72	5.02
6000	7.24	0.11	17.58	2.80	-6.06	22.56	1.73	1.03	6.68	4.97

Table B.24: Speed, pressure drop, eccentricity ratio, and virtual mass coefficients of the 2X clearance LOL pressure-dam seals

Speed	ΔP	ε_o	Mxx	Mxy	Myx	Myy	eMxx	eMxy	eMyx	eMyy
RPM	bar	-	kg	kg	kg	kg	kg	kg	kg	kg
1500	2.07	0.08	9.68	0.22	0.79	9.47	0.14	0.12	1.14	1.73
1500	4.14	0.08	10.33	0.08	1.61	10.91	0.25	0.27	0.66	0.81
1500	6.21	0.06	11.26	0.34	2.26	11.81	0.22	0.25	0.94	0.97
1500	7.24	0.08	11.87	-0.42	2.26	11.09	0.33	0.57	0.84	1.58
3000	2.07	0.34	3.90	0.55	1.07	6.01	0.59	0.71	0.84	1.85
3000	4.14	0.21	10.46	0.24	1.18	10.90	0.22	0.17	0.64	0.86
3000	6.21	0.19	11.58	0.24	2.49	11.77	0.24	0.17	0.76	0.91
3000	7.24	0.21	12.23	0.12	2.42	11.97	0.28	0.44	0.76	1.33
4500	2.07	0.08	3.53	0.88	3.47	1.94	0.24	0.28	1.74	1.50
4500	4.14	0.11	7.74	-0.04	4.31	8.56	0.45	0.19	2.40	1.38
4500	6.21	0.15	11.38	-0.23	4.21	12.66	0.36	0.21	2.75	1.12
4500	7.24	0.15	11.99	-0.18	4.21	12.98	0.47	0.24	2.81	1.12
6000	2.07	0.11	2.81	1.53	3.50	0.73	0.43	0.16	2.24	1.85
6000	4.14	0.13	5.79	1.12	5.65	4.71	0.32	0.14	3.12	1.94
6000	6.21	0.13	8.13	-0.10	7.54	8.12	0.48	0.58	3.13	3.29
6000	7.24	0.11	9.21	-0.60	6.71	10.93	1.09	0.35	2.79	2.71

APPENDIX C: EQUATIONS EXCLUDED FROM TEXT

Whirl Frequency Ratio

The following equations are used to arrive at the whirl frequency ratio presented in the results of this thesis, from San Andrès et al.[23]. The WFR, Φ, is given as:

$$\Phi^4 I_4 + \Phi^2(I_2 - 1) + \Phi_o^2 = 0, \tag{C.1}$$

where Φ_o^2 is:

$$\Phi_o^2 = \frac{(K_{eq} - K_{xx})(K_{eq} - K_{yy}) - K_{xy}K_{yx}}{\omega^2(C_{xx}C_{yy} - C_{xy}C_{yx})}, \tag{C.2}$$

K_{eq} is:

$$K_{eq} = \frac{K_{xx}C_{yy} + K_{yy}C_{xx} - K_{xy}C_{yx} - K_{yx}C_{xy}}{C_{xx} + C_{yy}}, \tag{C.3}$$

and I_1, I_2, and I_4 are:

$$I_1 = \frac{C_{yx}M_{xy} + C_{xy}M_{yx}}{C_{xx} + C_{yy}} \tag{C.4}$$

$$I_2 = \frac{K_{xy}M_{yx} + K_{yx}M_{xy} - I_1(K_{xx} + K_{yy}) + 2K_{eq}I_1}{C_{xx}C_{yy} - C_{xy}C_{yx}} \tag{C.5}$$

$$I_4 = \omega^2 \frac{I_1^2 - M_{xy}M_{yx}}{C_{xx}C_{yy} - C_{xy}C_{yx}} \tag{C.6}$$

Reynolds Equations

The following equations were used to find the axial, circumferential, and vector Reynolds numbers in the smooth and pressure-dam seals.

$$\begin{aligned} Re_z &= \frac{2\rho C_r}{\mu} W_0; \\ Re_\theta &= \frac{\rho C_r}{\mu} R\omega; \\ Re &= \sqrt{Re_\theta^2 + Re_z^2}, \end{aligned} \tag{C.7}$$

where Re_z, Re_θ and Re are the axial, circumferential, and vector Reynolds numbers, respectively. Also, ρ is the fluid density, C_r is the radial clearance, W_0 is the flow axial velocity, μ is the fluid dynamic viscosity, R is the shaft radius, and ω is the rotor speed. A Reynolds number below 1,000 indicates laminar flow, above 2,000 indicates turbulent, and in between is termed transitional [39].

APPENDIX D: FURTHER DISCUSSION ON SEAL LOCI

The seal motion of the pressure-dam seals in the LOD orientation is puzzling. the results show that under certain conditions, the recorded seal motion is opposite to the direction of load. In the LOL orientation, this phenomena is not observed. It was theorized that the seals had two static equilibrium positions that were 180°away from each other. Figure 55 shows the seal motion of the LOD seals as previously presented, at 2.1 bar. Additionally, the seal motion in the LOL orientation has been multiplied by (-1) and is also plotted.

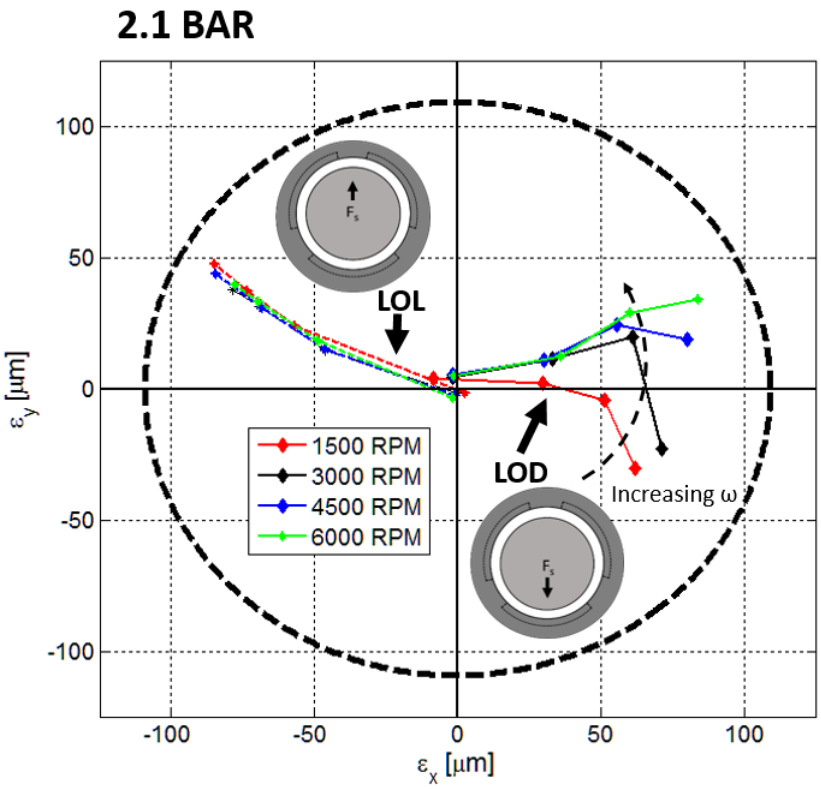

Figure 55: Plot of LOD and LOL seal loci on same plot. Note that the seal motion of the LOL seals has been multipled by (-1).

The figure is interesting, but does not confirm the initial hypothesis, primarily because the seal motion in the LOD orientation is sporadic when conditions are changed, but nearly constant in the LOL orientation.

Furthermore, Figure 56 shows static load versus the resulting eccentricity in the x-direction for both pressure-dam seal load orientations.

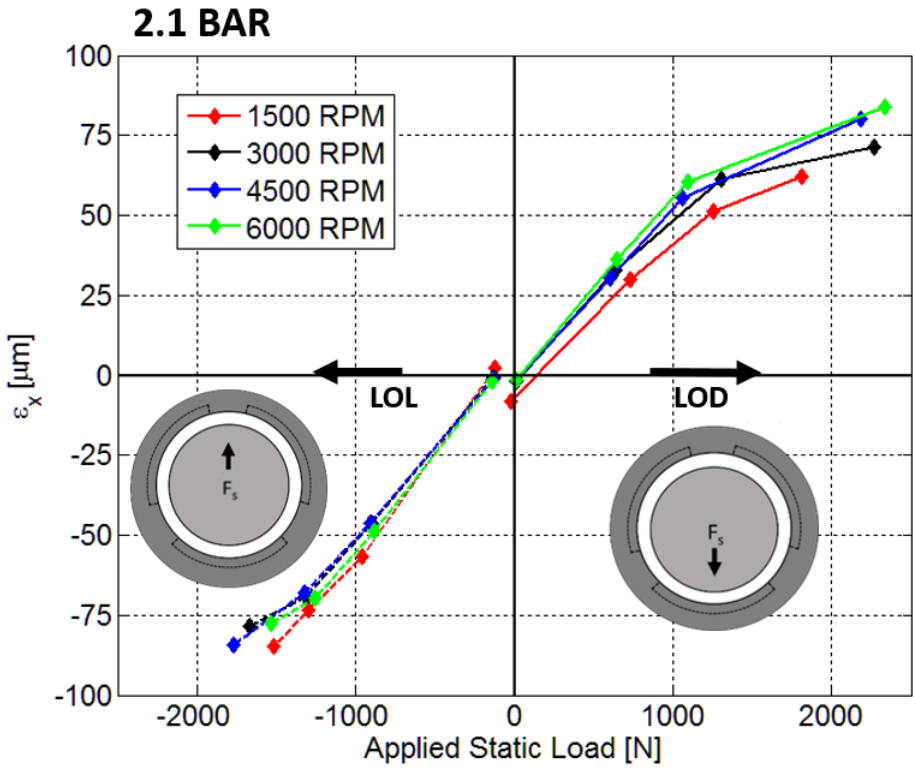

Figure 56: Plot of applied static load and the resulting ϵ_x for the pressure-dam seal in the LOD and LOL orientation. Note that the seal motion of the LOL seals has been multipled by (-1).

Note that the static load and the resulting eccentricity values are quite comparable in either load orientation. Figure 57 shows the static load versus the resulting eccentricity in the y-direction for both pressure-dam seal load orientations.

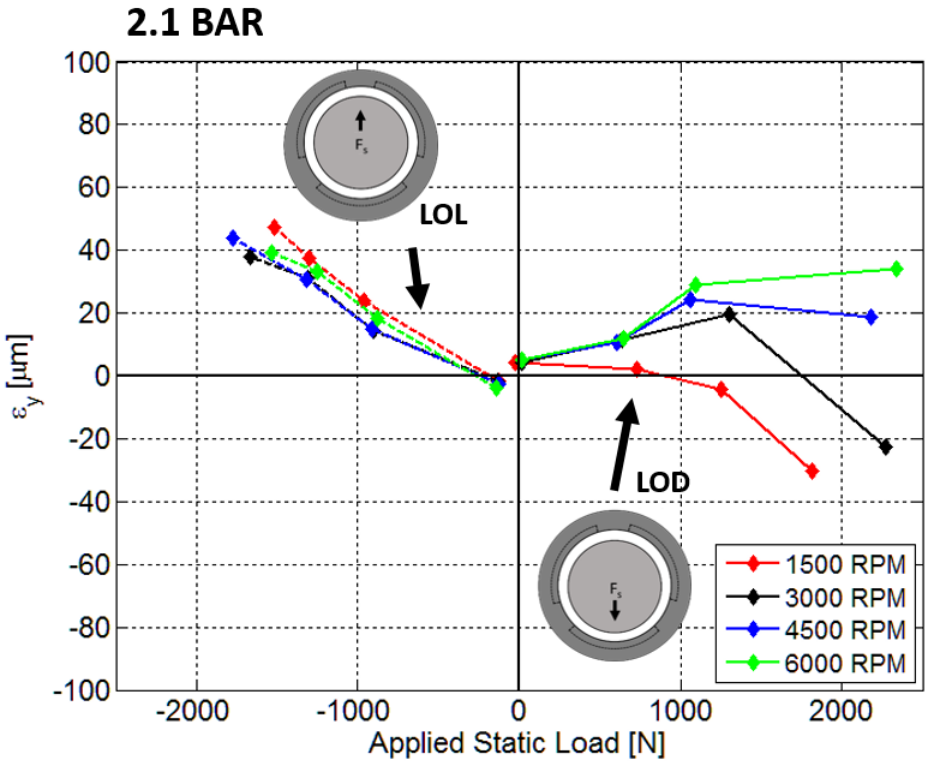

Figure 57: Plot of applied static load and the resulting ϵ_y for the pressure-dam seal in the LOD and LOL orientation. Note that the seal motion of the LOL seals has been multipled by (-1).

Trends in the y-direction are quite dissimilar. The author does not have an explanation for these trends.